Optimization of RadCom systems: A cognitive approach



AbdulMuneem Alselwi

Registration No. 63-FET/PhDEE-F13

A thesis submitted in partial fulfillment of the requirements for the Ph.D. degree in Electronic Engineering with specialization in Multifunction Systems at the Faculty of Engineering and Technology,

International Islamic University,

Islamabad.



Accession No. 75/25/38 VM Accession No. 75/25/38 VM

Structural optimization

Copyright

2022

by

AbdulMuneem Alselwi

All rights reserved.

DEDICATED TO

My Parents,

Wife,

Sister & Brothers,

and teachers.

CERTIFICATE OF APPROVAL

Title of Thesis: Optimization of RadCom systems: A cognitive approach

Name of Student: Mr. Abdulmuneem Abdulhadi Sharaf

Registration No: 63-FET/PHDEE/F13

Accepted by the Department of Electrical Engineering, Faculty of Engineering and Technology, International Islamic University (IIU), Islamabad, in partial fulfillment of the requirements for the Doctor of Philosophy degree in Electronic Engineering.

Viva voce committee:

Dr. Adnan Umar Khna (Supervisor)

Department of Electrical Engineering, Faculty of Engineering and Technology, IIU Islamabad, Pakistan.

Dr. Wasim Khan (Co-Supervisor)

ASM Professor DEE, FET, IIU Islamabad.

Prof. Dr. Aqdas Naveed Malik (Internal)

Professor DEE, FET, IIU Islamabad.

Dr. Hammad Omer (External External-I)

Assistant Professor, DEE, COMSETS, Islamabad

Dr. Muhammad Usman (External External-II)

Ex, Projector Director, NDC, NESCOM, Islamabad.

Dr. Suheel Abdullah Malik (Chairman, DEE)

Associate Professor, DEE, FET, IIU Islamabad.

Prof. Dr. Nadeem Ahmad Sheikh (Dean, FET)

Professor DME, FET, IIU Islamabad.

Rammoo

ABSTRACT

Implementing a cognitive architecture into a RadCom system design is an innovative paradigm for optimizing the system resources within the time-variant environment. Involving a closed-loop design into the current Radcom systems structure would allow the moving target to be tracked and simultaneously maintain the information transmission towards the direction of the intended communication receivers during each illumination. The proposed design provides the following benefits to the current RadCom system: 1) An efficient utilization of available resources, 2) Improvement of the tracking task of the system, 3) Enhancing the system throughput via an appropriate selection for information embedding strategy that would maintain the communication link towards the intended receiver regardless of its location, either in the main lobe or sidelobe (SL), within the transmit beampattern (BP).

In this thesis, we have employed convex optimization and beampattern modulation techniques and advanced array designs such as frequency diverse array (FDA) and/or multiple-input multiple-output (MIMO) configurations. This had facilitated the provision of the spatial and temporal structure required to implement radar and communication functions simultaneously.

The main contributions of this thesis include: 1) Proposed an unambiguous joint estimation algorithm for angle and range parameters of the radar target based on FDA-MIMO configuration, 2) Our proposed design involved various motion modes of the moving target during tracking scenario, namely, constant velocity (CV), constant acceleration (CA), and coordinated turn motion (CTM) models, 3) We have developed an

algorithm for the appropriate selection of the information embedding strategy towards to the intended communication direction 4) We have designed two signaling strategies, namely a phase-shift keying (PSK) and a novel amplitude phase-shift keying (APSK), for embedding the transmitted communication symbols. This proposed APSK information embedding strategy outperforms the existing SL signaling strategies in terms of the number of bits that can be embedded and bit error rate (BER) performance. It also allows different communication symbols to be transmitted to different communication users located in the SL directions, 5) The performance of the radar functionality is improved in terms of target detection and tracking, Cramer-Rao lower bounds (CRLBs) for range and angle estimations, and the signal-to-interference-plus-noise ratio (SINR). While for the communication functionality, the performance is enhanced in terms of symbol error rate (SER), secure information transmission, and overall throughput.

PUBLICATIONS AND SUBMISSIONS

- [1] A. Alselwi, A. U. Khan, I. M. Qureshi, W. Khan, and A. Basit, "Throughput Enhancement for the Joint Radar-Communication Systems Based on Cognitive Closed-Loop Design," *IEEE Access*, vol. 9, pp. 64785-64807, 2021.
- [2] A. Alselwi, A. U. Khan, I. M. Qureshi, W. Khan, and A. Basit, "Multi-user transmission for the joint radar communication systems based on amplitude phase shift keying modulation and waveform diversity," *International Journal of Microwave and Wireless Technologies*, pp. 1-15, 2021.
- [3] A. Alselwi, A. U. Khan, I. M. Qureshi, W. Khan, and A. Basit, "An architecture for Electronic Warfare Systems Inspired by the Theory of Cognition", *IEEE Intelligent Systems*, (Submitted).

ACKNOWLEDGEMENTS

This doctoral dissertation would not have been possible without the consistent help and support of many mentors, friends, and family members. I would like to take this opportunity to express my gratitude and appreciation to them.

First and foremost, I would like to thank the Almighty Allah for giving me the strength and patience to complete my Ph.D. studies. Next, I would like to express my gratitude to my supervisor Dr. Adnan Umar Khan who has provided mentoring, and support at both professional and personal levels in an uncountable number of situations. It has been an absolute pleasure and honor to be the student of Prof. Ijaz Mansoor Qureshi from whom I learned a lot and consider him to be one of my ideal teachers. Additional thanks go to the administrative staff of the electrical engineering department of the International Islamic University (IIU)-Islamabad, in particular, Mr. Imran for providing solutions to the numerous administrative-related issues I encountered.

My sincerest thanks to my dear family members, your support during this journey was vital for me. None of this would have been possible without their patience and understanding of the challenges that I had to overcome. I am forever grateful for their motivation, emotional and financial support throughout my studies.

The other half of "we", my amazing wife, Manal Bint-Dhaiban, thank you for your patience, love, and support. I appreciate your prodding me into action when I procrastinate "although, I will still frown when you interrupt my procrastination". However, I can always count on you to make me smile.

TABLE OF CONTENTS

ACKNOWLEDGEMENTS	
TABLE OF CONTENTS	iii
LIST OF FIGURES	
LIST OF TABLES	
LIST OF ABBREVIATIONS	ix
CHAPTER-1	1
INTRODUCTION	
1.1. Background	
1.2. Objectives And Contributions of The Thesis	4
1.3. Thesis Outline	7
CHAPTER-2	9
LITERATURE REVIEW	
2.1. Introduction	
2.2. Coexistence Approach	
2.2.1. Spectrum access opportunity (SAO)	
2.2.2. Interference channel model	
2.2.3. Precoder designs	12
2.2.4. Optimization designs	13
2.3. RadCom System Co-design Approach	
2.3.1 Time/Frequency sharing approaches	15
2.3.2 Antenna sharing approaches	
2.3.3 Waveform sharing approach	
2.3.3.1. Communication waveform-based approaches	
2.3.3.1.1. Spread spectrum waveform-based approach	
2.3.3.1.2. OFDM waveform-based approach	
2.3.3.2. Shared radar waveform approach	
2.3.3.2.1. Chirp waveform-based approach	
2.3.3.2.2. Frequency hopping waveform-based approach	
CHAPTER-3	
3.1. Introduction	
3.2. Proposed System Design	43

3.2	.1.	Signal model	48
3.2	.2.	Transmit beamspace design and information embedding schemes	50
3	3.2.2.1	. APSK-based information embedding scheme	51
3	3.2.2.2	. PSK-based information embedding scheme	54
3.2	.3.	Communication symbol detection at the communication receiver	58
3.2	.4.	Echo processing at the radar receiver	50
3.2	.5.	Joint angle and range estimation	53
3.2	.6.	Tracking algorithm	56
3.3.	Perf	ormance Analysis	71
3.3.	.1.	SINR analysis for radar	71
3.3.	2.	Detection analysis for radar target	12
3.3.	3.	CRLB analysis for radar	13
3.3.	4.	SER analysis for communication function7	/4
3.4.	Simu	lation Results7	15
3.5.	Sum	mary)3
CHAPTI			
4.1.		duction10	
4.2.		osed System Design10	
4.2.		Signal model10	
4.2.		Fransmit beamspace design and information embedding schemes11	
4	.2.2.1		
4	.2.2.2		
4.2.	3. (Communication symbol detection at the communication receiver	
4.2.		Echo processing at the radar receiver	
4.2.		Fracking algorithm12	
4.3.		rmance Evaluation12	
4.4.		nary14	
CHAPTE		14	
5.1.		nary14	
5.2.		e trends and challenges14	
APPEND	IX A.		1
APPEND	IX B.	152	2
APPEND	IX C.	15	3
		16	

LIST OF FIGURES

Figure 1.1: Cognitive design architecture for the proposed RadCom system
Figure 3.1: The proposed closed-loop design diagram for the RadCom system 44
Figure 3.2: The location of the communication station within the operating environment of
the proposed RadCom system, (a) the communication station is located within the sidelobe
directions of the radar transmit BP, and (b) both the radar target and the communication
station are located within the main lobe directions of the transmit BP 46
Figure 3.3: Constellation schemes with gray coding, (a) 16-APSK for $\beta = 4$ bits and (b)
16-PSK for a =4 bits
Figure 3.4: Signal Transmission diagram for the proposed system
Figure 3.5: Processing steps of IMM estimator with $r = 2$ modes
Figure 3.6: Spectral distribution of the interference and the two targets using, (a)
Conventional MIMO radar and (b) FDA-SA radar
Figure 3.7: The range resolution of two targets can be offered by the proposed system 78
Figure 3.8: Estimation results of the target parameters present in an interference
environment. Estimation of (a) Fundamental range difference, (b) Angle, and (c) range
ambiguity index 80
Figure 3.9: RMSE versus SNR for the Angle estimation in (a) interference-free
environment and (b) interference environment82
Figure 3.10: RMSE versus SNR for the Range estimation in (a) interference-free
environment and (b) interference environment
Figure 3.11: RMSE versus the number of snapshots for the Angle estimation in (a)
interference-free environment and (b) interference environment
Figure 3.12: RMSE versus the number of snapshots for the Range estimation in (a)
interference-free environment and (b) interference environment
Figure 3.13: CRLB versus SNR (a) Angle parameter and (b) Range parameter 88
Figure 3.14: (a) Real trajectory and measurements and (b) estimates of the different
estimators

Figure 3.15: RMSE in state estimates of KF (CV), KF (CA) filters, and IMM-KF estimator
for tracking a maneuvering target. (a) Angle errors. (b) Range errors
Figure 3.16: Mode probabilities of two-mode IMM algorithm for tracking a maneuvering
target
Figure 3.17: The detection performance of the proposed scheme design compared with
MIMO and FDA radar systems94
Figure 3.18: Transmit BPs for RadCom signaling strategies vs. angle when K=3 and apply:
(a)16- APSK strategy and (b) 32-APSK strategy
Figure 3.19: SER versus Eb NO when K=3 and: (a) the intended communication receiver
is located in the SL directions (b) the intended communication receiver is located within
the main beam
Figure 3.20: BER performance in the direction of the intended communication receiver in
(a) angle dimension and (b) range dimension
Figure 4.1: The proposed closed-loop design diagram for the RadCom system 107
Figure 4.2: Signal Transmission diagram for the proposed MIMO RadCom system118
Figure 4.3: Transmit BPs of the Traditional MIMO, Approach of [165], and the proposed
optimal beamspace design
Figure 4.4: RMSE performance comparison between the approaches under test, Traditional
MIMO, Approach of [165], and the proposed optimal beamspace design 126
Figure 4.5: Resolution performance comparison between the approaches under test,
Traditional MIMO, Approach of [165], and the proposed optimal beamspace design 127
Figure 4.6: (a) Real trajectory, (b) estimates of the EKF and the proposed EKF-IMM filters,
and (c) estimates of the EKF and the proposed EKF-IMM smoothers 130
Figure 4.7: RMSE in angle estimates of different non-linear filters and smoothers over
sampling steps in the scenario of tracking a maneuvering target
Figure 4.8: Model probabilities for two-mode (CV and CTM models) of maneuvering
target during tracking operation 132

Figure 4.9: Transmit BPs radiations for RadCom APSK-based signaling strategy vs. angle
when two bits are embedded towards the communication direction located in the SL
at 0 <i>i</i> = 45°
Figure 4.10: Single transmit BP radiation for RadCom PSK-based signaling strategy vs.
angle represents a single embedded communication symbol towards the communication
direction located at $\theta i \in \Theta = -10^{\circ} 10$.
Figure 4.11: Transmit BPs power radiations vs. angle for various RadCom signaling
strategies: (a) ASK-based communication scheme when $(L = C = 2)$, (b) PSK-based
communication scheme when $(R = C = 2)$, and (c) proposed APSK-based
communication scheme when $(L = R = C = 2)$
Figure 4.12: BER versus SNR for various SL-based signaling strategies; ASK, PSK, and
the proposed APSK142
Figure 4.13: Angular BER: when (a) the intended communication receiver is located
at $\theta t = 30^{\circ}$ in the SL directions and (b) the intended communication receiver is located
within the main beam spatial sector $\in \Theta = -10^{\circ} 10$, i.e., at $\theta i = 6^{\circ}$.

LIST OF TABLES

Table 1.1: Applications of the RadCom Systems Technology
Table 3.1: Stages involved for IMM algorithm implementation
Table 3.2: Parameter's design of the proposed system
Table 3.3: Simulation parameters used for target tracking scenario in example 3.4 89
Table 3.4: Average RMSE performance for angle parameters of different estimators 92
Table 3.5: Average RMSE performance for range parameters of different estimators 92
Table 3.6: Comparison between the proposed scheme design with recent existing
designs
Table 4.1: Simulation parameters used for target tracking scenario in example 4.2 128
Table 4.2: Average RMSE performance for angle parameters of different non-linear
estimators.

LIST OF ABBREVIATIONS

ADC	Analog to digital converters
ADMM	Alternating Direction Method of Multipliers
AM	Amplitude modulation
ATC	Air traffic control
APSK	Amplitude phase shift keying
BCJR	Bahl, Cocke, Jelinek and Raviv
BER	Bit error rate
BF	Beamforming
BP	Beampattern
BS	Base station
CA	Constant acceleration
СН	Costas hopping
СМ	Constant modulus
CP	Cyclic prefix
CPI	Coherent processing interval
СРМ	Continuous phase modulation
CRB	Cramer-Rao bound
CRLB	Cramer-Rao lower bound
СТМ	Coordinated turn motion
CV	Constant velocity
DFnT	Discrete Fresnel transform
DFT	Discrete Fourier transform
DL	Downlink
DOA	Direction of arrival
EKF	Extended Kalman filter
FDA	Frequency diverse array
FH	Frequency hopping
FIM	Fisher information matrix
FFT	Fast Fourier transform
FMCW	Frequency modulated continuous wave
FrFT	Fractional Fourier transform
ICSI	Interference channel state information
IDFT	Inverse discrete Fourier transform
IDFnT	Inverse discrete Fresnel transform
IFFT	Inverse Fast Fourier transform
ISI	Inter-symbol interference
JTP	Joint transmit platform
KF	Kalman filter
LFM	Linear frequency modulation

LDPC	Low-density parity-check
LoS	Line-of-sight
LPI	Probability of intercept
IMM	Interacting multiple models
INR	Interference-to-noise ratio
MI	Mutual information
MIMO	Multiple-input Multiple-output
MMSE	Minimum mean square error
MSE	Mean square error
MSK	Minimum shift keying
MU-MIMO	Multi-user MIMO
NLoS	Non-Line-of-sight
NSPP	Null space projection precoder
OFDM	Orthogonal frequency-division multiplexing
OCDM	orthogonal chirp division multiplexing
PA	Phased array
PAPR	peak-to-average power rate
PDF	Probability density function
PRF	Pulse repetition frequency
PSK	Phase shift keying
PU	Primary user
RF	Radio-frequency
RFID	Radio-frequency identification
RMSE	Root mean square error
SAO	Spectrum access opportunity
SCS	Subcarrier spacing
SER	Symbol error rate
SINR	Signal-to-interference-plus-noise ratio
SL	Sidelobe
SLL	Sidelobe level
SNR	Signal-to-noise ratio
SS	Spectrum sharing
SU	Secondary user
SVD	Singular value decomposition
UAV	Unmanned aerial vehicle
ULA	Uniform linear array
V2X	Vehicle-to-everything
ZF	Zero-forcing
	<u> </u>

CHAPTER-1

INTRODUCTION

In the past, radar and communication systems were developed as independent units. However, a cost-efficient solution that integrates both the functions in a single platform under the name of RadCom system was proposed to resolve the congestion problem within the spectrum space. Application of cognitive principles into the RadCom system design allows efficient utilization of the system resources and enhancement of its performance in terms of target tracking and overall throughput. This is a novel idea that has not been researched to the best of our knowledge.

In this chapter, we present the background of the joint radar and communication systems, and then the contributions of this thesis to the field of RadCom system design. In the end, we summarize the organization of the thesis.

1.1. Background

The Radio-frequency (RF) spectrum is a scarce resource used for several services such as navigation, broadcasting, surveillance, and communication. With the rapid growth of services and connected devices, especially in the wireless communication industry, the frequency spectrum is being progressively congested. By 2025, the ubiquitous number of connected devices is estimated to be 75 billion devices [1], which highlights an impending necessity for additional spectral resources to meet the requirement for high-quality services

provided to the users. As a result, the auction price for the available RF spectrum has risen sharply during recent years [2-4]. For these reasons, network providers are looking for opportunities to reuse the RF spectrum that is currently restricted to other services and applications [5, 6].

Radar has been evolving for many years and modern radar systems are used around the world offering a variety of applications including geophysical monitoring, air traffic control (ATC), surveillance for defense and security, and weather observation. Due to the large spectrum portions available, the radar frequencies are among the best options to be shared with different communication systems [6]. In particular, below 10 GHz, a large proportion of the spectral resources are utilized by the Radar, however currently it is shared with the new wireless communication systems e.g., LTE, 5G NR, and Wi-Fi [6]. At higher frequencies, the radar and communication platforms are anticipated to have smooth coexistence or even useful cooperation in the upcoming 5G network and beyond. However, sharing the available spectral resource would increase the interference with the radar frequency bands. Thus, the military and government organizations have raised concerns over the protection of critical radar tasks [7-9].

In recent years, intensive research has concentrated on the problem of RF spectrum congestion between radar and communications [6, 10, 11]. Generally speaking, there are two major research directions for joint radar and communication designs: (1) the coexistence approach and (2) the RadCom system co-design approach [12]. The coexistence approach aims to develop effective interference management procedures so that the two systems can operate without unduly disturbing each other. It is based on the exchange of information between radar and communication systems. On the other hand,

the RadCom techniques concentrate on designing dual-function systems that can concurrently perform remote sensing and wireless communication. It enables a single hardware platform to perform both detection and communication operations without compromising the performance of both functions [13, 14].

In many applications, the joint radar-communication platform design is useful [15, 16]. This has pushed comprehensive efforts to innovate methods that facilitate the integration process of both the functions [17-24]. It has been implemented in various novel applications, including covert communications, indoor positioning, and vehicular networks [24-26]. We have summarized the existing and potential applications of RadCom systems in Table 1.1. For instance, military applications sharing the aperture and spectral resources for radar and communications permit command integration, platform control, and system resources management more efficiently.

Table 1.1: Applications of the RadCom Systems Technology.

Civilian Applications	Radar-communications coexistence, Medical sensors, WiFi localization, vehicle-to-everything (V2X) network, Radar relay. Radio frequency identification (RFID), Unmanned aerial vehicle (UAV) communications and sensing, etc.
Military Applications	Multi-function RF system, UAV communications, and sensing, Radar assisted low-probability-of- intercept (LPI) communications, Passive radar, etc.

1.2. Objectives And Contributions of The Thesis

The main objective of this thesis is to develop a cognitive architecture for RadCom systems design. Our primary focus is utilizing the feedback information provided from the receiver side to enhance the performance of the RadCom systems. It will add the following benefits to the current RadCom system [17-24]:

- Utilization of spectrum and system resources more efficiently,
- Improving the tracking task for radar target and permitting a cognitive selection for an appropriate information embedding scheme that maintains the communication link towards the intended communication direction during each scan,
- Enhancing the throughput of the system.

A cognitive approach for RadCom system design is an innovative paradigm for optimizing the system resources within the time-variant environment. Fig. 1.1 represents the proposed cognitive architecture for the RadCom system design under consideration. The joint transmit platform (JTP) is illuminating the environment (targets and communication receivers) and the reflected signals are processed at the receiver to extract useful information about the target's features. The knowledge of the environment from one scan to the next is accumulating and the receiver makes decisions on the possible presence of the target within the environment on a continuous-time basis. The estimated target position \widehat{P}_n at time n is forwarded to the predictor position block to estimate the next target position \widehat{P}_{n+1} at time n+1. Next, the receiver feeds back this information to the transmitter, which compares \widehat{P}_{n+1} with the known location of the communication

receivers. Then the JTP illuminates the environment in light of resulted information and the cycle is then repeated over and over again.

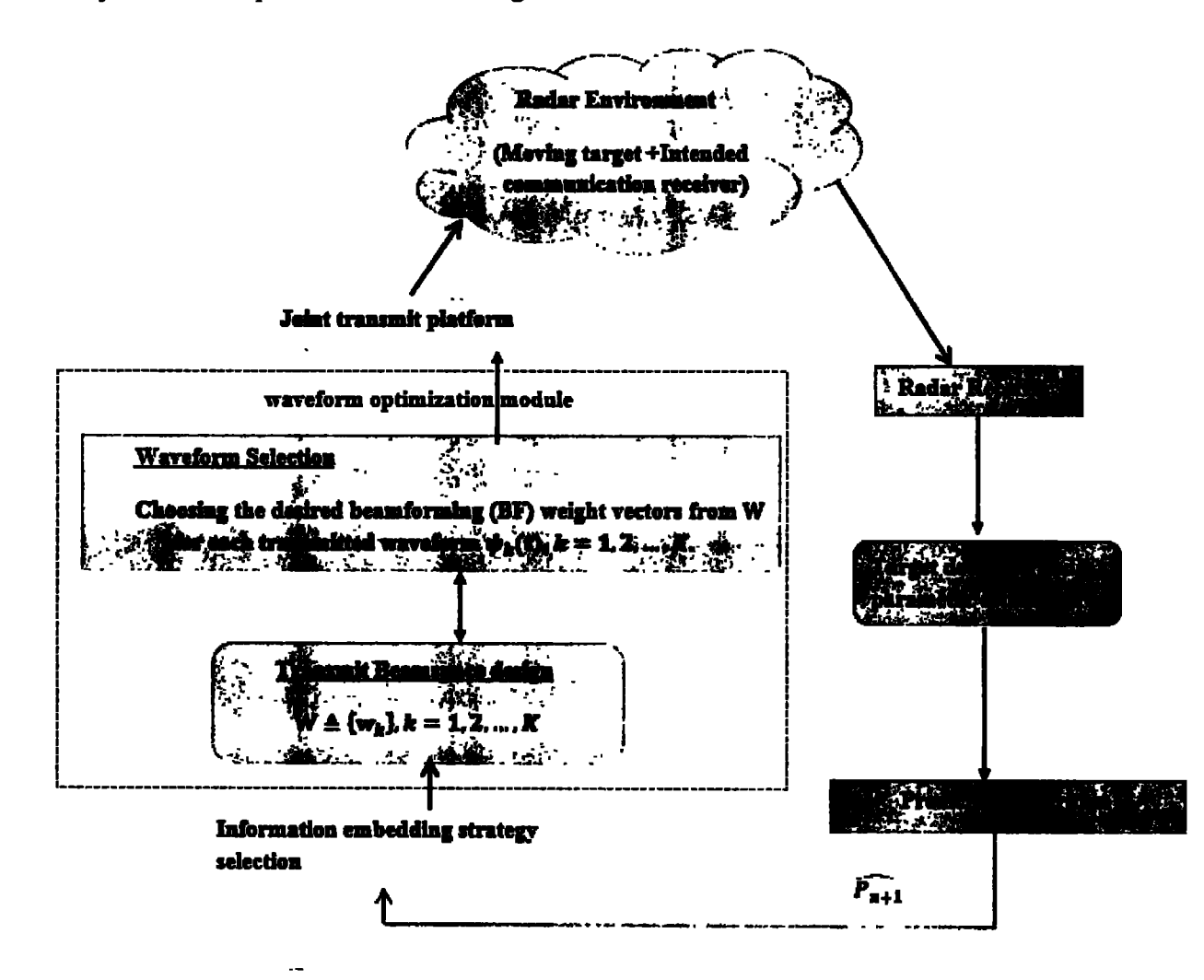


Figure 1.1: Cognitive design architecture for the proposed RadCom system.

This allows the JTP to select the appropriate information embedding strategy and accordingly design the optimum beamforming (BF) weight vectors for both functions. In this thesis, a novel two-stage optimization strategy is implemented, which can be summarized as follows:

Stage 1: BF weight vectors design

This involves that each transmitting BF weight vector is designed to represent a single communication symbol towards the communication direction without compromising the radar function performance.

• Stage 2: BF weight vectors selection

This involves selecting the BF weight vectors according to the information bits stream provided to the system for communication symbols transmission.

In this thesis, we have employed convex optimization techniques and advanced array designs e.g., frequency diverse array (FDA) and/or multiple-input multiple-output (MIMO) configurations as illustrated in Figs 3.4 and 4.2.

The main contributions can be summarized as follows:

- We proposed a closed-loop design for the RadCom system that permits tracking of the moving target while maintaining the information transmission in the direction of the intended communication receiver during each illumination,
- We have proposed an unambiguous joint estimation algorithm for angle and range parameters of the radar target based on FDA-MIMO configuration,
- In target tracking scenarios, we considered various motion modes of the moving target, namely, constant velocity (CV), constant acceleration (CA), and coordinated turn motion (CTM) models in our proposed designs.
- We have developed an algorithm for the appropriate selection of the information embedding strategy according to the location of the communication receiver within

the transmit beampattern, whether it is located within the main lobe or sidelobe (SL),

- We have designed two signaling strategies, namely PSK scheme and novel APSK scheme for embedding the transmitted communication symbols,
- The proposed APSK information embedding strategy outperforms the existing SLbased strategies in terms of data rate transmission and it also allows different communication symbols to be transmitted to different users,
- The performance of the radar functionality is improved in terms of target detection, parameters estimation, Cramer-Rao lower bounds (CRLBs) for range and angle estimations, and the signal-to-interference-noise ratio (SINR). While for the communication functionality, the performance is improved in terms of bit error rate (BER), secure information transmission, and overall throughput of the system.

1.3. Thesis Outline

This thesis is organized as follows:

- In Chapter 2, a literature review of the recent research progress in the RadCom system design is discussed.
- In Chapter 3, we developed an angle-range dependent RadCom system that utilizes an FDA-MIMO configuration. We have used an unambiguous joint estimation algorithm for the angle and range parameters of the target. In the target tracking scenario, we considered two motion modes of the moving target, CV and CA models, in our proposed design. For embedding the communication symbols, we utilize either the magnitude ratio and/or the phase shifts between the transmitted

waveform pairs. Performance metrics of the communication and the radar functions are analyzed.

- In Chapter 4, a collocated MIMO configuration is considered for the RadCom model design. MIMO configuration empowered with a cognitive architecture can facilitate efficient utilization of the system resources. In the target tracking scenario, we considered two motion modes of the moving target, CV and CTM models, in our proposed design. The proposed APSK signaling strategy provides a significant improvement in communication performance compared to the existing SL-based communication signaling in terms of data rate transmission and low BER. Moreover, the APSK scheme allows different communication symbols to be transmitted to different communication users within the SL region.
- Finally, Chapter 5 provides the concluding remarks and associated future works from this thesis.

CHAPTER-2

LITERATURE REVIEW

In this chapter, the recent advancement designs in the field of joint radar and communication systems are explored. Initially, the coexistence approaches are discussed, and then the co-design approaches for the RadCom system are investigated.

2.1. Introduction

In the past, radar and wireless communication have typically been independently studied entities. The objectives of radar systems are to achieve better estimation and resolution for the target's parameters in the presence of noise and surrounding clutter. On the other hand, wireless communication attempts to obtain the maximum possible capacity for information transmitted across a noisy wireless channel under complexity and power constraints. However, there is a lot in common between radar and wireless communication: Both systems send and receive electromagnetic (EM) waves and apply signal processing algorithms to the received signal to extract useful information. Thus, it is not an implausible idea to integrate these two functions/systems.

In recent years, the research in integrating radar and communication system designs has gained significant momentum. Such systems would constitute a unique cost-efficient solution especially when both functions are performed simultaneously via a common platform. Generally, there are two major research directions for joint radar and communication designs: 1) the coexistence approach, and 2) the RadCom system co-design approach. In the following, we discussed each approach independently in more detail.

2.2. Coexistence Approach

This approach has been focused on the access management of the shared spectrum and using interference mitigation techniques between the radar and communication systems under the assumption that they coexist as independent systems.

2.2.1. Spectrum access opportunity (SAO)

The radar bands are the best candidates to be shared with the communication system because of the large availability of their spectrum portions [6]. SAO approach can be treated as a part of cognitive radio technology, where the radar and communication system are considered as the primary user (PU) and secondary user (SU) of the shared spectrum, respectively. In such techniques, the SU senses the spectrum and then accesses it only if the spectrum is not occupied by the PU. To avoid imposing interference on the PU's operation, the SU should control its transmit power to guarantee that the PU's interference-to-noise ratio (INR) doesn't become excessive [27]. A similar method has been used in [28] where the main beam of the radar is rotating periodically to detect potential targets. Thus, the cellular base station (BS), i.e., SU can transmit only when it is located within the sidelobe (SL) region of the radar. The distance between the radar and BS is calculated given the acceptable INR level, and also the performance of the communication link is analyzed in terms of the downlink (DL) data rate.

Although they are easy to implement in practical scenarios, the aforementioned methods do not share the spectrum in reality. This is due to the SU (communication system) only being able to use the spectrum when the PU (radar system) is not occupying it. Also, the above contributions do not simply extend to facilitating multiple-input multiple-output

(MIMO) radar coexistence. Different from traditional radar systems, the MIMO radar emits orthogonal waveforms in all spaces to detect unknown targets and produces directional beams towards targets of interest [29, 30]. As a result, it is difficult for the BS to identify the SLs of the radar because the beampattern (BP) of the MIMO radar may vary randomly along with the target's movement. Thus, more powerful methods are required, such as the transmit precoder design, to eliminate mutual interference.

2.2.2. Interference channel model

Before the designing stage of the transmit pre-coded (TPC) signals, the channel state information must be first obtained about the interference channel state information (ICSI), i.e., the channel through which mutual interfering signals are propagated. Typically, the ICSI is obtained by utilizing pilot signals transmitted by the communication system to the radar system, where channel estimation techniques such as minimum mean squared error (MMSE) and least-squares (LS) [31] could be simply applied. However, these schemes can consume additional signaling and computational resources [20]. As another choice, the authors suggested in [32] to construct a dedicated coordination center linked to both systems via backhaul or wireless links, which would perform the entire coordination including transmitting precoder design and ICSI estimation. The coordination center would be part of the system which has a priority, e.g., as part of the radar system as presented in [20]. However, such a scheme would introduce significant overhead. In [33] the authors proposed a novel approach for channel estimation by utilizing the radar signal as a pilot waveform, in which the radar system is not aware of the communication operation. Since the radar adjusts its operating mode randomly, the BS must first identify the operating

modes of the system (searching or tracking) via hypothesis testing procedures and then estimate the channel.

2.2.3. Precoder designs

After the interference channel is estimated, i.e., ICSI is available, the transmit precoder can be designed at either the communication or the radar's side. In [34, 35], the concept of null space (NS) projection is applied, which requires the ICSI to be available at the radar system. The key concept is the transmitted precoded radar waveform is projected into the NS of its channel to the communication receiver. After the ICSI matrix is estimated by applying, e.g., the blind NS learning algorithm [36], the radar gets the right singular vectors of the ICSI matrix by using the singular value decomposition (SVD). Then, the radar constructs an NS projection precoder based on the vectors associated with the NS of the ICSI channel. The transmitted precoded radar signals are then projected onto the NS of the ICSI channel so that the received interference power at the BS is rigorously zero. However, such a scheme can seriously degrade the performance of the MIMO radar, e.g., causing the spatial orthogonality breakdown for the searching waveform. To deal with this problem, the authors of [37] designed an adaptive threshold for the singular values (SVs) of the ICSI matrix. Then, an NS projection precoder is constructed by the vectors associated with SVs that are less than the designed threshold. In this case, the performance of the radar can be improved but the received power of the interference at the BS will be increased.

Despite the aforementioned advantages, there are many flaws in NS projection-based methods. For example, the interference power is proportional to the SVs of the random channel, thus it cannot be precisely controlled. Additionally, the radar may miss the target when the target's response falls into the row space of the ICSI and then zero-forced via the

NS projection precoder. Fortunately, these drawbacks could be solved by using convex optimization approaches, where both systems' performance are optimized under controllable conditions [32, 38, 39].

2.2.4. Optimization designs

In this approach, the shared spectrum problem is formulated as optimization-based signaling with constraints. In [39], the authors employed a sub-sampling scheme to sample the receiving signal matrix of the echoes from the target at the radar receiver and roughly retrieves the target information by applying the matrix completion (MC) technique. The sub-sampling scheme modulates ICSI and enlarges its NS. This allows the communication system to formulate its transmitting precoder in such a way that the interference inflicted to the radar is minimized. In [39], the MC-MIMO radar sub-sampling matrix and communication signal covariance matrix are jointly optimized under the capacity and power constraints. This optimization problem is solved using the Lagrangian decomposition and alternate minimization techniques. By considering realistic constraints, the authors in [32] introduced the cluttered environment into the coexistence scenario, which must be reduced to maximize the radar effective SINR while ensuring communication performance. According to the observation that the persistent interference caused by the communication system upon the radar while the interference caused to the communication link by the radar is intermittent [32], the authors in [21] considered the coexistence issues of a pulsed radar and communication system, and the rate of the communication was computed as the summation of the weighted rates without and with the radar interference. Then, the optimization problem was formulated to maximize the

communication rate subject to the radar SINR and power constraints. Such a problem can be resolved in the closed-form if radar interference meets certain conditions.

The authors in [40] addressed the coexistence issue of the multi-user MIMO (MU-MIMO) communication system and the MIMO radar, in which a robust beamforming design is proposed at the BS, where the ICSI is assumed to be imperfectly known. They formulated an optimization problem that maximizes the radar detection probability while guaranteeing the SINR of the DL users and the BS power budget. In [41], the interference alignment is proposed for transmitting precoder design with an emphasis on the degree of freedom (DoF), considering the scenario of MU-radar coexisting with MU-communication. To minimize the CRB for estimating radar target parameters with the presence of MU-MIMO communication interference, a novel optimization approach has been developed in [42] based on the Alternating Direction Method of Multipliers (ADMM). As a further step, the authors in [43] proposed a beamforming design based on constructive interference [44] for the coexistence issue, in which the known DL-MU interference is exploited for enhancing the power of the useful signal. Accordingly, the SINR of the DL users is considerably improved compared to [40] given the same budget of the transmit power.

2.3. RadCom System Co-design Approach

In these approaches, both functions (radar and communications) coexist within the same platform, i.e., the system performs both functions using the same hardware device. As a result, the system resources would be shared among both functions. To enable their

coexistence while ensuring the performance requirements for each function, various resource-sharing methods have been proposed in the literature. In general, it can be categorized into three main divisions: time/frequency sharing approaches, antenna sharing approaches, and waveform sharing approaches.

2.3.1 Time/Frequency sharing approaches

These approaches are considered the simplest methods for facilitating the coexistence of the radar and communication functions onto the same platform while alleviating the cross-interference. Here, the transmitted waveform can be written as:

$$\mathbf{s}(t) = \mathbf{s}_r(t) + \mathbf{s}_c(t) \tag{2.1}$$

where $\mathbf{s}_r(t)$ and $\mathbf{s}_c(t)$ are the radar probing signal and communications signal, respectively. Typically, using orthogonality boosting by frequency and/or time division, the ability to transmit these two dedicated signals jointly with limited cross-interference can be achieved.

A straightforward mechanism is to allocate for each function a different time slot or a different frequency band. As a result, a trade-off in performance between both the functions is taking place. For instance, in [45], a RadCom system is implemented by using non-overlapping fixed frequency bands. In this approach, each function is assumed to use its predetermined band. In [46-52], the frame structure of the existing communication protocols is utilized for radar functionality. Here, the radar operation is an incidental result of the communication protocol and thus the communications function will not be disturbed or compromised. In the work presented in [47-49], due to its large bandwidth, the authors used the IEEE 802.11ad standard operating at 60 GHz, the millimeter wave (mmWave)

communication, for the RadCom system to provide better range resolution for radar and high data rates for communication. The IEEE 802.11ad standard frame consists of data and preamble blocks. To avoid using the data-dependent signals, the RadCom system reserves the data block for data transmission while the preamble block is utilized for radar probing. Once the transmission link is established, targets located within the beam directions can be detected reliably by the system. The simulation results in [47] showed that the detection rate of the radar can be achieved up to 0.99 given low SNR, i.e., above -2 dB. However, the estimation performance of the velocity is limited due to the short duration of the preamble block [48]. To overcome this limitation, one solution is to lengthen the duration of the preamble block but this would degrade the communication performance significantly. To solve this conflict, an optimization formulation is required for trading-off between the radar and communication functions. To do so, the authors in [53] introduced the idea of the fraction of data symbols, which is defined as the ratio of the data symbols in the frame to the data symbols in the IEEE 802.11ad standard frame. They formulated a convex optimization problem that minimizes the MSE bounds for the data symbol, velocity, and range estimations. The simulation results showed that the MMSE of the estimated range is improved by an amount of 3.3 cm²compared to [47]. Another optimization strategy is proposed in [54], which is based on sparse sensing methods to optimize the trade-off between the performance of both the functions and appended virtual preamble blocks during the coherent processing interval (CPI). As a further step, the authors in [50] have designed the virtual preamble sequences by applying a sub-Nyquist methodology. It minimizes the distortion in communication rate while maximizing the estimation accuracy of the velocity. The simulation results showed that the communication

rate distortion and the velocity error obtained by the virtual pulse methods are much lower than those achieved by the baseline method in [47].

Instead of using standard frames, the authors in [17] used time cycles for communication and radar operations. For each time cycle, the time portions are allocated to maximize the data communication rate and the radar estimation rate. Here, for each radar scan, the information of the target is obtained, and based on mutual information (MI) that is accomplished by the radar receiver the estimation rate can be determined. Depending on the information gained by the radar the time allocated to each function can vary from cycle to cycle. For example, if the information gained from the previous cycle time is little through the radar operation, then the allocation time for the radar function should be decreased. The simulation results for the methods proposed in [17, 47, 53] show the advantages of utilizing the cycle time or time frames to enhance both the sensing accuracy and data communication rate.

These design approaches implement radar function with minimum impact on the communication transmission at the cost of slightly limiting its radar capabilities. Since they utilize only the preamble portion as a radar signal, low power can be transmitted for radar due to the low duty cycle which results in reducing range detection. Moreover, the reflections due to data signal transmission may interrupt and submerge the echoes of the radar probing signal, i.e., the preamble, especially in cluttered environments where strong scatterers exist and it may cause the small targets to be missed by the radar.

2.3.2 Antenna sharing approaches

Typically, using orthogonality boosting by applying spatial beamforming, the ability to transmit the signal in (2.1) with limited cross-interference can be achieved. In particular, multiple antenna signal processing is utilized to alleviate mutual interference based on spatial beamforming design. While this type of signal processing was used in coexistence cases for separate radar and communication systems, it can also be employed for a RadCom system as well [55]. The main idea is projecting the radar waveform into the null space of its channel to the communication receivers [56] as a result, a zero-forcing (ZF) beamformer is constructed. In this scheme, the radar waveform is designed to alleviate mutual interference between both the functions, where certain performance constraints should be satisfied, while the communication waveform is beamformed.

The received signals at the radar target and the communication receiver are, respectively, given by:

$$y_r(\theta) = \mathbf{a}_r^T(\theta) \mathbf{s}_r + \mathbf{a}_c^T(\theta) \mathbf{W} \mathbf{s}_c + z_r(\theta)$$
 (2.2)

$$y_c = \mathbf{h}_r^T \mathbf{s}_r + \mathbf{h}_c^T \mathbf{W} \mathbf{s}_c + z_c$$
 (2.3)

where $\mathbf{a}_r(\theta)$ and $\mathbf{a}_c(\theta)$ are the steering vectors of the radar and communication transmitters, respectively, towards a direction θ , \mathbf{W} is the beamforming matrix applied to the communication signal, \mathbf{h}_r and \mathbf{h}_c represent the channel coefficient vectors between the radar and communication transmitters and the communication receiver, respectively, \mathbf{z}_r and \mathbf{z}_c represent noises of the radar and communication receivers modeled as white Gaussian with zero mean and variance σ^2 . Observing from (2.2) and (2.3) that, since the radar signal \mathbf{s}_r is already designed according to the radar BP so there is no need to apply a

beamformer with it. Also, the beamforming matrix W and radar transmit signal vectors \mathbf{s}_r can be jointly designed to mitigate cross-interference while certain performance requirements should be satisfied. For zero-forcing (ZF) beamforming, \mathbf{s}_r can be designed to be projected onto the null space of the radar communications interference channel, i.e., to be orthogonal to \mathbf{h}_r . Since the communication and radar functions are implemented within the common transmit platform, the beamforming matrix W can be designed to satisfy specific requirements for radar BP and communications performance independently. For example, in [57] different antenna elements are assigned for each function and \mathbf{h}_r might not be identical to \mathbf{h}_c . Note that, a priori knowledge about \mathbf{h}_r and \mathbf{h}_c in all cases is required.

Addressing the antenna elements, the allocation issue for the RadCom systems is presented in [58] in more detail. The authors proposed a random allocation mechanism for antenna elements array to improve the angular resolution for radar function and at the same time increase the communication data rate. The system is composed of a common uniform linear array (ULA) platform that includes a radar receiver and a communication transmitter and each antenna element can be connected with either of the two. The function of the radar receiver is to process the echoes received at the RadCom system while the communication transmitter is used to transmit information bits. At each time of information transmission, antenna elements are allocated according to the bits stream and the remaining are allocated for the radar receiver. In particular, the bits stream is partitioned into blocks each composed of spatial and constellation bits. Here, the spatial bits are used to define the combination of the ULA antenna elements while the constellation bits are mapped by using constellation schemes [59, 60]. The channel capacity can be improved when the number of spatial bits

is increased as compared to the MIMO system [61]. The radar performance is evaluated by using the CRB of the radar resolution, and the simulation results showed that the CRB of the proposed approach is much lower than that of the baseline method, i.e. when the antenna elements are spatially divided into the two subsystems. This indicated that the proposed approach is efficient.

A different spatial beamforming approach is presented in [62, 63] where the authors implemented a RadCom system based on a sparse transmit array design. The radar and communication functions are implemented within the common transmit platform, where the position of the antenna elements is selected to optimize specific radar tasks, and the rest is allocated for information transmission as a secondary function. However, the major disadvantage of this approach is that the communication data rate is very limited especially when more antenna elements are allocated to the radar for tracking tasks.

A major benefit of the frequency/time division and antenna approaches is that they can offer a wide selection of feasible performance combinations. For example, in frequency/time division, the overall performance is evaluated through how the system resources, including time slots and spectrum, are assigned for each function. The overall performance trade-offs can be significantly improved with the use of spatial beamforming, permitting radar and communication functions to operate concurrently at all time slots and full bandwidth usage [64]. However, prior knowledge about the channel is required for the spatial beamformer design, it may not be available for fast-moving target scenarios.

2.3.3 Waveform sharing approach

This is a well-known approach utilized in the literature of RadCom systems, particularly in autonomous systems because of its superb features, e.g., optimized utilization of the spectrum and low cost. The key idea is to integrate both radar and communication functions on the same transmitted signals. There are two approaches, communication waveform, and radar waveform approaches. The first one is based on how to utilize the communications signals to process and extract the target parameters from the return signals at the receiver, while the second approach is based on how to embed the information bits into the radar emissions.

2.3.3.1. Communication waveform-based approaches

These approaches utilize standard communication waveforms for radar probing and are suitable for processing the target returns. Firstly, we briefly review the spread spectrum waveform-based RadCom systems, and then a review of orthogonal frequency division multiplexing (OFDM) waveform-based RadCom systems is presented in more detail.

2.3.3.1.1. Spread spectrum waveform-based approach

In spread-spectrum communications, the signals can be transmitted over a larger bandwidth by applying spread coding techniques. It modulates the communication signals with pseudorandom sequences that possess a high spreading factor. The resulting waveforms inherit the spreading factor properties such as good autocorrelation that make them appropriate for radar measurements. Implementation of the RadCom system based on spread coding was discussed in [65-67]. The basic idea is as follows: first, use a digital modulation scheme such as the PSK scheme to map the data bits into data symbols. Then,

modulating each communication symbol with a code sequence. As a result, the transmitted signal would have a quasi-optimum autocorrection property of the code sequence, e.g., pseudorandom m-sequence [68]. The prior knowledge of code sequences at the receivers is assumed, for example, through the use of synchronization schemes. Therefore, the communication and radar receivers can, respectively, detect communication symbols and estimate target parameters by employing correlation processing and matched filtering. The simulation results in [65] show that the code sequences with longer lengths, such as msequences and Kasami codes [69], can estimate the targets of high ranges. However, from a radar measurements perspective, the dynamic range is limited by the properties of the transmitted code sequences, e.g., its imperfect autocorrelation. Besides, the integration time is restricted because of the Doppler effect and the maximum target velocity can be estimated is limited to 22.5 km/h (or 6.25 m/s) at 24 GHz carrier frequency and Doppler shift of I KHz. Consequently, the spread-spectrum approach is limited in real-time applications such as automotive applications which required a tremendous computational effort for velocity estimation of the targets. For wideband spread-spectrum signals, highspeed ADCs are required which leads to increasing the complexity and cost of the system implementation.

2.3.3.1.2. OFDM waveform-based approach

The OFDM signal is a popular wireless communications scheme that permits data transmission in parallel over multiple overlapped orthogonal subcarriers, and as a result, it improves significantly the spectral efficiency. Also, it has many advantages such as robustness against fast fading, handling the inter-symbol interference (ISI), easy equalization, and relatively low-cost hardware are required [70, 71]. In the context of

frequency-agile signals, the OFDM signal attracts the radar community because of its spectral flexibility, ability to withstand potential jammers, and its tolerance to doppler shifts [72, 73]. These properties made the OFDM signals a suitable choice to be used for radar measurements and indicate their potential to be utilized for RadCom systems [74-76]. The transmitter of the RadCom system initially mapped the data bits into communication symbols using digital communication schemes, e.g., BPSK, and then applied an inverse fast Fourier transform (IFFT) algorithm to translate the communication symbols into OFDM signals. Since the proposed system is monostatic, the transmitter can share the transmitted OFDM signals with the co-located radar receiver. The RadCom system transmits the OFDM signals to distant communication receivers and the reflected signals from objects are received at the radar receiver. To create a range profile and estimate the range of the target, the radar receiver correlates the reflected signal with the transmitted signal. The simulation results in [74] show that the ranges of two close targets, where the distance between them is 1.9 meters, can accurately be estimated by the proposed approach. However, the correlation-based processing of the OFDM signal depends on the correlation properties of the transmit data bits which may cause high sidelobes in the range profile. As a result, the accuracy of target detection would be reduced drastically, especially in multiple targets scenarios.

To remove data bits dependency, the radar processing eliminates the transmitted information bits from the received echoes signals by using the element-wise division for each subcarrier, and as a result, the received modulation symbol matrix $\mathbf{D}_{\mathbf{div}}$ is obtained [65, 76]. The target range and velocity information can be extracted, respectively, by applying a two-dimensional FFT processing. In particular, the discrete Fourier transform

(DFT) is applied to every row of D_{div} and then inverse DFT (IDFT) is applied for every column of the resulting matrix. As a result, the range and Doppler can be estimated independently. The simulation results showed that the proposed approach offers a higher peak-to-sidelobe ratio comparing with the correlation-based approach [74], which results in a significant improvement in the accurate estimation of the target parameters. For example, the velocity of the target that can be estimated by using the proposed approach is up to 253 m/s [77].

To address the randomness issue of the data bits, the authors in [78] propose a method that combined the OFDM scheme with the P4 code sequence [79], which is analogous to phase values produced by the PSK modulation. The basic idea is that the P4 sequence is first generated according to the rate of the data bits. A new sequence of the P4 codes is then generated from the old sequence by cyclically shifting the locations of the P4 code. Then, the random data bits are mapped into one of the codes in the complementary set and then modulated by the OFDM scheme. This method reduces the SLs of the autocorrelation functions produced by the reflected signal at the radar receiver. Thus, radar performance in terms of target detection would be improved. The results in [78] show that the RadCom system is capable of detecting a target with a velocity of 300 m/s.

Likewise, due to the ideal periodic autocorrelation features that m-sequence and its cyclic shifted versions [80, 81] possessed, the authors in [82] propose to combine it with the OFDM signal. Thus, employing m-sequence in RadCom signal design would enhance the radar performance in terms of range resolution and velocity estimation. The basic idea is that the m-sequence is first generated and then the random data bits are mapped into a time shift value that is used to produce the corresponding m-sequence. Then the resulting

sequence is modulated by the OFDM scheme. At the radar receiver, the DFT and cross-correlation are applied to estimate the velocity and the range of the targets, respectively. The results in [82] show that with an m-sequence of size 127, the system can detect two close targets, the spacing between them is ≈ 0.3 m, with a range of 12 km. Furthermore, the maximum data throughput that the system can be achieved is up to 1.96 Mbps.

Recently, due to the error-correction ability that Golay codes [83] possess, the authors in [84] propose to combine it with the OFDM modulation scheme not only to remove the data dependency but also to enhance the error-correction ability of the RadCom system. The modulation process of the data bits is similar to [82]. The simulation results in [84] show that radar performance is improved due to the significant decrease in the SL levels of the ambiguity functions. Moreover, the BER obtained is improved compared to BER achieved by the OFDM approach alone [74].

Most of the approaches mentioned above assume that the received OFDM signals are coherent, meaning that the subcarriers have the same phase shifts, which is not true for the case of wideband OFDM signals [85]. In this case, the conventional target detection algorithms, e.g., the correlation-based algorithm as used in [82], may not be reliable to estimate the phase shifts of the received OFDM signals, and this results in significant degradation of the RadCom system performance. To overcome this issue, the authors in [86] used linear and cubic spline interpolation techniques [87] to convert the OFDM wideband signals into nearly their corresponding narrowband. Thus, the target parameters can be estimated at the radar receiver by using the conventional target detection algorithms, e.g., the correlation-based. The results of the Monte Carlo simulation in [86] show that the performance of the detection process with the interpolation techniques is outperformed by

the counterpart without using the interpolation techniques in terms of a lower RMSE of the estimated parameters. In [88, 89], the OFDM modulation scheme is utilized with the stepped frequency approaches to provide a high-resolution range-Doppler profile in narrowband transmissions. However, the wideband OFDM systems required a high rate of the analog to digital converters (ADCs), which affects the power consumption and cost of the systems.

Note that in the OFDM sharing signaling mentioned above, the IFFT algorithm is usually utilized to convert data bits on subcarriers to samples in the time domain. According to the central limit theorem, several samples would have large magnitudes. This leads to the high peak-to-average power rate (PAPR) problem [90] which imposes the transmit electronic circuit to operate in the saturation region that induces signal distortions. High PAPR results in less power can be transmitted that reduces the range detection performance for the radar and degrades the BER performance for the communication.

To address the PAPR issue, the authors in [91] used an active constellation extension algorithm [92]. The basic idea of the proposed technique is setting a threshold for the target amplitude so that any amplitude of the output sample is higher than this threshold is clipped. This process would reduce the performance of the RadCom system. To address this problem, the error vector magnitude and cross-correlation methods [93], due to their independence upon the transmitted data, are employed at the communication and radar receivers, respectively. The simulation results showed that the PAPR is significantly reduced, however, the BER attained by the proposed technique is slightly increased compared to the BER obtained in [82]. Moreover, amplitude threshold optimization is difficult. As an alternative solution, the weighted OFDM schemes in [94, 95] are proposed

to control the maximum PAPR. However, these schemes degrade the system performance in terms of spectral efficiency by adding some subcarriers that don't carry data [94, 95].

To improve the data rate and spectrum efficiency while minimizing the PAPR, the authors in [96] propose orthogonal chirp division multiplexing (OCDM) [97] to be combined with OFDM. The OCDM waveform is composed of multiple orthogonal chirp signals, some of which are reserved to generate peak canceling signals and the rest are utilized for information embedding. Thus, at the transmitter, the communication symbols are modulated with the OCDM waveforms using the inverse discrete Fresnel transform (IDFnT) [98], thereafter, the resulted symbols are modulated again by applying the OFDM modulation scheme. At the radar and communication receivers, the FFT and DFnT algorithms are utilized to detect the targets and communication symbols. The results in [96] show that the radar performance is improved in terms of the sharp shape of the ambiguity function AF and low SLs and the maximum achieved data rate is $2N^2$, where N is the number of chirps. For power optimization, if prior knowledge of the channel is available, the authors in [99, 100] optimized the power allocated between various subcarriers according to data rate and conditional information of the radar.

The aforementioned schemes addressed two important issues of utilizing the OFDM signal for the RadCom system designs. The first issue was the randomization nature of the data bits and the second was the high PAPR. However, since the OFDM signal is used to fulfill the requirements for both the functions, i.e., radar sensing and communication transmission, designing the OFDM signal parameters such as length of the cyclic prefix (CP) and the subcarrier spacing (SCS) would have also a significant impact on the performance of both the functions. For this case, the authors in [101] provided conditions

for CP and SCS design that should be satisfied to ensure the performance of both the functions which depends on the channel characteristics. In particular, the length of the CP is designed to be larger than the maximum excess delay to prevent ISI, and SCS should be smaller than the coherence bandwidth according to the maximum velocity and unambiguous range.

A different approach is combining OFDM with multiple-input multiple-output (MIMO) radar to increase the data rate and improve the target resolution. This scheme can be implemented by allocating different subcarriers for different distinct transmit elements [29]. Various methods have been proposed for subcarriers division among the transmit elements. These methods include random assignments, equidistant, and non-equidistant dynamic subcarrier interleaving [102-104].

To conclude this subsection, the shared communication waveform-based RadCom approaches are extensively studied, particularly using OFDM signaling, and make it an attractive RadCom approach design. However, some limitations and shortcomings should be accounted for: Firstly, the communication receivers must be located within the radar main beam so that they can observe high SNRs, secondly, enormously cost hardware circuit elements are required to produce wideband OFDM signal and also to sample their reflections, and finally, from an automotive applications perspective, in the scenario of moving vehicles, the reflected OFDM signals exhibit misalignment among their subcarriers which may extremely degrade the performance of radar [73, 105].

3

2.3.3.2. Shared radar waveform approach

Traditionally, radar systems employed two types of waveforms, i.e., sweep or chirp and frequency hopping waveforms. Both waveforms have been proposed to be used for the RadCom system designs. In these approaches, the embedding of the communication symbols into the radar emissions is achieved without compromising the radar functionality.

2.3.3.2.1. Chirp waveform-based approach

The chirp is a waveform in which the frequency decreases (down chirp) or increases (up chirp) with time, i.e., the chirp rate [106]. The transmitter of the radar performs chirp modulation, either frequency modulated continuous wave (FMCW) or linear frequency modulation (LFM), before chirps transmission. The radar receiver extracts the direction, range, and velocity of the target by applying the matched filtering algorithm. In particular, it estimates the differences in frequency and phase between the received and transmitted waveforms. The LFM waveforms improve the radar performance in terms of range resolution, in which it can detect closed targets located at long distances without increasing the pulse width. Furthermore, it is robust against eavesdropping and jamming, and due to its feature of constant modulus (CM), the hardware components of the radar system are simplified [106]. In recent years, chirp signals have been utilized to transmit data bits [107]. In particular, utilizing the chirp rate to transmit a bit of information 0 or 1. This indicates that the chirp signal can be employed for the RadCom systems.

However, the generation of the chirp waveforms typically requires a huge range of frequencies which leads to a low spectrum efficiency. To address the spectrum efficiency problem, the authors in [108, 109] combined the chirp modulation with the OFDM scheme.

Here, the OFDM first modulates the data symbols to produce OFDM signals and then multiplied the resulting signal with the chirp waveform. The signal processing at the radar receiver applied the de-chirping process, i.e., multiplying the echo signal with the conjugated chirp waveform. Then, post-de-chirping, the baseband signal is processed with the 2D-FFT algorithm to estimate the velocity and the range of the target. At the OFDM receiver, the baseband signal is processed with the baseband processing to demodulate the communication symbols. The simulation results showed that the proposed method can detect a target located at a distance of 60 meters and with a velocity of 3m/s. However, parameters used to generate the chirp signal at the transmitter must be known at the receiver, which demands some synchronization arrangements. Furthermore, the OFDM is a modulation scheme with a non-constant envelope and a high PAPR which causes severe distortion of the transmitted waveforms.

To overcome these drawbacks, the authors in [110] proposed a scheme that combines the minimum shift keying (MSK) with LFM modulation. The MSK scheme, also known as continuous phase modulation (CPM), modulates the data symbols with signals that possess continuous phases. The procedure that integrates the LFM waveform with the MSK signal is similar to the procedure presented in [108]. The constant envelope feature of the MSK signal made the LFM-MSK waveform more robust against the distortion caused by the radar amplifier nonlinearities. However, as discussed in [111], the spectrum of the LFM-MSK waveform is a function of information bits. Accordingly, it may exceed the operating bandwidth of the LFM radar system, in cases where all the information bits involved in the LFM pulse are "1" or "0". This causes an increase in energy leakage and a deterioration in both communication and detection performances.

To confine the spectrum within the operating bandwidth of the system and prevent energy leakage, a simple approach is placing the data bits within the middle of the chirp pulse and no data bits should be placed on the edge of the signal. However, this results in discontinuing in the phases between successive LFM pulses, and therefore an expansion of the large spectrum may occur. To avoid these shortcomings, an integrated waveform design is proposed in [112] which is based on a three-phase modification of the LFM-MSK signals. The key idea is to append a sequence of "1" bits and a sequence of "0" bits at the beginning and the end of the chirp signal, respectively. The results show that the spectrum obtained via the proposed scheme is always confined within the spectrum of the LFM waveform. However, due to the redundant bits used in the proposed approach, the achieved data throughput is very limited. For redundant bits reduction, the methods based on the rate-shift algorithm [113] and continuous phase modulation (CPM) partial response [114] can be utilized. For example, the rate shift is applied to the upper bound on the time-varying transmission of the LFM-MSK signal. Thus, the data transmission rate is adapted so that it is always close to the available maximum transmission rate. The simulation results in [113] show that, given the same BER, the proposed rate-shift method can enhance the throughput of the system up to 60% compared to the constant-rate LFM-MSK waveform.

The RadCom systems presented in [110, 112, 113] are considered scenarios of a single communication receiver, where the transmitter can only convey the information bits to a single communication user. It should be noted that the frequencies, i.e., subcarriers, contained in the LFM signals are orthogonal to each other, and thus, the above approaches, such as [110], can be implemented in multi-user transmissions where each user is allocated to a single subcarrier in the LFM signal. Such an implementation can be found in [115],

where the authors considered a scenario that includes a single RadCom transmitter and multi-user communication. First, each information bit that will be transmitted to a user is modulated with BPSK. Then, the communication symbol is multiplied with/embedded into a single subcarrier of the transmitted LFM signal. This indicates that one symbol is conveyed on a single subcarrier during each radar pulse. Thus, if there are M subcarriers in the LFM signal, then M communication bits can be transmitted during each radar pulse. In practical applications, the proposed method would have a low capacity which may not meet the high-speed communication requirements.

To realize high-speed communication requirements, the authors in [116] proposed that the information bits are modulated by CPM schemes before transmitting them to the users. To do this, the information bits sequence is firstly transformed into a bipolar sequence by applying the amplitude modulation (AM). Then, CPM is used to modulate the bipolar AM levels into phase symbols. Thereafter, the communication symbols are multiplied with/embedded into the subcarriers of the transmitted LFM signal. Each communication receiver can detect the transmitted communication symbols by applying CPM demodulation followed by decoding. The proposed method significantly improves spectrum efficiency and data transmission. In particular, the data transmission rate achieved by the proposed approach is almost $K \log_2 K$ times greater than that obtained by the baseline approach [115], where K is the number of symbols transmitted on each subcarrier during one pulse. It also achieved BER nearly identical to that obtained by [115] without interference from adjacent channels. Moreover, the range and velocity AFs are almost identical to the LFM waveform, which means that the proposed approach can successfully perform the detection operation.

To improve the BER performance, the authors in [117] propose to combine the BER with the low-density parity-check (LDPC) code [118]. In particular, before embedding the symbols sequence into the LFM waveform, the LDPC codes are placed in the sequence. At the communication receiver, both the CPM demodulation and the BCJR algorithm [119] are used together to detect and decode the communication symbols. The simulation results showed that the BER is improved by 1.8 dB compared to the BER obtained in [116]. However, introducing the BCJR algorithm and LPDC coding may cause a high latency to occur for the proposed scheme.

A different approach was proposed by the authors in [120], where the fractional Fourier transform (FrFT) is used to process the echoes received at the RadCom system. Besides, it permits the chirp signals to be used as subcarriers instead of sinusoids. Therefore, to embed information bits through the radar transmissions, they utilized the quasi-orthogonality of different LFM rates while preserving the performance of an LFM pulse radar. Hence, the performance of the FrFT signal is equivalent to that of the chirp pulse in terms of false alarm and detection probabilities while preserving a comparable performance to that of the communication OFDM signal. However, this approach comes at the cost of a slight degradation of the performance in terms of the Doppler and range resolutions.

As another alternative, by utilizing the structure of the chirp signal for allowing a communication feature, the authors in [121] proposed a RadCom waveform comprised of multiple chirps that vary in their time alignments and start frequency points. In particular, each chirp is divided into two allocated segments and is corresponding to one communications symbol. The signal processing at the radar receiver applied several correction factors and the 2D-FFT algorithm within one channel to estimate the velocity

and the distance of the targets. At the communication receiver, the baseband signal is processed with the baseband processing to demodulate the communication symbols Moreover, to demodulate the communication symbols precisely the synchronization between the receiver and transmitter should be guaranteed. The simulation results show that the proposed method can detect a target located at a distance of 9 meters with a velocity of 15m/s and the achievable SER is $\approx 28.57 \, \text{kBd/s}$. The proposed communications method has almost no effect on radar functionality and may attain good data throughput with low power schemes. However, along with the structure of the proposed RadCom waveform, one drawback might arise related to the phase-locked loop features used in the proposed scheme. The shift between the two fragments of one communications symbol may not be accurate, which could result in some distortion exhibited as disparate breaks between consecutive chirps. Another disadvantage is that the unambiguous range of the radar is decreased, which is related to the length of the chirp, compared to its counterpart regarding the traditional chirp sequence.

2.3.3.2.2. Frequency hopping waveform-based approach

Frequency hopping (FH) is the procedure of transmitting waveforms by changing their operating frequency rapidly among different frequencies. The FH waveforms are simply generated, possess a constant-modulus property, and are imperviable to eavesdropping and interference. Therefore, they are traditionally employed in military applications.

In [122], the authors used the FH signals to embed communication symbols in the RadCom systems. The system is equipped with a joint transmit MIMO platform and generates M FH orthogonal signals via code optimization method [123] that ensures perfect

ambiguity function AF for radar detection. Next, employing PSK constellation to modulate the information bits and then embed them into the transmitted FH signals. During each radar pulse, the P codes are used for modulating the phase of the transmitted FH signals. Thus, MP communication symbols can be embedded, where each P represents a distinct communication symbol. The matched filtering is applied at the communication receiver to estimate the phases of the received signals and then detect the information bits. The simulation results in [122] showed that when the BPSK scheme is employed to modulate the information bits the SER of 10^{-6} can be achieved. However, it didn't show how the proposed method affects radar performance. Also, the proposed method requires an accurate estimate of the CSI which is difficult to achieve in practice.

To address these limitations, the authors in [124] divided the received signal into K subpulses and then applied the FFT algorithms with the K sub-pulses to define their spectral components. Accordingly, the FH codes are estimated to detect the communication symbols. The results show that the radar performance is improved in terms of the sharp shape of the AF with low SLLs and the obtained BER, where SNR is set to be -9 dB, is nearly 10^{-6} . The greatest advantage of the proposed method is that the CSI estimation is not required for the communication symbols detection as compared with [122] and thus the complexity of the communication receiver design is significantly reduced.

By utilizing both the space-division multiple access (SDMA) and waveform diversity of the MIMO communication and MIMO radar, respectively, a RadCom system is proposed to detect the target within the main lobe directions of the radar while transmitting communication symbols within the sidelobe directions [125-127]. The authors in [125] used amplitude shift keying (ASK) to modulate the SLL where each power level represents

a distinct communication symbol. Likewise, the authors in [126] used PSK to embed the information bits as the phases of the signals transmitted towards the intended communication receiver at the sidelobe. Remarkably, the embedded information via the PSK strategy can be reliably decoded by the communication receiver located within the main beam directions. Therefore, multi-user communication can be achieved by changing the SLLs at different angles.

To avoid any degradation in the radar performance, the BP invariance approach has been adopted in [128, 129] where the embedding of the information bits is achieved via shuffling the transmitted signals across the antenna elements. Thus, the permutation matrices would contain embedded communication symbols. However, in the aforementioned approaches, a communication symbol is typically embedded into one or many radar pulses, which leads to a low data throughput that depends upon the pulse repetition frequency (PRF) of the radar. Besides, the SL embedding strategies can only operate if the communications receiver is benefiting from a line-of-sight (LoS) channel. The received symbol in the multipath channel will be significantly distorted due to the dispersed signals coming from Non-LoS (NLoS) paths, to which the main lobe and SL powers can contribute.

The frequency diverse array (FDA) radar uses a small frequency offset across the array elements and an angle-range-time-dependent BP is obtained [130]. Thus, the FDA provides extra degrees of freedom (DoF) in the range dimension that would enable the system to resolve the targets with different ranges even if they are at the same angle. Also, it transmits the embedded coded FH waveforms and each waveform is orthogonal to each other with a frequency offset. The simulation results showed that the radar performance is improved in

terms of the better range-Doppler resolution and the achieved data rate transmission is limited by the number of employed waveforms and PRF of the system.

In recent years, Costas hopping (CH) signals [131] are proposed for the RadCom system design. The CH signals offer a thumbtack-shaped AF, unsusceptible to interference, and are easy to generate. The authors in [132] employed CH signals as a RadCom waveform. The system used the construction algorithm [131] to generate the CH waveforms, and then the information bits are embedded in each waveform using the phase modulation. The FDA transmits the embedded CH waveforms and they are orthogonal to each other with a frequency increment. The results show that the CH waveform-based scheme improves the system performance compared to [122] in terms of SINR for the radar and SER for the communication receiver. This means that it has better robustness towards noise and interference. However, phase synchronization is required for the proposed approach which can be a challenge to implement.

To overcome the phase synchronization issue, the authors in [133] utilized the phaserotational invariance method to embed the information bits into the radar radiations. This
approach is based on designing the transmit BF vectors such that each beamforming vector
exhibits the same radiation pattern but provides a different phase profile. The key idea can
be demonstrated as follows: Suppose that, during each radar pulse, there are N bits to be
embedded into the radar radiation towards the communication receiver. The joint transmit
platform generates 2N pairs of BF vectors where each pair represents a different value of
the phase rotations. Then, each sequence of N bits is mapped into a distinct value of the
phase rotations. At the communication receiver, after the matched filtering process, the bits
sequence can be estimated by taking the phase difference between two received BF vectors.

The simulation results show that the proposed method outperforms the communication signaling strategies based on SLL control [125, 126, 134] in terms of BER performance. Most importantly, phase synchronization arrangement is not required for the proposed method.

To enhance the data rate obtained by the approach in [133], more orthogonal waveform pairs are employed as proposed in [135]. In this case, multiple sequences of information bits can therefore be transmitted on different waveform pairs during each radar pulse. The simulation results showed that up to 15 bits can be embedded per radar pulse, while in [133] only 8 bits can be embedded given the same SNR and BER. This indicates that the proposed method enhances the data rate significantly. As another approach, the authors in [136] have developed a method for throughput enhancement by exploiting the silent period (when the primary radar function is inactive) for information transmission.

To conclude, we have reviewed and discussed various shared-based approaches for the RadCom system designs. They vary significantly regarding their features such as communication throughput, radar performance, hardware requirements, and computational complexity. For example, employing OFDM transmissions for the RadCom system can enhance the spectrum efficiency and system throughput. The major limitation of this approach is that the communication receiver should be located within the radar main beam directions of the system radiations. Moreover, OFDM transmission experiences high PAPR and requires costly hardware, and its radar functionalities are compromised when implemented by a moving target.

Although few works have been made to characterize the allowable compromise between radar and communication functions in RadCom systems designs [12], so far no unified joint standard exists that permits rigorous evaluation between various approaches. Therefore, it is necessary to understand the benefits and drawbacks of each approach so that the RadCom systems can be designed accordingly in a proper manner.

CHAPTER-3

THROUGHPUT ENHANCEMENT FOR THE RadCom SYSTEMS BASED ON COGNITIVE CLOSED-LOOP DESIGN

In this chapter, we proposed a closed-loop design for an angle-range dependent RadCom system that permits tracking of the moving target while maintaining the communication link towards the intended communication receiver during each illumination. The transmit platform of the frequency diverse array (FDA) is composed of M antenna elements and partitioned into K equally overlapped subarrays (SAs) transmitting orthogonal waveforms. We utilized the system configuration array design to permit joint estimation for the angle and range parameters of the target and also to construct (K-1) waveform pairs that enhanced the performance of the communication function in terms of throughput without compromising the performance of the radar function. We have designed two signaling strategies, APSK and PSK schemes, for embedding the transmitted communication symbols within transmitting BPs that utilize either the magnitude ratios and/or phase shifts between the radar waveform pairs towards the communication direction during each illumination

The simulation results verify that the communication performance is enhanced in terms of low symbol error rate (SER), secure information transmission, and increased throughput, while for radar applications the performance is improved in terms of target detection, parameter estimation, and tracking performance. It also showed that the proposed symbol mapping APSK scheme provides a high data rate transmission compared

to the existing SL-based information embedding schemes. Besides, the CRLB for range and angle estimation and the SINR for the proposed RadCom system are analyzed.

3.1. Introduction

The majority of the current RadCom systems are producing only an angle-dependent transmit BP and imposing a constraint for the communication receiver to be present within the SL directions to decode the transmitted information. In [134] the authors proposed a time-modulated array technique exploiting the radar SL for the communication operation as a secondary function and the radar emission performed in the main lobe as a primary function via controlling the instantaneous BPs during the same radar pulse. Likewise, a multi-waveform SL-based dual-function system used convex optimization to produce multiple transmit BPs with multiple SL power levels, and each level represents a distinct information symbol towards the communication direction in the SL region [125]. There are two constraints for the amplitude modulation SL-based RadCom systems. Firstly, the communication throughput of the system is relatively very low and secondly, the communication stations should be in the SL regions of the radar transmit BPs, which is not always possible in practical scenarios. Different modulation schemes have been developed in the existing literature of the RadCom system design for embedding communication symbols within the radar emissions [107, 126, 127, 137, 138].

All these embedding information schemes were proposed for the traditional phased array (PA) radar where the waveform diversity cannot be utilized. To overcome this limitation, a MIMO configuration is employed in RadCom system designs [128, 139, 140].

To realize the dual function operation, the transmitted orthogonal waveforms are linearly combined in the far-field region to perform a radar emission in a specific direction and the information transmission in another spatial direction [141]. Communication symbols embedded into the MIMO emissions have been developed employing waveform permutations [129] and PSK modulation scheme [142], where the achievable communication throughput is limited by the number of employed orthogonal waveforms and the PRF. In [122] the authors introduced FH codes to increase the transmission symbol rate of the system. Another approach is presented in [137, 138], where the authors developed a two-stage design for emission radiation at the far-field to obtain a much higher transmission data rate. However, the issues with this approach are: (i) the radar detection performance is affected due to the loss of transmit power that is dedicated for communication operation, (ii) the communication stations should be located within the radar SL region. Despite the advantages of MIMO and PA radars, they can only generate angle-dependent BP [143].

To overcome this constraint, the FDA was first proposed by Antonik [130]. It uses a small frequency offset across the array elements and an angle-range-time dependent BP is obtained [144]. It is exploited to resolve the range ambiguity and improve the detection and estimation performance of the moving target in a cluttered environment [145]. The authors in [146] utilized the degrees of freedom (DoF) and developed radar waveforms that serve various functions simultaneously. Thus, the FDA provides extra DoF in the range dimension that would enable the system to resolve the targets with different ranges even if they are at the same angle. Also, it transmits the embedded coded FH waveforms and each waveform is orthogonal to each other with a frequency offset. In [136] the FDA with the

OFDM modulation is used to implement a RadCom system that exploited only the SL control during active time and silent period (when the primary radar function is inactive) for information transmission. The simulation results showed that the communication performance is enhanced in terms of the achieved data rate transmission.

In this chapter, during each illumination, the detection and tracking of the moving target by the proposed RadCom system are assumed to be the primary function of the system while maintaining the information bits transmission towards the intended communication direction is considered as the secondary function. Here, we proposed a closed-loop design for a range-angle-dependent RadCom system, where the radar receiver provides updated information about the target position to the transmitter. Then, the transmitter compares the updated position of the target with the known location of the communication receiver. This feedback information enables the transmitter to select a suitable signaling strategy and optimum BF weight vectors for both functions during each scanning cycle.

3.2. Proposed System Design

The cognitive system establishes a closed-loop that embodies the transmitter, receiver, and operational environment. The system is reconfigured (updating the transmission parameters) according to the feedback information injected from the receiver to the transmitter. Fig. 3.1. depicts the functional blocks of the proposed system design. The receiver side includes the radar receiver, memory, and an interacting multiple model (IMM) estimator block, while the transmitter includes five sub-blocks that contain a signaling strategy selector, memory, transmit BF design, BF weight vectors selector and

joint transmit platform. We divided the joint transmit platform into K overlapped SAs, each is composed of (M-K+1) antenna elements and transmits an orthogonal waveform. Moreover, during each radar pulse, the BF weight vector \mathbf{w}_1 is adopted as the primary weight vector and $\psi_1(t)$ selected as a reference waveform associated with \mathbf{w}_1 and, as a result, the (K-1) waveform pairs are constructed.

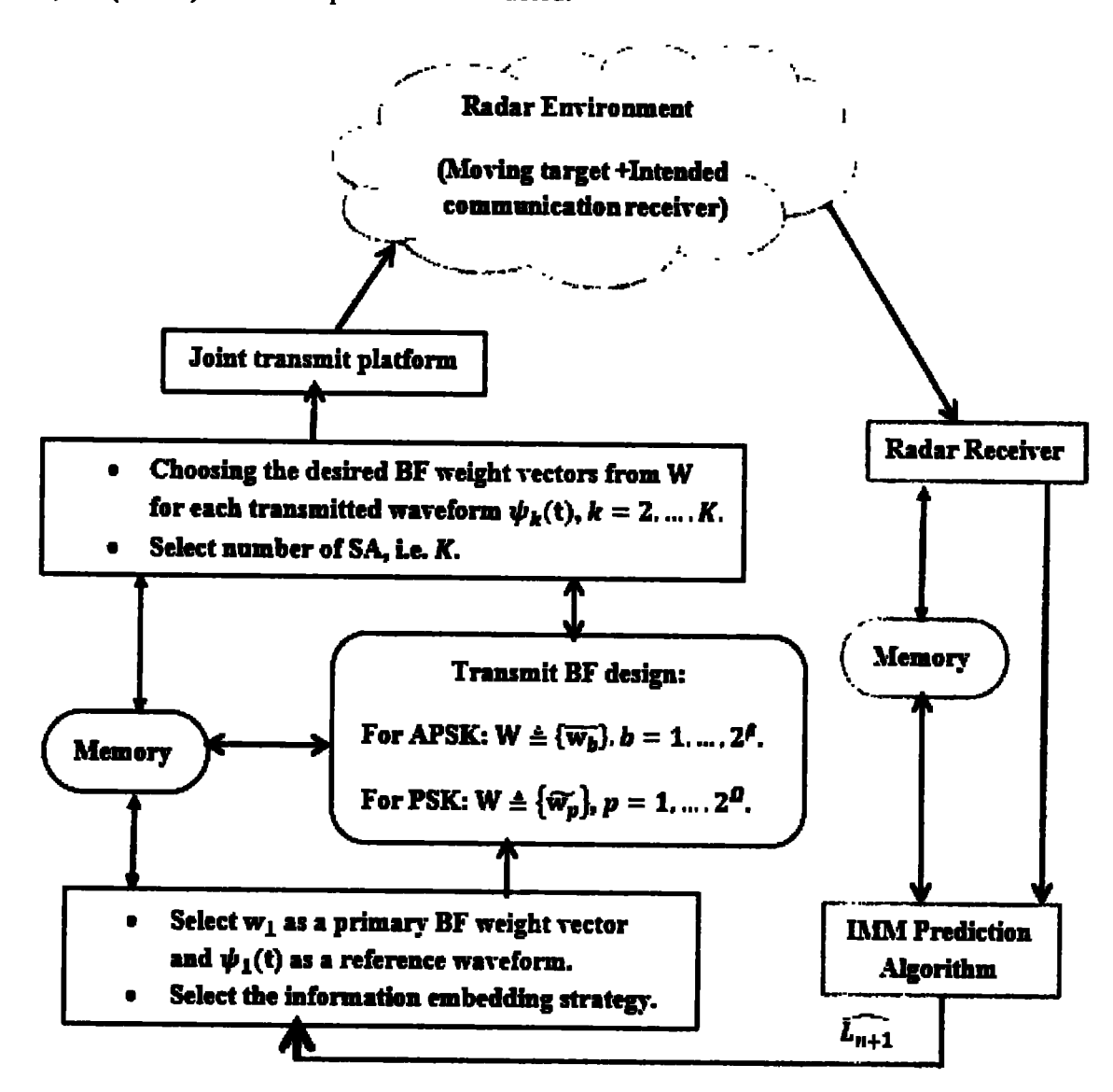


Figure 3.1: The proposed closed-loop design diagram for the RadCom system.

Once the proposed system is linked to the radar operational environment, the joint transmit platform illuminates the environment which contains a potentially moving target located at (θ_t, r_t) , where θ_t and r_t are angle and range of the radar target of interest, respectively, and intended communication receiver located at (θ_c, r_c) , where θ_c and r_c are angle and range of the communication receiver, respectively. Here, we assume that the position of the communication receiver is known and fixed while the location of the radar target is changing with time. Accordingly, the system performs a tracking task for the moving target as the primary function while the information is transmitted towards the intended communication receiver as a secondary function during each illumination. Thereafter, the radar receiver estimates the target parameters such as the direction of arrival (DOA), range, and velocity utilizing the reflected signals from the environment. It is worth mentioning that the memory is built from the initial scans and stores the previous and updated estimations of the target parameters. The estimated target position $\widehat{L}_n = (\widehat{\theta}_t, \widehat{r}_t)$ at time n is forwarded to the predictor position block to estimate the next target position $\widehat{L_{n+1}}$ at time n+1, for the mathematical definitions for the $\widehat{\theta_t}$ and $\widehat{r_t}$ please see (3.50) and (3.56), respectively. Next, the receiver feeds back the predicted position of the target to the transmitter, which compares $\widehat{L_{n+1}}$ with the known location of the communication receiver (θ_c, r_c) .

Here, there are two cases related to the location of the communication receiver within the radar transmit BP directions according to the target motion within the radar environment as illustrated in Fig. 3.2.

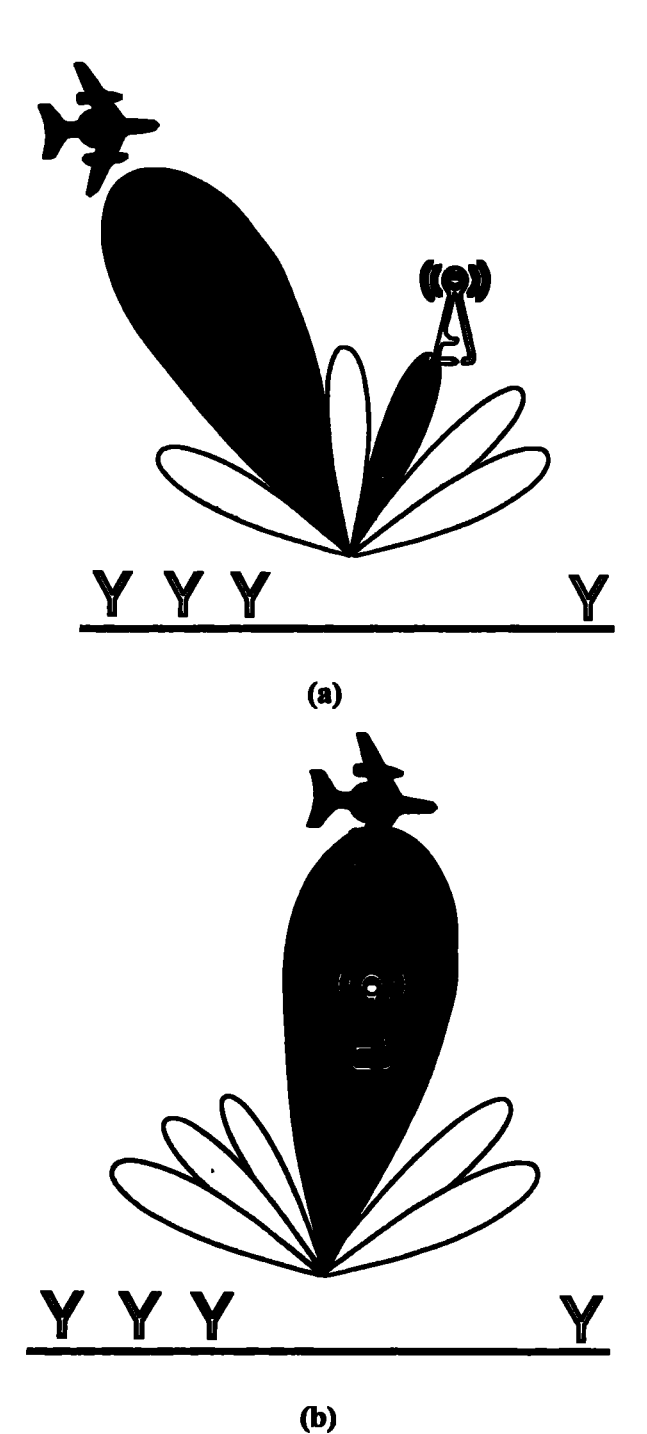


Figure 3.2: The location of the communication station within the operating environment of the proposed RadCom system, (a) the communication station is located within the sidelobe directions of the radar transmit BP, and (b) both the radar target and the communication station are located within the main lobe directions of the transmit BP.

In the first case, when the communication receiver is located outside the main lobe directions (Fig. 3.2 (a)), the transmitter selects the proposed APSK strategy to embed the information bits by utilizing the phase shifts and the magnitude ratios between the (K-1) waveform pairs. While in the second case, when the communication receiver is located within the main beam directions (Fig. 3.2 (b)), the transmitter selects the PSK-based communication strategy, where the information bits are embedded only in the phase shifts between the (K-1) waveform pairs. Hence, the optimum performance for target detection is maintained. Thus, regardless of the communication station location within the radar operation environment, the proposed cognitive selection of the information embedding strategy maintains the communication link towards the communication receiver during each radar scan. As a result, the overall throughput of the system is enhanced.

Many applications would possibly benefit from the availability of our proposed RadCom system, in particular, traffic control and military applications. For example, the scenarios where a stationary command/control post with the coordination capability is linked with a network that contains multiple spatially diverse RadCom systems. In this case, the system can not only detect enemies but also performs strategic communications functions. On the battlefield, the command/control post can utilize this information to increase the detection probability, precision, and improve electronic warfare. It is worthy to mention that, the memory is initially built from the initial scans and stores the actions that have been taken by the transmitter. Since the system is a monostatic platform, we assume that the feedback is always stable and the system operates iteratively. In the following, we elaborate on each part of the design paradigm independently.

3.2.1. Signal model

Consider an angle-range dependent RadCom platform equipped with a joint transmit antenna array consisting of M radiating elements placed as a uniform linear array (ULA) configuration with an inter-element spacing of d_T . The frequency radiated from the m^{th} element is:

$$f_m = f_c + m \Delta f, \qquad m = 0, 1, 2, ..., M - 1$$
 (3.1)

where f_c and Δf denote the carrier frequency and the incremental frequency across each element in the array, respectively, with $\Delta f \ll f_c$. Furthermore, we divided the joint transmit platform into K overlapped SAs, and each is composed of M-K+1 antenna elements. In this case, the steering vector of the k^{th} SA towards the direction (θ, r) is defined as:

$$\mathbf{a}_{k}(\theta, r) = \mathbf{u}_{k} \odot \mathbf{a}(\theta, r) \tag{3.2}$$

where \odot represents the element-wise product, u_k and $a(\theta, r)$ are the $M \times 1$ vectors expressed, respectively, as:

$$\mathbf{u}_{k}(m) = \begin{cases} 1 & m = k, k+1, \dots, M-K+k \\ 0 & otherwise. \end{cases}$$
 (3.3)

$$\mathbf{a}(\theta,r) = \left[1, e^{-j\left(\frac{2\pi f_c d_T \sin \theta}{c} - \frac{2\pi \Delta fr}{c}\right), \dots, e^{-j\left(\frac{2\pi f_c (M-1) d_T \sin \theta}{c} - \frac{2\pi (M-1) \Delta fr}{c}\right)}\right]^T$$
(3.4)

where c represents the speed of light, r represents the slant range between the first element and the observed point located at the far-field, and $[.]^T$ stands for the transpose operator. Equation (3.4) can be rewritten into a compact form as:

$$\mathbf{a}(\theta, r) = \mathbf{a}(\theta) \odot \mathbf{a}(r) \tag{3.5}$$

where

$$\mathbf{a}(\theta) = \left[1, e^{-j\left(\frac{2\pi f_C d_T \sin \theta}{c}\right)}, \dots, e^{-j\left(\frac{2\pi f_C (M-1) d_T \sin \theta}{c}\right)}\right]^T \tag{3.6}$$

$$\mathbf{a}(r) = \left[1, e^{j\left(\frac{2\pi\Delta fr}{c}\right)}, \dots, e^{j\left(\frac{2\pi(M-1)\Delta fr}{c}\right)}\right]^{T}$$
(3.7)

Let $\{\psi_k(t)\}\$, k=1,...,K, be the possible unit-energy orthogonal radar waveforms transmitted from each SA, such that:

$$\int_{T} \left| \psi_{k}(\mathbf{t}) \right|^{2} dt = 1 \tag{3.8}$$

$$\int_{T} \psi_{k}(t) \, \psi_{k'}^{*}(t) \, dt = \delta(k - k') \tag{3.9}$$

where T and t represent the time between radar pulses and the time duration within each pulse, respectively, (.)* denotes the complex conjugate operator, and δ (.) is the Kronecker delta function.

At the input of the joint transmit platform, the baseband form of the emitted signals is given by:

$$\mathbf{s}(\mathsf{t},\mathsf{\tau}) = \sqrt{\frac{E}{K}} \sum_{k=1}^{K} \mathbf{w}_{k}^{*} \psi_{k}(t) \tag{3.10}$$

where τ denoting the pulse number, E is the total transmit energy and \mathbf{w}_k is the BF weight vector associated with the k^{th} SA. Note that the total energy E is distributed equally among K waveforms so that during one radar pulse the transmitted energy equals to E. The signal in (3.10) can be rewritten as:

$$\mathbf{s}(\mathbf{t},\tau) = \sqrt{\frac{E}{\kappa}} \, \mathbf{W}^* \, \mathbf{\psi}(t) \tag{3.11}$$

where $\mathbf{W} \triangleq [\mathbf{w}_1, \mathbf{w}_2, ..., \mathbf{w}_k]$ is the $M \times K$ transmit weight BF matrix and $\mathbf{\psi}(t) \triangleq [\psi_1(t), ..., \psi_k(t)]^T$ is the $K \times 1$ orthogonal waveforms vector.

Here, the **W** and $\psi(t)$ are assumed to be optimized to fulfill the requirements of the primary radar function while the information transmission being a secondary function can be achieved by modulating the transmit BPs. To utilize the waveform diversity at the radar receiver, the transmit signals should be orthogonal at all Doppler shifts and time-delays within the velocity and range specifications of the FDA-MIMO radar. Achieving orthogonal signals with common spectrum contents is impractical and, therefore, in [147] several methods have been studied for designing waveforms with low cross-correlations.

3.2.2. Transmit beamspace design and information embedding schemes

Here, we demonstrate the design of the transmit beamspace matrix W and the signaling schemes for the proposed RadCom system. Let $\Theta = [\theta_{min}, \theta_{max}]$ and $R = [r_{min}, r_{max}]$ be the set of angles and ranges, respectively, that form a spatial sector where the main beam operates, while keeping the power in the SL region $(\overline{\Theta}, \overline{R})$ below a certain predetermined threshold. Since the radar receiver feeds back the target's next position $\widehat{L_{n+1}}$ to the transmitter, this information is utilized to design a W to fulfilling the requirements of both the functions and improve their performance.

According to [133], there is $2^{M-1} - 1$ BF weight vectors that could be produced from the primary BF weight vector, so that all have the same transmit BP. Thus, \mathbf{w}_1 is selected as a primary transmit BF weight vector from $\mathbf{W} = [\mathbf{w}_1, ..., \mathbf{w}_{2^{M-1}}]$ and $\psi_1(t)$ as a reference waveform during each radar pulse.

The \mathbf{w}_1 can be calculated by solving the convex optimization problem as follows:

$$\begin{aligned} & \min_{\mathbf{w}_1} \max_{\boldsymbol{\theta}, r} \left| \mathbf{w}_1^{\mathsf{H}} \mathbf{a}_1(\boldsymbol{\theta}, r) \right|, & \boldsymbol{\theta} \in \boldsymbol{\Theta}, \ r \in R, \\ & \text{Subject to} \quad \mathbf{w}_1^{\mathsf{H}} \mathbf{a}_1(\boldsymbol{\theta}_t, r_t) = 1, & \boldsymbol{\theta}_t \in \boldsymbol{\Theta}, r_t \in R, \\ & \mathbf{w}_1^{\mathsf{H}} \mathbf{a}_1(\boldsymbol{\theta}_c, r_c) = \varepsilon_{max}, & \boldsymbol{\theta}_c \in \overline{\boldsymbol{\Theta}}, r_c \in \overline{R}. \end{aligned}$$
(3.12)

Here, (θ_t, r_t) is the expected radar target position, (.)^H stands for the Hermitian operator, and the ε_{max} is a positive number that indicates the highest allowable SL level at the location (θ_c, r_c) . If there are multiple targets located in different directions then for a given joint transmit subarrays configuration each \mathbf{w}_k is designed separately to concentrate the transmit power towards the direction of the targets θ_t while maintaining the power radiation in the SL region under a specific level.

In the following, we introduced two signaling strategies used for the information embedding scheme.

3.2.2.1. APSK-based information embedding scheme

Consider the following scenario, when the radar target is moving and the communication receiver is located within the sidelobe directions of the radar transmit BPs. In this case, as the communication receiver (θ_c, r_c) remains outside the main beam direction, the proposed RadCom system can serve the communication receiver with information bits by selecting the proposed APSK communication scheme. According to the authors in [148], the *M*-ary APSK has a better performance compared with the traditional *M*-ary QAM. Since the *M*-ary APSK needs a smaller number of amplitude levels to represent binary bits. The *M*-ary APSK is a more suitable option for information embedding since the SL levels have to be limited.

According to [149], the optimal ring configurations for 8-APSK, 16-APSK and 32-APSK schemes based on the highest inter-ring and intra-ring distances are (1, 7), (5, 11), and (5, 11, 16) structures, respectively. Therefore, we need only two distinct amplitude levels for 8-APSK and 16-APSK schemes to embed three and four information bits, respectively, and three distinct amplitude levels are required for 32-APSK to embed five information bits. During each radar pulse, the *M*-ary APSK schemes can embed the information bits by controlling the phase shifts and the magnitude ratio levels between K-1 waveform pairs radiated towards the communication receiver located at (θ_c, r_c) in the SL region. Thus, after \mathbf{w}_1 is determined from (3.12), the k^{th} BF vector \mathbf{w}_k is selected from $\mathbf{W} = \{\overline{\mathbf{w}_b}\}$, $(b = 1, ..., 2^{\beta})$, and each information symbol comprises β bits. The BF weight vectors, $\overline{\mathbf{w}_b}$ $(b = 1, ..., 2^{\beta})$, for the APSK signaling strategy, are derived from \mathbf{w}_1 by solving the following convex problem:

$$\min_{\mathbf{w}_b} |\mathbf{w}_1 - \overline{\mathbf{w}_b}|$$

Subject to
$$\overline{\mathbf{w}_b}^H \mathbf{a}_k(\theta_c, r_c) = A_k e^{-j\phi_k}$$
; $b = 1, ..., 2^\beta$; $k = 2, ..., K$. (3.13)

where A_k is the amplitude ratio and φ_k is the phase shift and are given, respectively, as:

$$A_k = \left| \frac{\mathbf{w}_b^H \mathbf{a}_k(\theta_c, r_c)}{g_1} \right|, \tag{3.14}$$

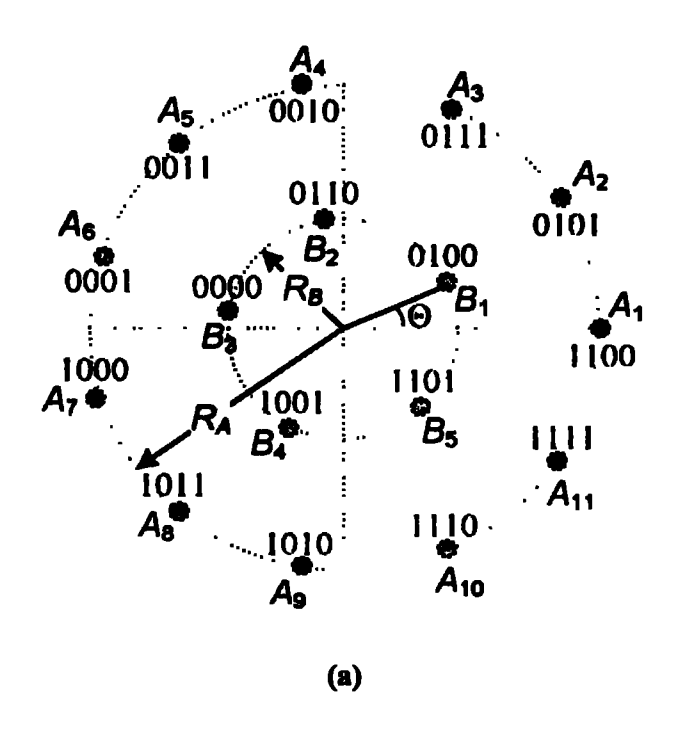
$$\varphi_k = angle\left(\frac{\mathbf{w}_b^H \mathbf{a}_k(\theta_c, r_c)}{g_1}\right) \tag{3.15}$$

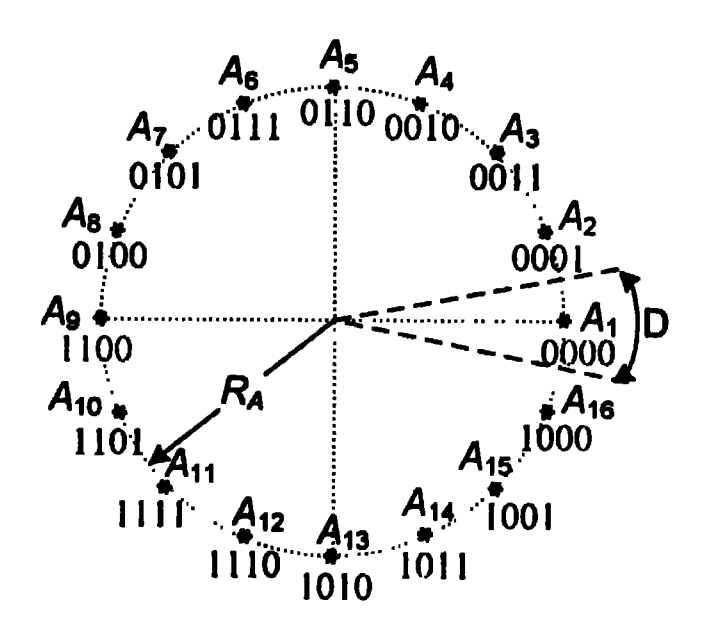
where $g_1 \triangleq \mathbf{w_1}^H \mathbf{a_1}(\theta_c, r_c)$, is the transmit gain associated with the primary BF vector $\mathbf{w_1}$ towards the communication receiver located at (θ_c, r_c) .

Here, the b^{th} BF vector $\overline{\mathbf{w}_b}$ is designed to achieve a magnitude ratio A_k as well as phase shift $e^{j\phi_k}$ towards the communication receiver location (θ_c, r_c) . Note that, each

magnitude ratio term A_k and the phase shift term $e^{j\varphi_k}$ can assign any of the permissible magnitude ratios L and phase shifts R, respectively, that are required by the M-ary APSK scheme. For example, to embed four bits of information i.e. $\beta=4$, the 16-APSK with (5, 11) structure is applied, it follows that L=2 (l_1 and l_2) and R=5 and 11 for l_1 and l_2 , respectively. Thus, during each radar pulse, by solving (3.13), all possible BF weight vectors $\overline{\mathbf{w}_b}$ ($b=1,...,2^\beta$) will be generated, for further illustration please see Fig. 3.18 in section 3.4 (Example 3.5).

The APSK constellation for $\beta = 4$, applying grey mapping, is plotted in Fig. 3.3 (a), where R_B and R_A denote the radius of the inner and outer rings, respectively, and Θ represents the angle formed between the first communication symbol of the inner and outer rings.





(b) Figure 3.3: Constellation schemes with gray coding, (a) 16-APSK for $\beta=4$ bits and (b) 16-PSK for $\Omega=4$ bits.

3.2.2.2. PSK-based information embedding scheme

Consider the following scenario when the radar target and the communication receiver are both located within the main beam direction of the radar transmit BPs as shown in Fig. 3.2(b). Thus, to maintain the target detection performance and communication transmission a PSK-based communication will be selected by the transmitter for information embedding. Therefore, after \mathbf{w}_1 is determined from (3.12), the k^{th} BF vector \mathbf{w}_k is selected from $\mathbf{W} = \{\widetilde{\mathbf{w}_p}\}, (p = 1, ..., 2^n)$, where each symbol consists of Ω bits. The BF weight vectors $\widetilde{\mathbf{w}_p}$, $(p = 1, ..., 2^n)$, for the PSK signaling strategy, are derived from \mathbf{w}_1 by solving the following convex problem [135]:

$$\min_{\widetilde{w_p}} \left| w_1 - \widetilde{w_p} \right|$$

Subject to
$$\widetilde{\mathbf{w}_p}^H \mathbf{a}_k(\theta_c, r_c) = g_1 e^{-j\phi_k}$$
; $p = 1, ..., 2^n$; $k = 2, ..., K$. (3.16)

Here ϕ_k is the phase shift and can be written as:

$$\phi_k = angle\left(\frac{\widetilde{w_p}^H \mathbf{a_k}(\theta_c, r_c)}{g_1}\right) \tag{3.17}$$

let's assume that four bits of information are available for transmission to the communication receiver located at (θ_c, r_c) . The constellation diagram for $\Omega = 4$ bits is plotted in Fig. 3.3(b), where the D is representing the decision region for the symbol A_1 .

The transmitted signal (3.11) can be rewritten as:

$$\mathbf{s}(\mathbf{t},\tau) = \sqrt{\frac{E}{\kappa}} \,\mathbf{W}^* \,\mathbf{B}(\tau) \,\mathbf{\psi}(t) \tag{3.18}$$

Here, **W** is the $M \times 2^{M-1}$ beamspace matrix and **B**(τ) \triangleq [$\mathbf{b}_1(\tau)$, $\mathbf{b}_2(\tau)$, ..., $\mathbf{b}_K(\tau)$] is $2^{M-1} \times K$ selection matrix that selects the desired BF weight vector from **W** for each $\psi_k(t)$, k = 1, ..., K. The k^{th} selection vector $\mathbf{b}_k(\tau)$ is $2^{M-1} \times 1$ vector such that only one element in $\mathbf{b}_k(\tau)$ is equal to 1 and the remaining elements are zeros. Notice that, the transmit beamspace matrix **W** acts as the dictionary of the optimized BF weight vectors.

Hence, our proposed design for an angle-range dependent RadCom system is different from the current literature of the radar-communication framework. It facilitates the tracking of the moving targets and simultaneously maintains the communication link towards the intended communication receiver during each illumination. As a result, the overall performance and the throughput of the system are enhanced.

Algorithm 3.1. illustrates the selection mechanism of the information embedding strategy during each radar illumination.

ALGORITHM 3.1: Algorithm for information embedding scheme selection during each radar illumination.

At the radar receiver (one cognitive cycle): $L_{n-1} = [\theta_{t,n-1}, r_{t,n-1}]$ (previous estimated target's parameters).

- 1: Estimate the parameters for the moving target at a time t_n , i.e. currently estimated parameters $\widehat{L_n}$.
- 2: Update the information library with new estimated values.
- 3: Forward the new estimated values to the predictor position algorithm (IMM algorithm) to estimate the next position of the moving target $\widehat{L_{n+1}}$.
- 4: Feedback $\widehat{L_{n+1}}$ to the transmitter.
- 5: At the transmitter: Compare $\widehat{L_{n+1}}$ with the known location of the communication receiver (θ_c, r_c) .
- 6: \mathbf{w}_1 is selected as a primary transmit BF weight vector from \mathbf{W} and $\psi_1(t)$ is selected as a reference waveform.
- 7: if $((\theta_c, r_c) \in (\Theta, R))$
- 8: Select *M*-ary PSK modulation scheme for information embedding towards (θ_c, r_c) , then (3.12) and (3.13) are applied.
- 9: else
- 10: $((\theta_c, r_c) \in (\overline{\Theta}, \overline{R}))$
- 11: Select *M*-ary APSK modulation scheme for information embedding, then (3.12) and (3.16) are used.
- 12: end if
- 13: Go to step 1

In Algorithm 3.1., the radar receiver estimates the target parameters such as the direction of arrival (DOA), range, and velocity utilizing the reflected signals from the environment. The estimated target position $\widehat{L_n}$ at time n is forwarded to the predictor position block to estimate the next target position $\widehat{L_{n+1}}$ at time n+1. Next, the receiver feeds back the predicted position of the target to the transmitter, which compares $\widehat{L_{n+1}}$ with the prior knowledge of the communication receiver location (θ_c, r_c) . Then, whenever the location of the communication receiver is within the main beam directions, the transmitter selects the PSK-based communication strategy for information transmission. On the other hand, whenever the location of the communication receiver is outside the main beam directions, the transmitter selects the proposed APSK strategy for information transmission. Thus, during each radar scan, the proposed cognitive selection of the information embedding strategies maintains the communication symbols transmission to the intended communication receiver.

Note that, such a transmit beamspace design requires careful design to make sure that the radar operation is not disturbed. This demands that the autocorrelation for different waveform designs remains constant regardless of the alteration in transmitting information symbols. In the context of the communications operation, the cross-correlation between different pairs of transmitting information symbols and associated waveforms should be as small as possible.

The transmission framework of the proposed system configuration is illustrated in Fig. 3.4.

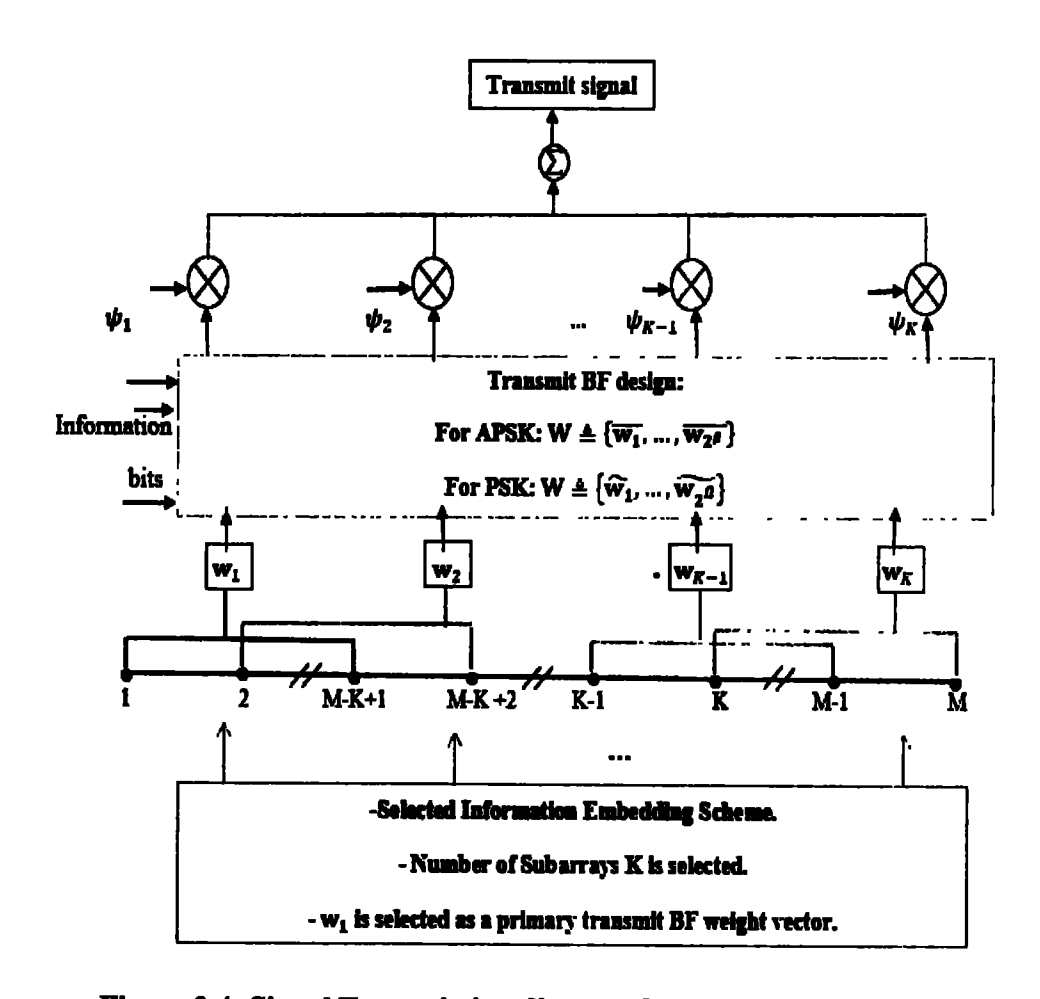


Figure 3.4: Signal Transmission diagram for the proposed system.

3.2.3. Communication symbol detection at the communication receiver

For communication symbol detection, the communication receiver located at (θ_c, r_c) , within the system illumination regions, is assumed to have a perfect knowledge of the $\psi_k(t)$, $k=1,2,\ldots,K$. Therefore, the received signal at the output of the single element communication receiver located at (θ_c, r_c) can be written as:

$$x_c(t;\tau) = \alpha_{ch}(\tau) \left[\mathbf{a}^T(\theta_c, r_c) \ \mathbf{s}(t;\tau) \right] + z_c(t;\tau)$$
 (3.19)

where $\alpha_{ch}(\tau)$ represents a complex channel response during the τ^{th} radar pulse and $z_c(t;\tau)$ is the white Gaussian noise with zero mean and variance σ^2 .

Equation (3.19) can be rewritten as:

$$x_c(t;\tau) = \sqrt{\frac{E}{K}} \alpha_{ch}(\tau) \left[\sum_{k=1}^{K} g_k \psi_k(t) \right] + z_c(t;\tau), \quad 1 \le k \le K. \quad (3.20)$$

where $g_k \triangleq \mathbf{w}_k^H \mathbf{a}_k(\theta_c, r_c)$ is the received gain associated with the k^{th} BF weight vector towards the communication receiver located at (θ_c, r_c) . Then, by matched-filtering the $x_c(t; \tau)$ to $\psi_k(t)$, $1 \le k \le K$, during each radar pulse yields:

$$y_{c,k}(\tau) = \frac{1}{T} \int_0^T x_c(t; \tau) \psi_k(t) dt$$

$$= \sqrt{\frac{E}{K}} \alpha_{ch}(\tau) \left(\mathbf{w}_k^H \mathbf{a}_k(\theta_c, r_c) \right) + \widetilde{z}_k(\tau)$$

$$= \sqrt{\frac{E}{K}} \alpha_{ch}(\tau) g_k + \widetilde{z}_k(\tau), \qquad 1 \le k \le K. \quad (3.21)$$

Here $\widetilde{z_k}(\tau)$ represents the output noise obtained after matched filtering and is modeled as zero-mean white Gaussian noise with variance σ^2 . The output of matched-filtering of the $x_c(t;\tau)$ to $\psi_1(t)$, the reference waveform associated with the primary BF weight vector \mathbf{w}_1 , yields:

$$y_{c,1}(\tau) = \sqrt{\frac{E}{\kappa}} \alpha_{ch}(\tau) g_1 + \widetilde{z_1}(\tau)$$
 (3.22)

Now, let's define the k^{th} received communication symbol as:

$$C_k\left(\theta_c, r_c\right) \triangleq \frac{y_{c,k}(\tau)}{y_{c,1}(\tau)}, \quad 2 \le k \le K. \tag{3.23}$$

where the k^{th} received communication symbol $C_k(\theta_c, r_c)$ has a magnitude ratio component $|C_k(\theta_c, r_c)|$ and a phase shift component $angle(C_k(\theta_c, r_c))$ in the direction of communication receiver (θ_c, r_c) .

Thus, during the tracking operation, the intended communication receiver located at the SL region decodes the transmitted symbol as:

$$\widehat{A_k} = |C_k(\theta_c, r_c)| \tag{3.24}$$

and

$$\widehat{\varphi_k} = angle(C_k(\theta_c, r_c))$$
 (3.25)

On the other hand, if the communication receiver would be located at main beam directions, during the tracking task, then A_k in (3.24) is set as constant and the embedded phase information ϕ_k can be estimated using (3.25) and mapped to the Ω bits.

3.2.4. Echo processing at the radar receiver

The reflected signal from the far-field point located at (θ, r) can be modeled as:

$$r(t, \theta, r) = \sqrt{\frac{E}{K}} \alpha(\tau) \sum_{k=1}^{K} \mathbf{w}_{k}^{H} \mathbf{a}_{k}(\theta, r) e^{-j \delta_{k, T}(\theta, r)} \psi_{k}(t), \ 1 \le k \le K \quad (3.26)$$

where $\alpha(\tau)$ is the reflection coefficient of the desired point in the far-field located at (θ, r) , and $\delta_{k,T}(\theta, r)$ denotes the transmit time delay of the wave propagation from the k^{th} SA to the far-field point located at (θ, r) and is given by:

$$\delta_{k,T}(\theta,r) = \frac{r_k}{c} - \frac{d_T}{c}(k-1)\sin\theta, \quad 1 \le k \le K$$
 (3.27)

where r_k is the slant range from the k^{th} SA to the far-field point located at (θ, r) . Equation (3.26) can be rewritten as:

$$r(t,\theta,r) = \sqrt{\frac{E}{\kappa}} \alpha(\tau) \mathbf{q}^{T}(\theta,r) \mathbf{\psi}(t)$$
 (3.28)

where $\mathbf{q}(\theta, r)$ is the $K \times 1$ vector and can be given by:

$$\mathbf{q}(\theta, r) = [\mathbf{w}_{1}^{H} \mathbf{a}_{1}(\theta, r)e^{-j\delta_{1,T}(\theta, r)}, ..., \mathbf{w}_{K}^{H} \mathbf{a}_{K}(\theta, r)e^{-j\delta_{K,T}(\theta, r)}]^{T}$$
(3.29)

Let's assume that, the co-located radar receiver consists of N receive antennas array with a ULA shape with an inter-element spacing of d_R . It is further assumed that the target in the far-field would be seen by the transmit and the receive arrays from the same direction. Therefore, the $N \times 1$ vector of the received array observations from a far-field target located at (θ_t, r_t) can be expressed as:

$$\mathbf{x}_{r}(t;\tau) = r(t,\theta_{t},r_{t}) \mathbf{b}(\theta_{t}) + \mathbf{n}_{d}(t;\tau) + \mathbf{n}_{r}(t;\tau)$$

$$= \sqrt{\frac{E}{K}} \alpha_{t}(\tau) [\mathbf{q}^{T}(\theta_{t}, r_{t}) \mathbf{\psi}(t)] \mathbf{b}(\theta_{t}) + \mathbf{n}_{d}(t;\tau) + \mathbf{n}_{r}(t;\tau)$$
(3.30)

where $\alpha_t(\tau)$ is the reflection coefficient of the t^{th} target during the τ^{th} radar pulse, assume that it obeys the Swerling-II model [106], $\mathbf{n}_d(t;\tau)$ is zero mean independent circularly Gaussian stochastic process representing the interference signals received from SL regions with variance σ^2_t , i=1,...,D, and $\mathbf{n}_r(t;\tau)$ is the $N\times 1$ zero mean independent white Gaussian noise vector with variance σ^2 during the τ^{th} radar pulse. The radar steering vector of the receive arrays $\mathbf{b}(\theta)$ can be expressed as:

$$\mathbf{b}(\theta) = \left[1, e^{jk_0 d_R \sin \theta}, \dots, e^{jk_0 (N-1) d_R \sin \theta}\right]^T \tag{3.31}$$

where $k_0 = 2\pi/\lambda$ is the wavenumber.

After the down-converting process followed by matched filtering to the measured signals $\mathbf{x}_{\tau}(t;\tau)$, the output of the matched filtered to the *kth* waveform can be expressed as:

$$\mathbf{y}_{r,k}(\tau) = \sqrt{\frac{E}{K}} \alpha_t(\tau) \left[\mathbf{w}_k^H \mathbf{a}_k(\theta_t, r_t) e^{-j \delta_{k,T}(\theta_t, r_t)} \mathbf{b}(\theta_t) \right] + \widetilde{\mathbf{n}_d}(\tau) + \widetilde{\mathbf{n}_r}(\tau) \quad (3.32)$$

Here $\widetilde{\mathbf{n}}_d(\tau)$ and $\widetilde{\mathbf{n}}_r(\tau)$ are zero mean independent circularly Gaussian stochastic processes representing the interference signals and additive Gaussian noise, respectively, after matched-filtering.

Thus, the $KN \times 1$ virtual received data vector after matched filtering can be written as:

$$\mathbf{y}_{r} = \left[\mathbf{y}_{r,1}^{T}(\tau), \dots, \mathbf{y}_{r,K}^{T}(\tau) \right]^{T}$$

$$= \sqrt{\frac{\varepsilon}{\kappa}} \alpha_{t} \left[\mathbf{q}(\theta_{t}, r_{t}) \otimes \mathbf{b}(\theta_{t}) \right] + \widetilde{\mathbf{v}}$$
(3.33)

where \otimes denotes the Kronecker product and $\widetilde{v}(\tau)$ is the $KN \times 1$ stacked vector denoting the interference received signals plus white noise vector components.

For the Doppler application, if the target has a radial velocity v_r , then the received signals are shifted in frequency by Doppler shift, $f_d=\frac{2v_r}{\lambda}$. Since $\Delta f\ll f_c$, the f_d due to Δf can be neglected. Let

$$\mathbf{a}_r(\theta_t, r_t) = \mathbf{q}(\theta_t, r_t) \otimes \mathbf{b}(\theta_t) \tag{3.34}$$

Then, we further extend (3.33) to include the moving target scenario as:

$$\mathbf{y}_{r(mov)} = \sqrt{\frac{E}{K}} \alpha_t \left[\mathbf{a}_d(f_d) \otimes \mathbf{a}_r(\theta_t, r_t) \right] + \widetilde{v}$$
 (3.35)

where $\mathbf{a}_d(f_d)$ is the Doppler vector which can be expressed as:

$$\mathbf{a}_{d}(f_{d}) = \left[1, e^{j2\pi f_{d}T}, \dots, e^{j2\pi(L-1)f_{d}T}\right]^{T}$$
(3.36)

where L is the sampling number. Then, (3.33) can be rewritten as:

$$\mathbf{y}_{r(mov)} = \sqrt{\frac{E}{K}} \alpha_t \, \mathbf{\kappa}_{mov} \left(\theta_t, r_t, f_d \right) + \widetilde{\mathbf{v}} \tag{3.37}$$

where $\kappa_{mov}(\theta_t, r_t, f_d)$ represents a joint range-angle-Doppler steering vector and is given by:

$$\kappa_{mov}(\theta_t, r_t, f_d) = \mathbf{a}_d(f_d) \otimes \mathbf{a}_r(\theta_t, r_t)$$
 (3.38)

The Doppler frequency can be expressed, for the constant velocity and accelerated moving target, respectively, as:

$$f_d = \frac{2v_o}{\lambda} \tag{3.39}$$

and

$$f_d = \frac{2(v_o + a_s t_s)}{\lambda}$$
 (3.40)

where v_o , a_s , and t_s denote the constant velocity, acceleration, and slow time dimension, respectively.

It may be visible from (3.37) that, the joint estimation of range-angle-Doppler parameters for the moving targets can be achieved by utilizing FDA-MIMO radar and when it is combined with the MIMO coherent-time integration, the Doppler resolution can be significantly improved. Hence, the FDA-MIMO radar has three-dimensional angle-range-Doppler (ARD) processing capabilities, this leads to further improvement of the SNR and attains the attributes of a low-observable moving target.

3.2.5. Joint angle and range estimation

As shown from (3.4) and (3.31), respectively, the transmit steering vector is angle and range dependent while the receive steering vector is only angle-dependent. Thus, we can define the transmit and receive spatial frequency, respectively, as:

$$f_{s,T} = \frac{f_c d_T \sin \theta}{c} - \frac{\Delta f r}{c} \tag{3.41}$$

$$f_{s,R} = \frac{f_c d_R \sin \theta}{c} \tag{3.42}$$

Therefore, on the received data, this range dependence in $f_{s,T}$ can be compensated by employing a compensating vector, which can be given as:

$$\mathbf{g}(r_a) = \left[1, e^{j\left(\frac{2\pi\Delta f r_a}{c}\right)}, \dots, e^{-j\left(\frac{2\pi(M-1)\Delta f r_a}{c}\right)}\right]^T$$
(3.43)

where r_a is the a priori estimate of the range of the target, which can be calculated as (r_a = bin size × range bin number). Let us define the fundamental range difference as:

$$\Delta r = r_f - r_a \tag{3.44}$$

where r_f is the fundamental target's range. The Δr can be modeled as a uniform random variable distributed on the interval $\left[-\frac{c}{4B}, \frac{c}{4B}\right]$, where B is the bandwidth of the transmitted signal.

The range of the target in the presence of range ambiguity can be given as:

$$r_t = r_f + (i - 1)r_{uamg} (3.45)$$

where i is the range ambiguity index of the target, and r_{uamg} is the maximum unambiguous range which can be calculated as:

$$r_{uamg} = \frac{c}{2PRF} \tag{3.46}$$

As shown in (3.42), the $f_{s,R}$ depends only on an angle. Thus, the $\mathbf{g}(r_a)$ can be expressed in the joint transmit-receive spatial frequency domain as:

$$\mathbf{h} = \mathbf{1}_N \otimes \mathbf{g}(r_a) \tag{3.47}$$

where $\mathbf{1}_N$ is an $N \times 1$ vector, for which all elements of the vector are equal to 1.

The received data after the compensation process is applied can be expressed as:

$$\mathbf{y}_{r,comp} = \left(\sqrt{\frac{E}{K}} \ \alpha_t \ [\ \mathbf{q}(\theta_t, \ r_t) \ \otimes \mathbf{b}(\theta_t) \] + \widetilde{\mathbf{n}_d} + \widetilde{\mathbf{n}_r} \right) \odot \mathbf{h}$$

$$= \sqrt{\frac{E}{K}} \alpha_t \mathbf{W}^H \left[\left(\mathbf{a}(\theta_t) \odot \mathbf{a} \left(\Delta r + (i-1) r_{uamg} \right) \right) \otimes \mathbf{b}(\theta_t) \right] + \widetilde{\mathbf{n}_d} + \widetilde{\mathbf{n}_r} \quad (3.48)$$

The derivation of (3.48) is provided in Appendix A.

Due to the coupling of the angle and range parameters in the transmit domain, they can't be estimated from (3.48) directly. Thus, to circumvent this problem, we reconstruct $y_{r,comp}$ using the reconstruction operator, mat (.). The snapshot of the compensated data is reconstructed into an $N \times K$ data matrix $Y_{r,comp}$ as:

$$\mathbf{Y}_{r,comp} = \left[\text{mat}(\mathbf{y}_{r,comp}) \right]^T$$

$$= \sqrt{\frac{E}{\kappa}} \alpha_t(\tau) \mathbf{W}^* \left[\mathbf{a}(\theta_t) \odot \mathbf{a} \left(\Delta r + (i-1)r_{uamg} \right) \right]^T \mathbf{b}(\theta_t) + \widetilde{\mathbf{N}_t}(\tau) + \widetilde{\mathbf{N}_r}(\tau) (3.49)$$

The maximum likelihood estimator (MLE) for the target's angle is given by:

$$\widehat{\theta_t} = \arg \max_{\theta_t} \left| \sum_{k=1}^K \mathbf{w}_R^H(\theta_t) \, \mathbf{Y}_{r,comp}(k) \right| \tag{3.50}$$

where $\mathbf{w}_R(\theta_t) = \mathbf{Q}_R^{-1} \mathbf{b}(\theta_t)$ is the MVDR beamformer with \mathbf{Q}_R representing the covariance matrix of the received noise-plus- interference, and $\mathbf{Y}_{r,comp}(k)$ is the k^{th} column of $\mathbf{Y}_{r,comp}$ that includes the received data related to the k^{th} transmit SA.

Thus, the adaptive weight can be constructed in the transmit-receive dimensions as:

$$\mathbf{w}\left(i,0,\widehat{\theta_{t}}\right) = \mathbf{Q}_{\mathsf{T-R}}^{-1} \,\mathbf{u}\left(i,0,\widehat{\theta_{t}}\right) \tag{3.51}$$

where $\mathbf{u}(i,0,\widehat{\theta_t})$ is the steering vector in the transmit-receive domains and is given by:

$$\mathbf{u}(i,0,\widehat{\theta_t}) = \mathbf{b}(\widehat{\theta_t}) \otimes \left[\mathbf{a}(\widehat{\theta_t}) \odot \mathbf{a}((i-1)r_{uamg}) \right]$$
(3.52)

Next, we estimate the range ambiguity index as:

$$\hat{i} = \arg \max_{i=1,2..N_{amg}} \left| \mathbf{w}^{H} \left(i, 0, \widehat{\theta_{t}} \right) \mathbf{y}_{r,comp} \right|$$
 (3.53)

where N_{amg} represents the number of ambiguous ranges. And the adaptive weight will be

$$\mathbf{w}\left(\hat{\imath}, \Delta r, \widehat{\theta_t}\right) = \mathbf{Q}_{\mathsf{T-R}}^{-1} \mathbf{u}\left(\hat{\imath}, \Delta r, \widehat{\theta_t}\right) \tag{3.54}$$

Thus, the Δr is estimated as:

$$\widehat{\Delta r} = \arg \max_{\Delta r} \left| \mathbf{w}^{H} \left(\hat{\imath}, \Delta r, \widehat{\theta_{t}} \right) \mathbf{y}_{r,comp} \right|$$
 (3.55)

Hence, the true range can be estimated as:

$$\widehat{r_t} = r_a + \widehat{\Delta r} + (\widehat{\imath} - 1)r_{uama} \tag{3.56}$$

Hence, we can interpret this unambiguous angle and range estimation scheme as estimating the angle of the targets in the $f_{s,R}$ domain, and thereafter resolving the ambiguity in the range extent, and finally the range is estimated in the $f_{s,T-R}$ domains.

3.2.6. Tracking algorithm

In tracking scenarios, a maneuvering target (MT) is considered as a nonlinear dynamical system characterized by several possible operation regimes, which can be described as a sudden change in the dynamic motion equation of the system. Consequently, a maneuvering target represents a challenge to attain filter consistency (FC). This sort of problem is often referred to as a hybrid-state or jump Markov estimation problem [150]. One approach to treat this type of problem is the adaptive Kalman filter (KF). For tracking the MT, the adaptive KF is observing the residuals of innovations with their covariance errors in real-time, detecting a failure in FC, and adapting its parameters to retrieve FC. Unfortunately, using this approach will not provide reliable tracking performance, and this is due to the performing data association and adjusting the filter parameters at the same time will lead to unreliable decision making [151, 152]. Another alternative approach for tracking the MT scenario is modeling the situation as the state estimation problem with

Markovian switching coefficients [153]. The IMM estimator is a typical approach for such an estimation problem [154].

The dynamic and measurement equations for the MT can be expressed as:

$$\mathbf{x}_{n+1} = \mathbf{F}_n(\theta_{n+1}) \, \mathbf{x}_n + \mathbf{G}_n(\theta_n) \, \boldsymbol{v}_n(\theta_n) \tag{3.57}$$

$$\mathbf{z}_n = \mathbf{H}(\theta_n) \, \mathbf{x}_n + \mathbf{w}_n \tag{3.58}$$

where \mathbf{x}_n is the target's state vector at discrete time t_n , \mathbf{F}_n is the transition matrix of the system, θ_n is a finite-state Markov chain with transitional probability p_{si} of switching from s mode to i mode, \mathbf{G}_n denotes the errors related to the state of the target. Likewise, \mathbf{z}_n is the measurement vector at discrete time t_n , \mathbf{H} is the measurement matrix. The random sequences \mathbf{v}_n and \mathbf{w}_n are mutually independent, zero-mean white Gaussian, with covariances \mathbf{R}_n and \mathbf{Q}_n , respectively.

Stages and parameters involved for IMM estimator implementation are provided in Table 3.1.

Table 3.1: Stages involved for IMM algorithm implementation.

Mixing stage: Starting with the state x_{n-1}^i and the mode probability μ_{n-1}^i for each of r modes:

Predicted model probability:
$$\mu_{n-1}^i = \sum_{s=1}^r \mu_{n-1}^s \ p_{si}$$
 (3.59)

Mixing probabilities:
$$\mu_{n-1 \setminus n-1}^{s|i} = \frac{\mu_{n-1}^{s}}{\mu_{n-1 \setminus n-1}^{l}} p_{si}$$
 (3.60)

Mixing estimate:
$$\mathbf{x}_{n-1 \setminus n-1}^{0l} = \sum_{s=1}^{r} \mu_{n-1 \setminus n-1}^{s \mid i} \mathbf{x}_{n-1 \setminus n-1}^{s}$$
 (3.61)

Mode Conditioned Estimates stage: Starting with $\mathbf{x}_{n-1 \setminus n-1}^{0i}$ and $\mathbf{P}_{n-1 \setminus n-1}^{0i}$ for each of r modes:

Predicted state:
$$\mathbf{x}_{n \setminus n-1}^{l} = \mathbf{F}_{n-1}^{l} \mathbf{x}_{n-1 \setminus n-1}^{0l}$$
 (3.63)

Predicted covariance:
$$\mathbf{P}_{n \setminus n-1}^{i} = \mathbf{F}_{n-1}^{i} \mathbf{P}_{n-1 \setminus n-1}^{0i} \left(\mathbf{F}_{n-1}^{i} \right)^{T} + \mathbf{G}_{n-1}^{i} \mathbf{Q}_{n-1}^{i} \left(\mathbf{G}_{n-1}^{i} \right)^{T}$$
 (3.64)

Measurement residual:
$$\widetilde{\mathbf{z}_n^I} = \mathbf{z}_n - \mathbf{H}_n^I \mathbf{x}_{n \setminus n-1}^I$$
 (3.65)

Residual covariance:
$$\mathbf{S}_{n}^{i} = \mathbf{H}_{n}^{i} \mathbf{P}_{n \setminus n-1}^{i} \left(\mathbf{H}_{n}^{i}\right)^{T} + \mathbf{Q}_{n}$$
 (3.66)

Filter gain:
$$\mathbf{K}_{n}^{i} = \mathbf{P}_{n \setminus n-1}^{i} \left(\mathbf{H}_{n}^{i} \right)^{T} \left(\mathbf{S}_{n}^{i} \right)^{-1}$$
 (3.67)

Update state:
$$\mathbf{x}_{n \setminus n}^{i} = \mathbf{x}_{n \setminus n-1}^{i} + \mathbf{K}_{n}^{i} \mathbf{z}_{n}^{i}$$
 (3.68)

Update covariance:
$$\mathbf{P}_{n \setminus n}^{i} = \left[\mathbf{I} - \mathbf{K}_{n}^{i} \mathbf{H}_{n}^{i}\right] \mathbf{P}_{n \setminus n-1}^{i}$$
 (3.69)

Mode Likelihood Computations stage:

Model likelihood:
$$\Pi_n^i = \frac{1}{\sqrt{|2\pi s_n^i|}} e^{\left[-\frac{1}{2}(\widetilde{z_n^i})^T (s_n^i)^{-1} \widetilde{z_n^T}\right]}$$
(3.70)

where |. |denotes the matrix determinant.

Mode Probability Update stage:

Model probability:
$$\mu_n^i = \frac{\Pi_n^i}{\sum_{s=1}^r \mu_{n-1 \backslash n-1}^s} \mu_{n-1 \backslash n-1}^i$$
 (3.71)

Combination of State Estimates stage:

Filtered state estimate:
$$\mathbf{x}_{n \setminus n} \triangleq E[\mathbf{x}_n | \mathbf{z}_n]$$

$$= \sum_{i=1}^{r} \mu_n^i \mathbf{x}_{n \setminus n}^i \tag{3.72}$$

where E[.] denotes the expectation operator.

Filtered covariance:
$$\mathbf{P}_{n \mid n} \triangleq E[(\mathbf{x}_n - \mathbf{x}_{n \mid n}) (\mathbf{x}_n - \mathbf{x}_{n \mid n})^T | \mathbf{z}_n]$$

$$= \sum_{i=1}^r \mu_n^i \left[\mathbf{P}_{n \mid n}^i + (\mathbf{x}_{n \mid n}^i - \mathbf{x}_{n \mid n}) (\mathbf{x}_{n \mid n}^i - \mathbf{x}_{n \mid n})^T \right] \qquad (3.73)$$

Fig. 3.5 shows a schematic representation of IMM processing steps with r = 2 modes.

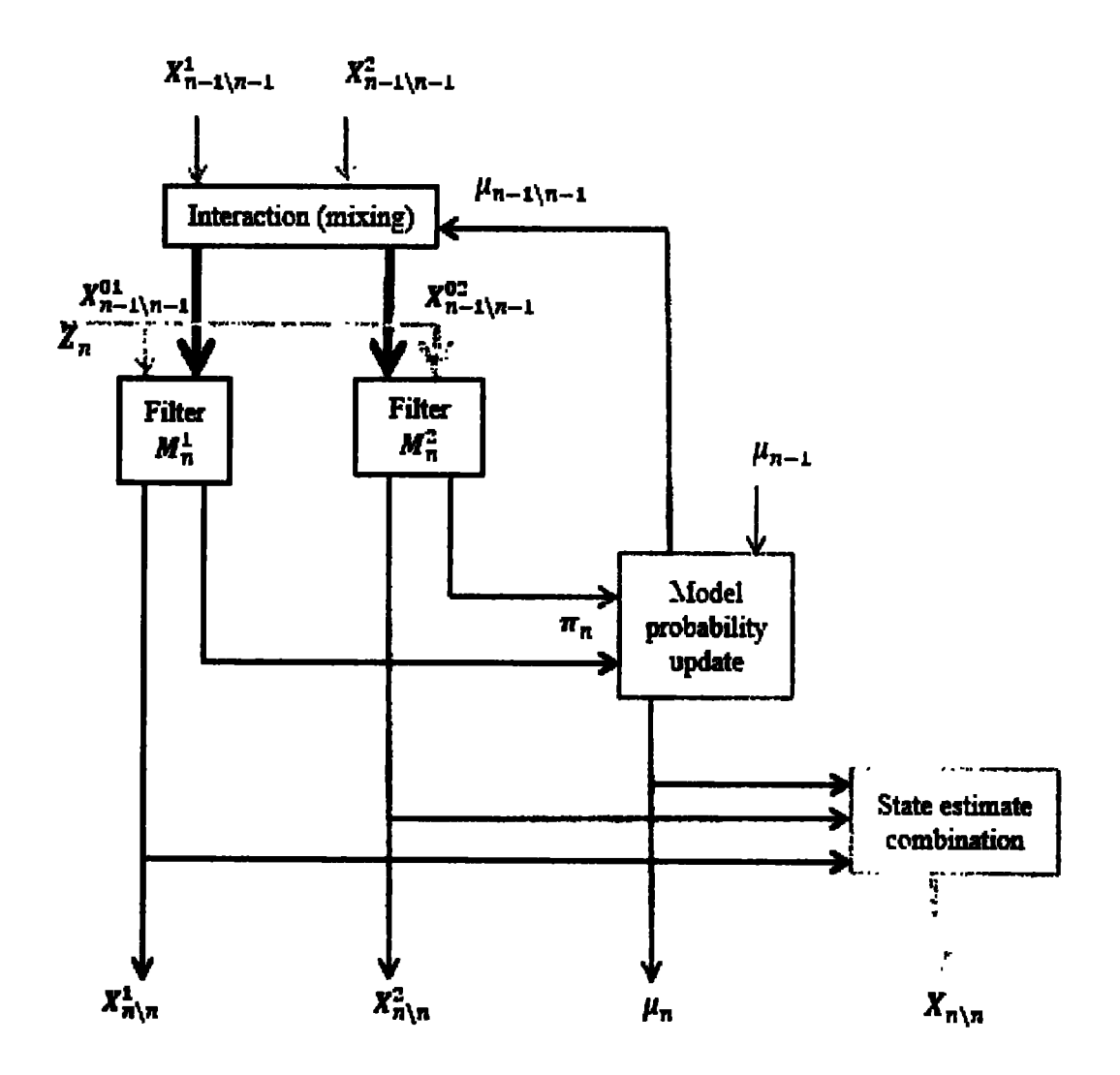


Figure 3.5: Processing steps of IMM estimator with r=2 modes.

For many tracking systems, x_n is projected in the Cartesian system and retained stabilized in a frame of reference relative to the position of the platform. The state vector can be expressed in Cartesian coordinate's space as:

$$\mathbf{x}_{n} = [x_{n} \ \dot{x_{n}} \ \dot{x_{n}} \ \dot{y_{n}} \ \dot{y_{n}} \ \dot{y_{n}} \ \dot{z_{n}} \ \dot{z_{n}} \ \ddot{z_{n}}]^{T}$$
(3.74)

where (x_n, y_n, z_n) , $(\dot{x_n}, \dot{y_n}, \dot{z_n})$ and $(\ddot{x_n}, \ddot{y_n}, \ddot{z_n})$ denote the position, the velocity, and the acceleration components of the target at discrete time t_n , respectively. We consider two

motion modes for the MT, namely, constant velocity (CV) and constant acceleration (CA) models in our proposed design [155].

The dynamical constraint for CV and CA motion models can be expressed in Cartesian coordinate's space as:

$$\mathbf{F}_{n} = \begin{bmatrix} \mathbf{A}_{n} & \mathbf{0}_{m \times m} & \mathbf{0}_{m \times m} \\ \mathbf{0}_{m \times m} & \mathbf{A}_{n} & \mathbf{0}_{m \times m} \\ \mathbf{0}_{m \times m} & \mathbf{0}_{m \times m} & \mathbf{A}_{n} \end{bmatrix}$$
(3.75)

where $\mathbf{0}_{m \times m}$ denotes m by m matrix of zeros and \mathbf{A}_n is expressed for CV and CA motions respectively, as:

$$\mathbf{A}_{CV} = \begin{bmatrix} 1 & \tau_n \\ 0 & 1 \end{bmatrix} \tag{3.76}$$

$$\mathbf{A}_{CA} = \begin{bmatrix} 1 & \tau_n & \frac{\tau_n^2}{2} \\ 0 & 1 & \tau_n \\ 0 & 0 & 1 \end{bmatrix}$$
 (3.77)

where $\tau_n = t_n - t_{n-1}$ denotes the sampling time, t_n represents the period of measurement n.

The covariance matrix of the input noise for CV and CA motion models are characterized by $G_n Q_n G_n^T$ that is given by:

$$\mathbf{G}_{n}\mathbf{Q}_{n}\mathbf{G}_{n}^{T} = \begin{bmatrix} q_{n}^{x} \mathbf{B}_{n} \mathbf{B}_{n}^{T} & \mathbf{0}_{m \times m} & \mathbf{0}_{m \times m} \\ \mathbf{0}_{m \times m} & q_{n}^{y} \mathbf{B}_{n} \mathbf{B}_{n}^{T} & \mathbf{0}_{m \times m} \\ \mathbf{0}_{m \times m} & \mathbf{0}_{m \times m} & q_{n}^{z} \mathbf{B}_{n} \mathbf{B}_{n}^{T} \end{bmatrix}$$
(3.78)

where $\mathbf{B}_{n}\mathbf{B}_{n}^{T}$ is expressed for CV and CA motions, respectively, as:

$$(\mathbf{B}_{n}\mathbf{B}_{n}^{T})_{CV} = \begin{bmatrix} \frac{\tau_{n}^{4}}{4} & \frac{\tau_{n}^{3}}{2} \\ \frac{\tau_{n}^{3}}{2} & \tau_{n}^{2} \end{bmatrix}$$
(3.79)

$$(\mathbf{B}_{n}\mathbf{B}_{n}^{T})_{CA} = \begin{bmatrix} \frac{\tau_{n}^{4}}{4} & \frac{\tau_{n}^{3}}{2} & \frac{\tau_{n}^{2}}{2} \\ \frac{\tau_{n}^{3}}{2} & \tau_{n}^{2} & \tau_{n} \\ \frac{\tau_{n}^{2}}{2} & \tau_{n} & 1 \end{bmatrix}$$
 (3.80)

However, the performance of the IMM algorithm and its effectiveness has been documented in the literature [152, 154, 156].

3.3. Performance Analysis

In this section, we analyze the performance of the proposed RadCom system design for both functions, i.e. target detection performance and communication symbol transmission in terms of SER.

3.3.1. SINR analysis for radar

The target detection performance depends upon the output SINR of the adaptive MVDR beamformer. Therefore, from (3.33) the observation vector \mathbf{y}_r includes the target signal part which is assumed to be an unknown deterministic signal and interference plus noise part which is assumed to be zero mean independent circularly Gaussian with variances σ^2_d and σ^2 , respectively. Assume that there are D jammers present in the radar environment, the covariance matrix \mathbf{Q} of the interference plus noise can be written as:

$$\mathbf{Q} = \sum_{d=1}^{l} \sigma^2_d \mathbf{v}(\theta_d, r_d) \mathbf{v}^H(\theta_d, r_d) + \sigma^2 \mathbf{I}$$
 (3.81)

where $\mathbf{v}(\theta, r) = \mathbf{q}(\theta, r) \otimes \mathbf{b}(\theta)$, and I is the identity matrix.

The output SINR can be written as:

$$SINR = \frac{\sigma_s^2 |\mathbf{w}_R^H \mathbf{v}(\theta, r)|^2}{\mathbf{w}_R^H \mathbf{Q} \mathbf{w}_R}$$

$$= \frac{\sigma^2_s |\mathbf{v}^H(\theta_t, r_t) \mathbf{v}(\theta, r)|^2}{\mathbf{v}^H(\theta_t, r_t) \mathbf{Q} \mathbf{v}(\theta_t, r_t)}$$
(3.82)

where σ_s^2 is the variance of the average target signal.

3.3.2. Detection analysis for radar target

To analyze the detection performance of the radar target, a statistical hypothesis testing model for received data is constructed as:

$$\begin{cases} H_0: \mathbf{y}_r = \widetilde{\mathbf{v}} & (target \ is \ absent) \\ H_1: \mathbf{y}_r = \sqrt{\frac{E}{K}} \ \alpha_t [\ \mathbf{q}(\theta_t, r_t) \otimes \mathbf{b}(\theta_t)] + \widetilde{\mathbf{v}} & (target \ is \ present) \end{cases}$$
(3.83)

Based on Neyman-Pearson's approach for statistical inference, the likelihood ratio test can be used to analyze the detection probability for a radar target and is given as [157]:

$$\prod = \log \frac{\Pr(\mathbf{y}_r; H_1)}{\Pr(\mathbf{y}_r; H_0)}$$

$$= \left| \left\| \sqrt{\frac{\varepsilon}{\kappa}} \, \alpha_t(\tau) \, \mathbf{q}(\theta_t, r_t) \right\|^2 \, \|\mathbf{b}(\theta_t)\|^2 + \widetilde{v} \, \right|^2 \gtrsim_{H_1}^{H_0} \varepsilon \quad (3.84)$$

where ε is the threshold used to partition the decision region for the detection process.

The probability of detection P_D can be given by [158]:

$$P_D = Q_M(\sqrt{2 \, SNR}, \sqrt{-2 \, \ln P_{FA}})$$
 (3.85)

where P_{FA} is the probability of false alarm and Q_M (.) is known as Marcum's Q function [106] which can be given by:

$$Q_M(\alpha, t) = \int_{\varepsilon}^{+\infty} t \exp[-0.5(t^2 + \alpha^2)] I_0(\alpha t) dt$$
 (3.86)

where $I_0(\cdot)$ is the modified Bessel function of the first kind.

3.3.3. CRLB analysis for radar

In this subsection, we evaluate the lower-bound performance of the FDA-MIMO radar in terms of the CRLBs for the angle and range parameters. The deterministic angle and range of the target are represented in vector form as $\Phi = [\theta_t, r_t)]^T$. From (3.33), the observation data y_r follows a circularly Gaussian distribution with mean y_s and covariance matrix \mathbf{Q} , where:

$$y_s = \sqrt{\frac{E}{\kappa}} \alpha_t(\tau) [\mathbf{q}(\theta_t, r_t) \otimes \mathbf{b}(\theta_t)]$$
 (3.87)

Thus, if the α_t is known, the corresponding CRBs expression for the target parameters of interest is [159]:

$$\mathbf{D}^{-1}_{\Phi} = \frac{2NE}{K} |\alpha_t|^2 \operatorname{Re} \left\{ \left(\frac{\partial \mathbf{u}(\theta_t, r_t)}{\partial \Phi} \right)^H \mathbf{Q}^{-1} \left(\frac{\partial \mathbf{u}(\theta_t, r_t)}{\partial \Phi} \right) \right\}$$
(3.88)

where N is the number of snapshots and

$$\mathbf{u}(\theta_t, r_t) = \mathbf{b}(\theta_t) \otimes \left[\mathbf{W}^H \left(\mathbf{a}(r_t - r_a) \odot \mathbf{a}(\theta_t) \right) \right]$$
(3.89)

In this case, the Fisher information matrix (FIM) can be given as:

$$\mathbf{F} = \frac{2NE}{K} |\alpha_t|^2 \begin{bmatrix} \|\mathbf{w}_{r_t}\|^2 & \text{Re}\{\mathbf{w}_{r_t}^H \mathbf{w}_{\theta_t}\} \\ \text{Re}\{\mathbf{w}_{r_t}^H \mathbf{w}_{\theta_t}\} & \|\mathbf{w}_{\theta_t}\|^2 \end{bmatrix}$$
(3.90)

where the two auxiliary vectors \mathbf{w}_{r_t} \mathbf{w}_{θ_t} can be defined, respectively, as:

$$\mathbf{w}_{r_t} \triangleq \mathbf{Q}^{-1/2} \, \mathbf{u}_{r_t}(\theta_t, r_t) \tag{3.91}$$

$$\mathbf{w}_{\theta_t} \triangleq \mathbf{Q}^{-1/2} \, \mathbf{u}_{\theta_t}(\theta_t, r_t) \tag{3.92}$$

where $\mathbf{Q}^{-1/2}$ is the square root matrix of the positive definite matrix \mathbf{Q}^{-1} , $\mathbf{u}_{r_t}(\theta_t, r_t)$

$$\frac{\partial u(\theta_t, r_t)}{\partial r_t} \text{ and } \mathbf{u}_{\theta_t}(\theta_t, r_t) = \frac{\partial u(\theta_t, r_t)}{\partial \theta_t}.$$

Thus, the corresponding closed-form CRLBs for angle and range parameters are equivalent to the inverse of FIM and can be expressed, respectively, as:

$$\mathbf{D}_{\theta_t} = \frac{K}{2^{NE|\alpha_t|^2}} \frac{\|\mathbf{w}_{r_t}\|^2}{\|\mathbf{w}_{r_t}\|^2 \|\mathbf{w}_{\theta_t}\|^2 - \left(\text{Re}\{\mathbf{w}_{r_t}^H \mathbf{w}_{\theta_t}\}\right)^2}$$
(3.93)

$$\mathbf{D}_{r_{t}} = \frac{K}{2NE |\alpha_{t}|^{2}} \frac{\|\mathbf{w}_{\theta_{t}}\|^{2}}{\|\mathbf{w}_{r_{t}}\|^{2} \|\mathbf{w}_{\theta_{t}}\|^{2} - (\text{Re}\{\mathbf{w}_{r_{t}}^{H} \mathbf{w}_{\theta_{t}}\})^{2}}$$
(3.94)

3.3.4. SER analysis for communication function

Firstly, let us consider the scenario when the communication receiver is located outside the main lobe directions, i.e., in the SL region, and then the transmitter selected M-ary APSK for embedding the information towards the communication direction during the current scan. Assume that each symbol (signal point) to be transmitted is mapped into 4 bits, i.e., $\beta = 4$ bits, (see Fig. 3.3(a)), and these symbols are equally probable. Calculating the distances between the symbols in the 16-APSK constellation are presented in Appendix B. Each symbol on the outer and inner circles has a probability of 11/16 and 5/16, respectively, to be selected for transmission towards the communication direction.

Thus, the SER for the proposed 16-APSK signaling with (5, 11) structure is written as:

$$p \approx \frac{11}{8} \sum_{i=2}^{11} Q\left(\sqrt{\frac{d^2_{A_1 A_i}}{2KN_o}}\right) + \frac{5}{8} \sum_{i=1}^{11} Q\left(\sqrt{\frac{d^2_{B_1 A_i}}{2KN_o}}\right) + \frac{5}{8} \sum_{j=2}^{5} Q\left(\sqrt{\frac{d^2_{B_1 B_j}}{2KN_o}}\right) + \frac{11}{8} \sum_{j=1}^{5} Q\left(\sqrt{\frac{d^2_{A_1 B_j}}{2KN_o}}\right)$$
(3.95)

Here Q (.) is the Gaussian error function. Similarly, for the 8-APSK with (1, 7) structure, the 32-APSK with (5, 11, 16) structure, and the 64-APSK with (4, 10, 15, 17, 18) structure, the SER is calculated in a similar procedure.

Now, let us consider the scenario when the target and the communication receiver are both located in the radar main beam directions, and then the transmitter selected the *M*-ary PSK for the information embedding scheme. Assume that each symbol (signal point) to be transmitted is mapped into 4 bits, i.e., Ω =4 bits, (see Fig. 3.3(b)), and are equiprobable. The probability density function (PDF) of the 16-PSK is derived in Appendix C. The decision region can be described as $D = \{\phi \colon {}^{-\pi}/_{M} < \phi \le {}^{\pi}/_{M}\}$; therefore, the SER of the 16-PSK is given by:

$$p \approx 1 - \int_{-\pi/16}^{\pi/16} \left(\frac{1}{2\pi} e^{-\xi/K \sin^2 \phi} \int_0^\infty v e^{-\frac{(v - \sqrt{2\xi/K} \cos \phi)^2}{2}} dv \right) d\phi$$
 (3.96)

Similarly, for the 8-PSK, the 32-PSK, and the 64-PSK, the SER can be evaluated in a similar procedure.

3.4. Simulation Results

In this thesis, MATLAB has been used as the main computing and programming environment. Also, other useful solvers and toolboxes have been integrated with MATLAB for performing the simulations. In particular, we have used the MATLAB convex (CVX) toolbox to solve all the optimization problems. Moreover, we modeled the communication system protocol in MATLAB.

Here, we present simulation examples to demonstrate the performance features of the proposed system design. In all examples, we assume a ULA FDA with $\Delta f = 300$ KHz and consisting of M = N = 14 antenna elements spaced $^{\lambda}/_{2}$ apart. Moreover, the surveillance region where the RadCom system operates is $-90^{\circ} \le \theta \le 90^{\circ}$ and $0 \text{ m} \le r \le 20 \times 10^{5} \text{m}$. Besides radar functions within the main beam, we assumed that the information bits are delivered to the communication receiver located at (θ_c, r_c) . It is also assumed that the power level in the SL region is at least 20 dB lower than the main beam

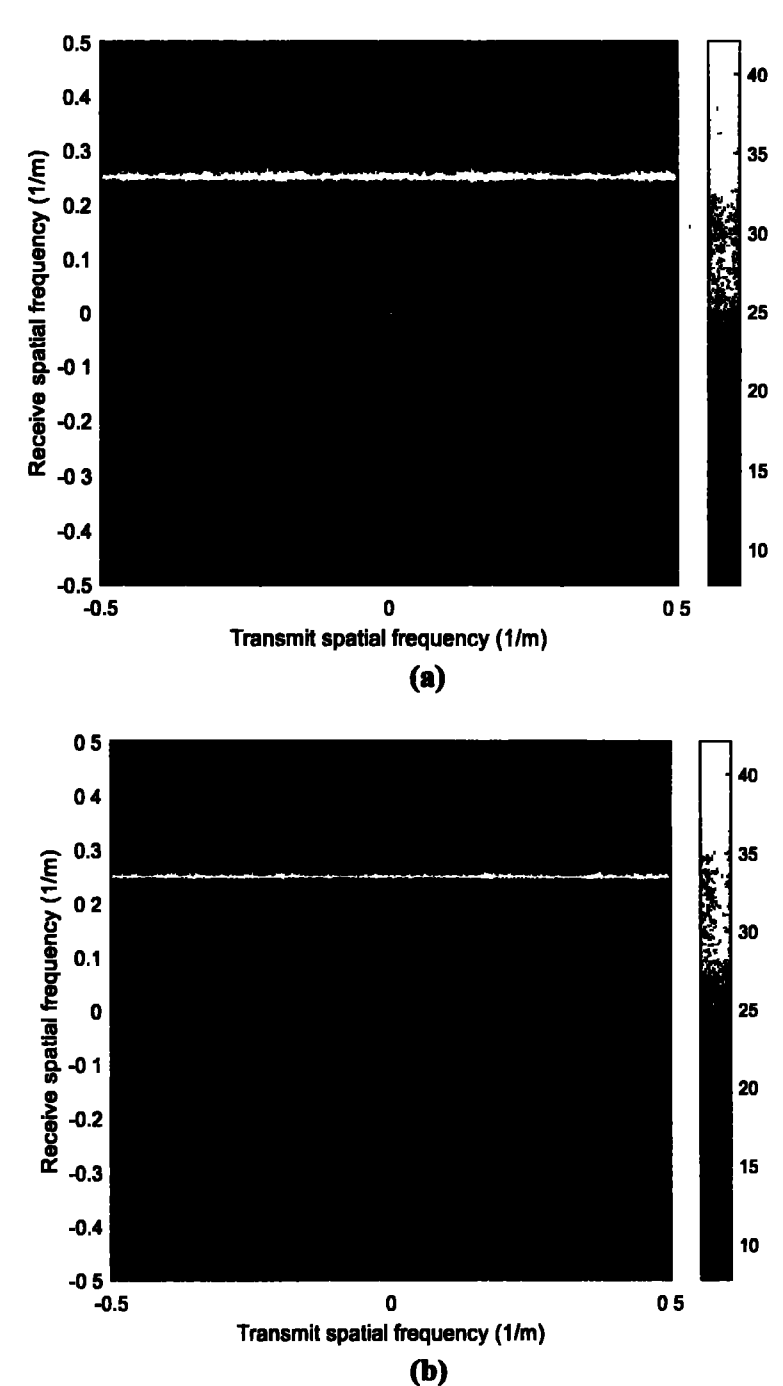
thus the maximum allowable value of $\varepsilon_{max}=0.1$ is selected. The simulation parameters are summarized in Table 3.2.

Table 3.2: Parameter's design of the proposed system.

Parameter	Description	Value
f _c ;	Carrier frequency	10 GHz
PRF	Pulse repetition frequency	5 KHz
71.9	Wavelength	3 cm
В	Waveform bandwidth	15 MHz
N. A.	Incremental frequency and	300 KHz
r _{uamg}	Maximum unambiguous range	30 Km
$d_T = d_R^{\tau}$	Element spacing	1.5 cm
M = N	Element number	14
Name 1	Ambiguity number	44.30
<i>P</i>	Number of pulses	200
62.45	Range olution	
θ_t	Interference angle	30°
INR	Interference to noise ratio	30 dB = 3

Example 3.1 (Spectral distribution of the targets in the presence of the interference and range ambiguity):

In this example, we consider a situation where there are two targets located in the same angle and range bin but they are from different ambiguous range zones. Assuming there are 1000 range bins and the estimate of a priori range r_a can be calculated as 10 m × 1000 = 10 km. The fundamental range difference Δr on the two targets is uniformly distributed on [-5m, 5m], and the SNRs of the targets are assumed to be 0 dB and 5 dB, respectively.



(b)
Figure 3.6: Spectral distribution of the interference and the two targets using, (a)
Conventional MIMO radar and (b) FDA-SA radar.

In the case of conventional MIMO radar, as shown in Fig. 3.6(a), since the two targets are located within the same angle, this results in the targets being overlapped and can't be resolved in the spatial frequency dimension. On the other hand, in the case of FDA-SA radar, the two targets can be resolved based on the spatial spectrum spreading in the transmit dimension as seen from Fig. 3.6(b). This is due to the spatial frequency dimension of the FDA-SA radar that can be divided into two straps and each target from a different ambiguous zone belongs to the one strap corresponding to the range ambiguity index i = 1,2 and the width of each strap determines by the Δr .

By utilizing the range dependency of the transmit steering vector, the accuracy of the range estimation can be improved which leads to further enhancement in the range resolution. Fig. 3.7 illustrates the resolvability improvement in the range offered by the proposed system.

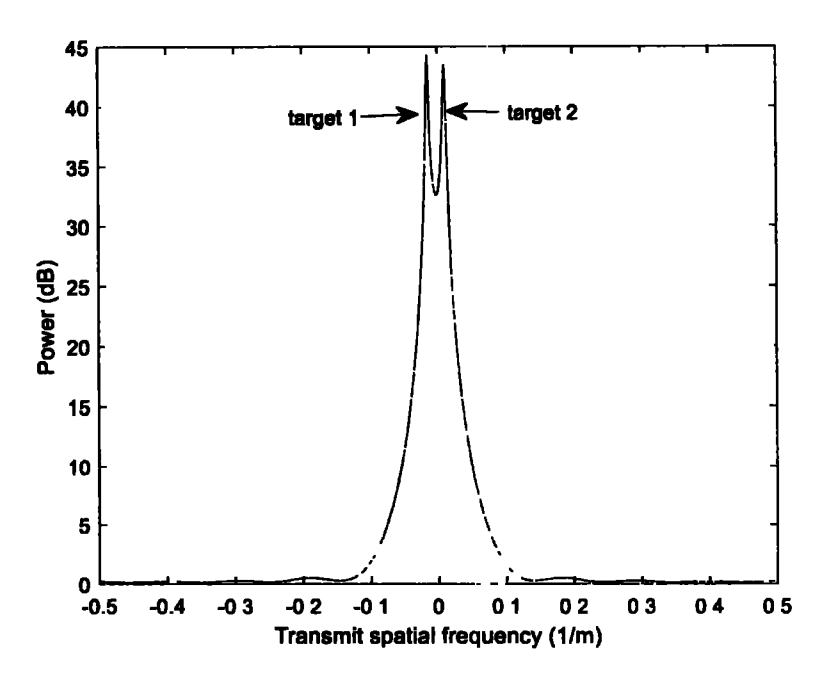
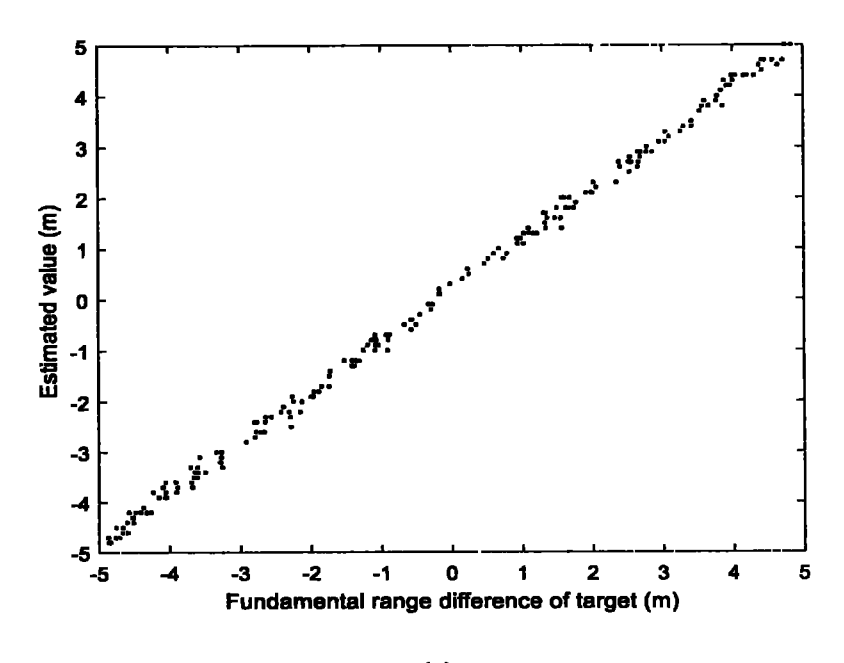


Figure 3.7: The range resolution of two targets can be offered by the proposed system.

It shows the spectrum of two targets in the same ambiguous-range region where the distance between them is 5 meters. It is shown from Fig. 3.7 that the two targets can be distinguished from each other. Thus, the proposed FDA-MIMO system offered a higher resolution in range compared to the traditional radar.

Example 3.2 (joint angle and range estimation):

In this example, we assess the performance of the joint estimation for the angle and range parameters of the target. Therefore, we carried out 200 Monte Carlo simulations and during each trial, the sample number is 200 with assumptions that the target is located at 2° , and the SNR is 0 dB. The range ambiguity index i and the fundamental range difference Δr parameters are selected to be the same as in example 3.1 except that they are fixed for each experiment. Figures 3.8(a), (b), and (c) plot the estimated results of the fundamental range difference Δr , angle, and range ambiguity index i, respectively. Fig. 3.8 shows that the results are very close to their true values.



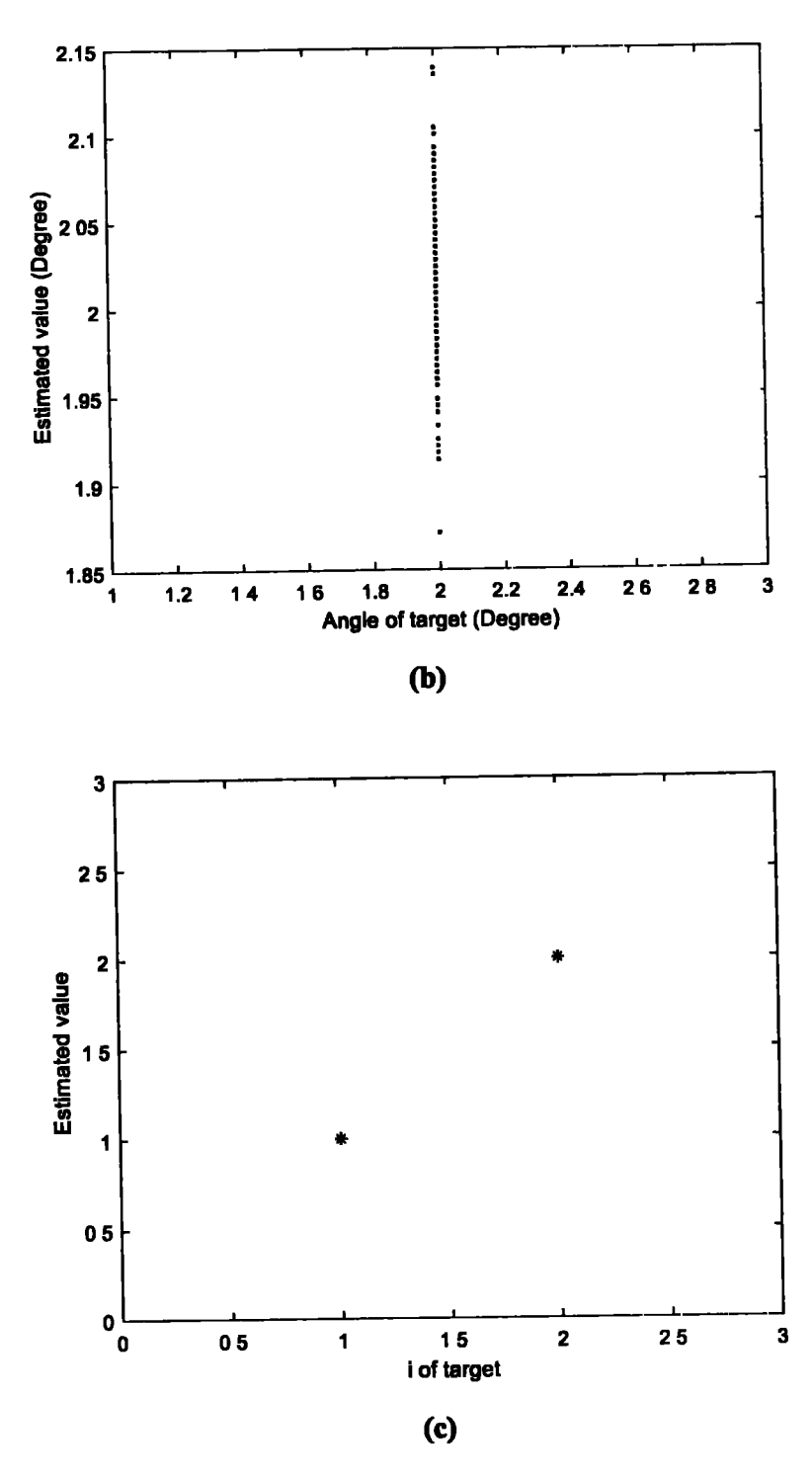


Figure 3.8: Estimation results of the target parameters present in an interference environment. Estimation of (a) Fundamental range difference, (b) Angle, and (c) range ambiguity index.

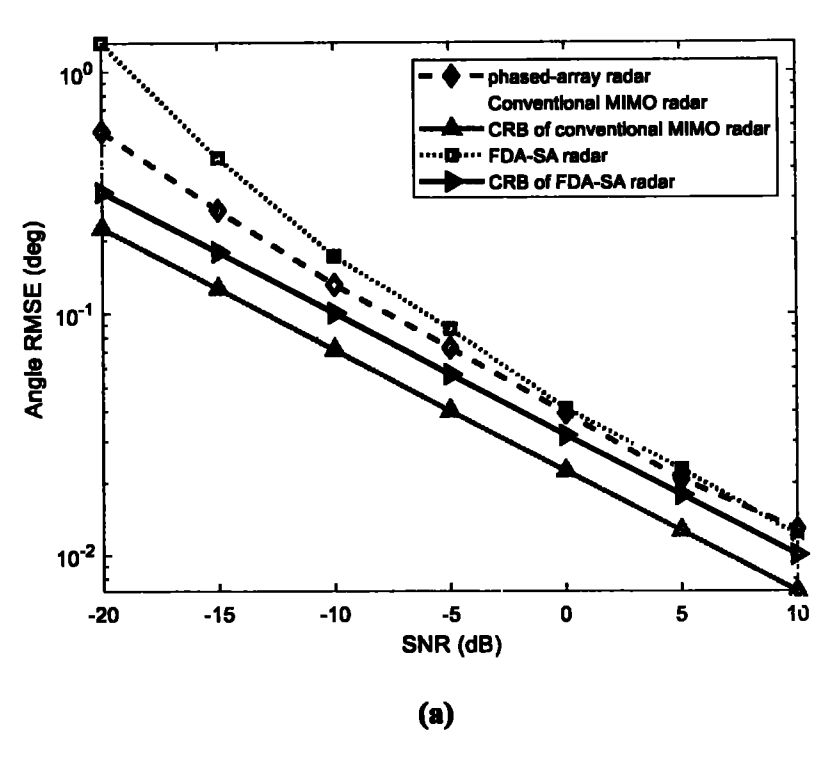
Here, the root mean square errors (RMSEs) is used as a performance criterion, which can be calculated as follows:

RMSE
$$(\theta) = \sqrt{\frac{1}{TM_c} \sum_{t=1}^{T} \sum_{j=1}^{M_c} (\widehat{\theta_{t,j}} - \theta_t)^2}$$
 (3.97)

RMSE
$$(r) = \sqrt{\frac{1}{TM_c} \sum_{t=1}^{T} \sum_{j=1}^{M_c} (\widehat{r_{t,j}} - r_t)^2}$$
 (3.98)

where $\widehat{\theta_{t,j}}$ and $\widehat{r_{t,j}}$ denote the estimates of the angle and range for the t^{th} target in the j^{th} Monte Carlo run, respectively, T and M_c denote the total number of targets and Monte Carlo runs, respectively.

Figs. 3.9 and 3.10 show the RMSEs of the angle and range estimates, respectively, attained from 200 Monte Carlo simulations versus the input SNR under interference-free and interference environments. For comparison purposes, the corresponding CRBs are plotted as well.



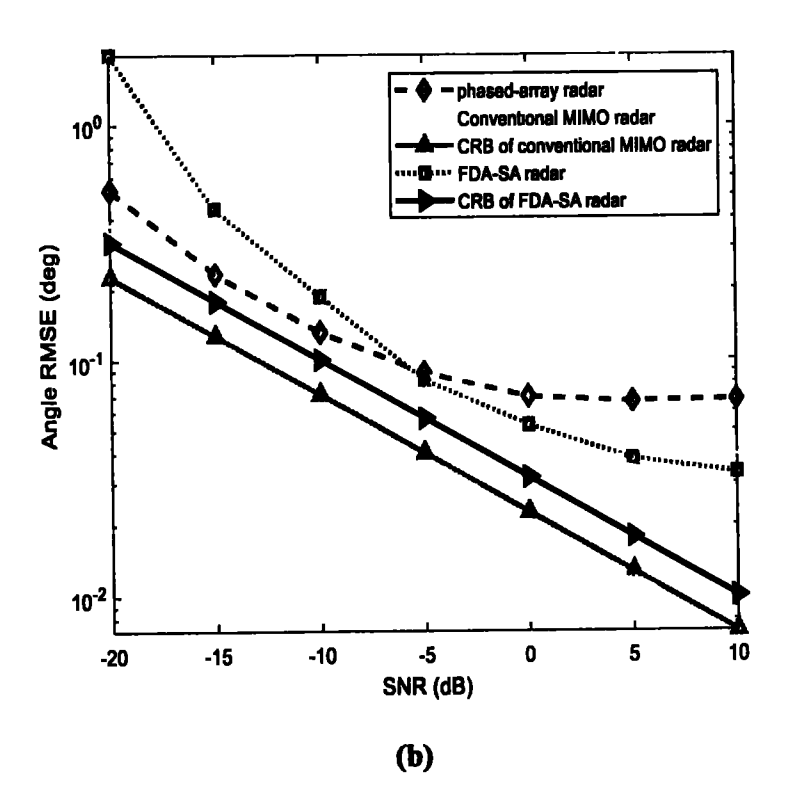


Figure 3.9: RMSE versus SNR for the Angle estimation in (a) interference-free environment and (b) interference environment.

The observations extracted from Fig. 3.9 are the following: (i) in the interference-free environment, the RMSEs estimates are close to the CRB as compared to the counterpart of the interference case. The CRB of the conventional MIMO radar is smaller than that of FDA-SA radar, this is because of the large aperture of the MIMO array created by the virtual radiated elements, (ii) in the interference environment, there is a bias in the angle estimation at high SNRs, and (iii) the accuracy of the estimation of the FDA-SA radar is close to that of the phased array (PA) radar.

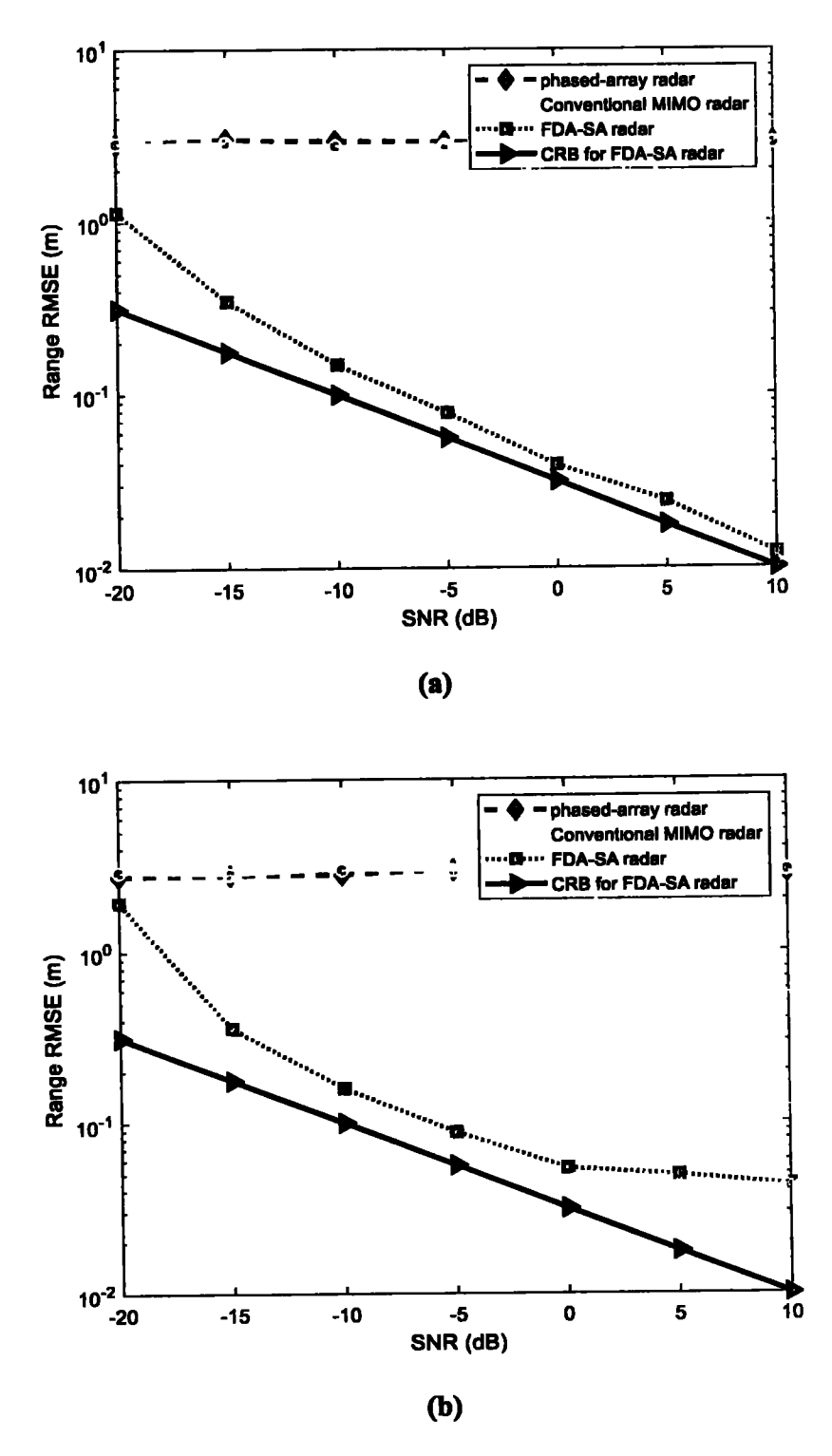
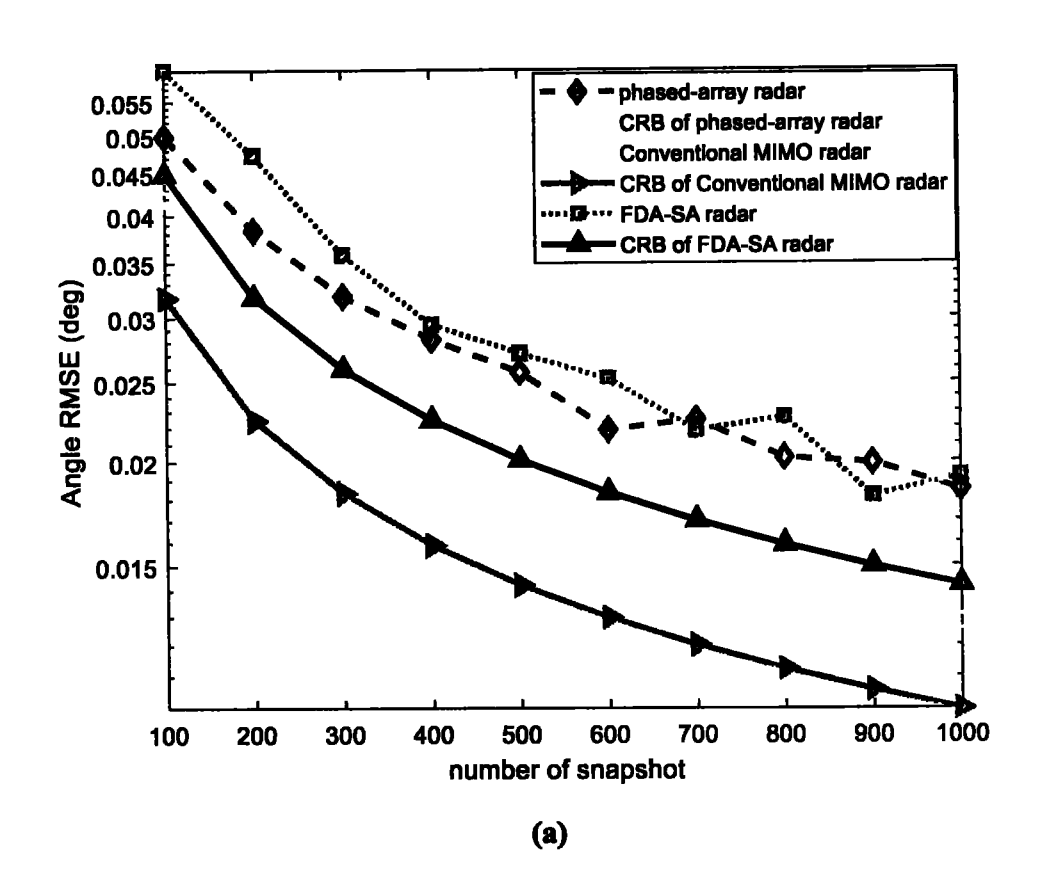


Figure 3.10: RMSE versus SNR for the Range estimation in (a) interference-free environment and (b) interference environment.

From Fig. 3.10 we can extract the following observations: (i) in the interference environment case, the estimates are also biased at high SNRs, (ii) Since the transmit spatial frequency $f_{s,T}$ of PA and MIMO radars are only angle-dependent and the range resolution is depending on the waveform bandwidth which is fixed, therefore the accuracy of the range estimation can't be further improved, and (iii) in the FDA-SA radar, the accuracy of the range estimation can be considerably improved at high SNR, since the $f_{s,T}$ is angle-range dependent.

Figs. 3.11 and 3.12 plot the RMSEs of the angle and range estimates, respectively, with respect to the number of snapshots at SNR, fixed to 0 dB.



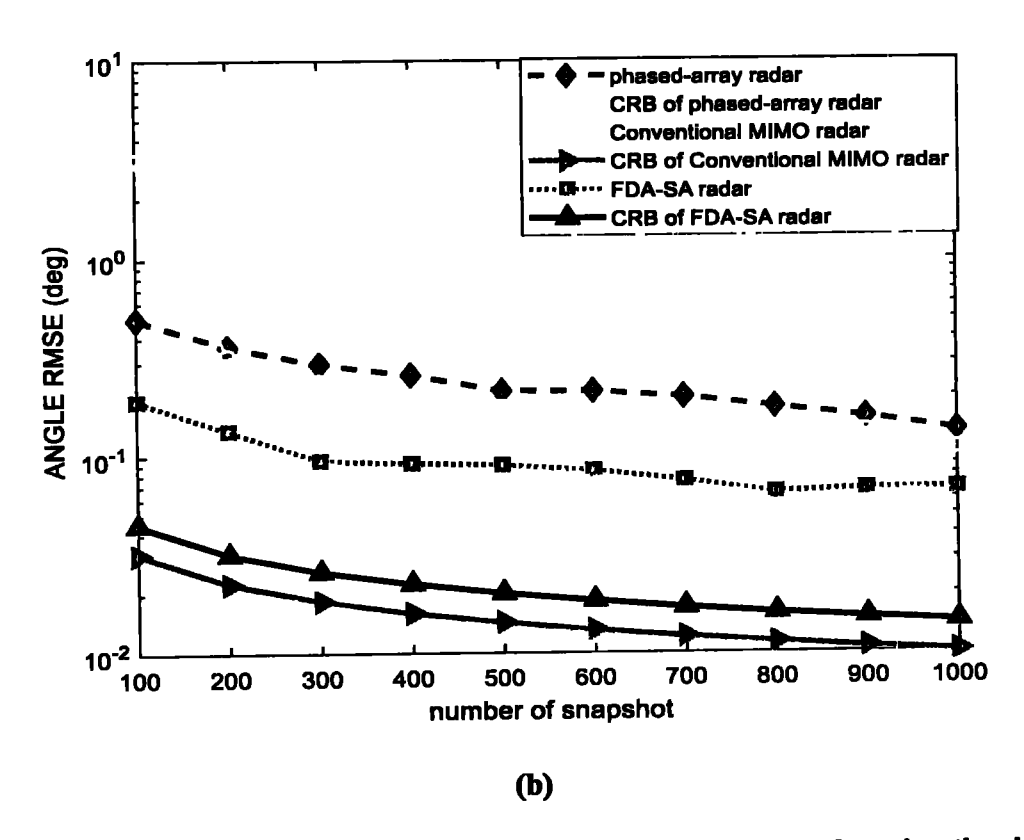
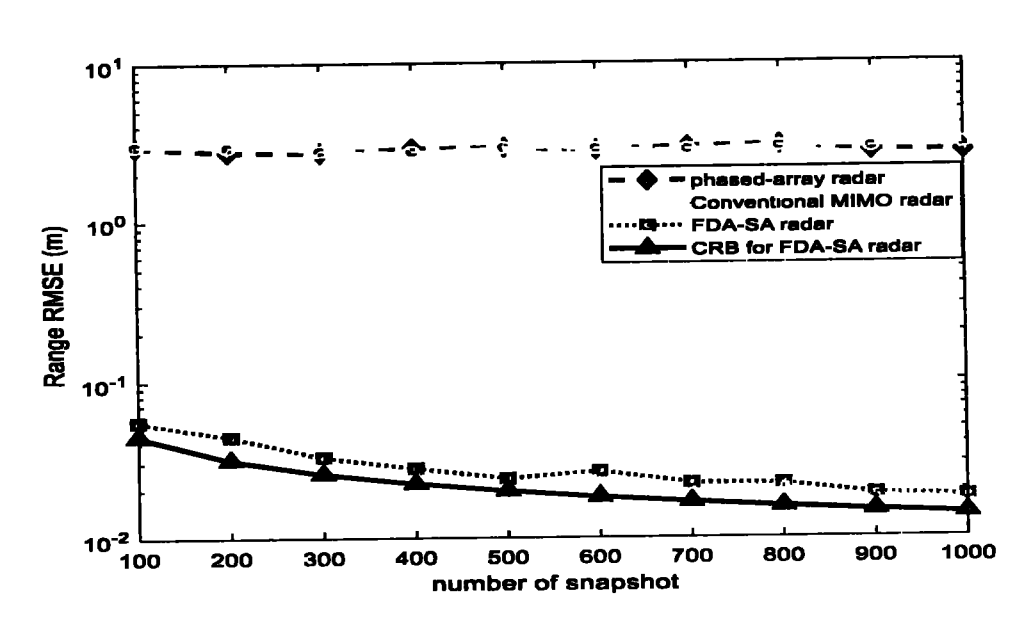


Figure 3.11: RMSE versus the number of snapshots for the Angle estimation in (a) interference-free environment and (b) interference environment.



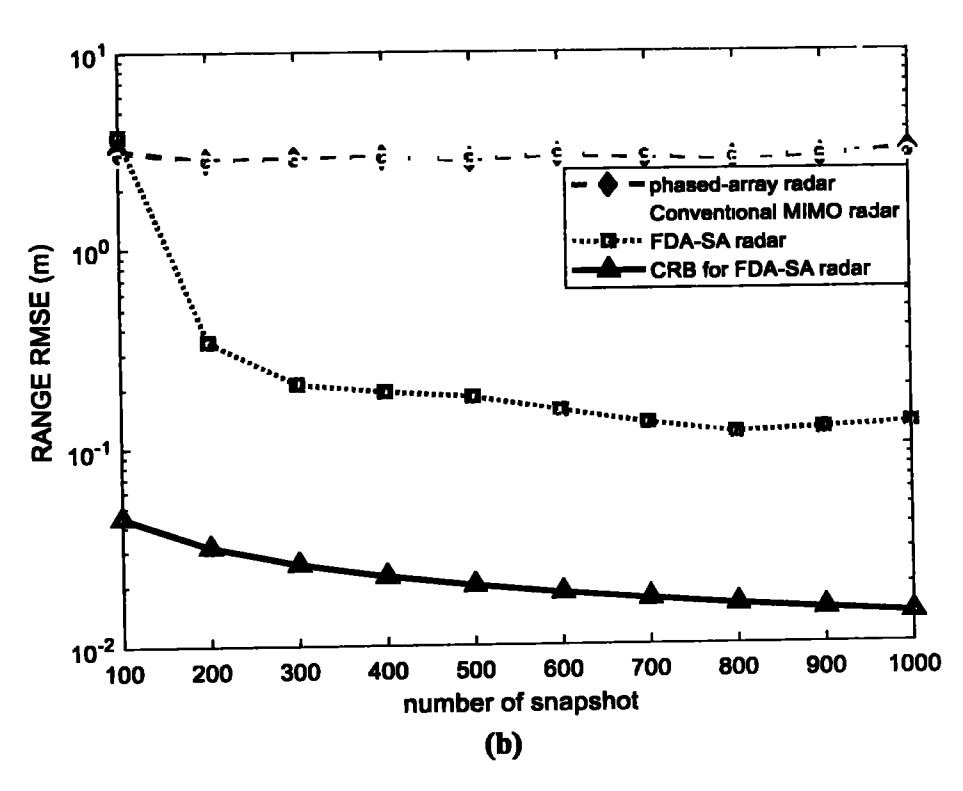


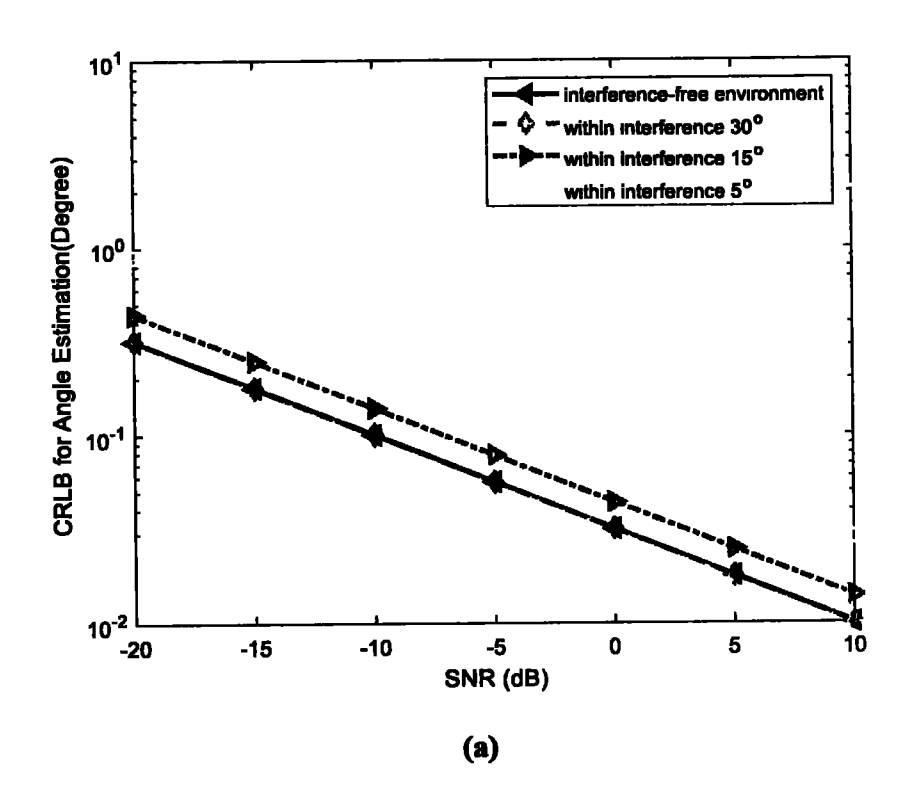
Figure 3.12: RMSE versus the number of snapshots for the Range estimation in (a) interference-free environment and (b) interference environment.

It is shown from Figs 3.11(a) 3.12(a) that, in the interference-free environment the RMSEs of angle and range estimates of the FDA-SA radar are close to their corresponding CRBs. Fig 3.11(a) shows less than 3dB loss in angle estimation performance for FDA-SA radar compared with the conventional MIMO radar performance. In the interference environment as shown in Figs. 3.11(b) and 3.12(b), the angle and range estimation accuracies of the FDA-SA radar, respectively, are higher than those of the conventional MIMO and PA radars. Since the FDA-SA radar can provide a degree of freedom in the range domain, the accuracy of the range estimation is enhanced evidently.

Therefore, despite the performance loss in angle estimation for the FDA-SA radar, it can provide high range resolution and handle efficiently with range ambiguity.

Example 3.3 (CRLB for target parameters):

In this example, we assess the CRLBs performance for the target located at 0° and assuming that the INR is fixed to 30 dB and there are three interferences located at 5°, 15°, and 30°, respectively. Fig. 3.13 plots the CRLBs versus the SNR for angle and range with the presence of interferences and interference-free cases.



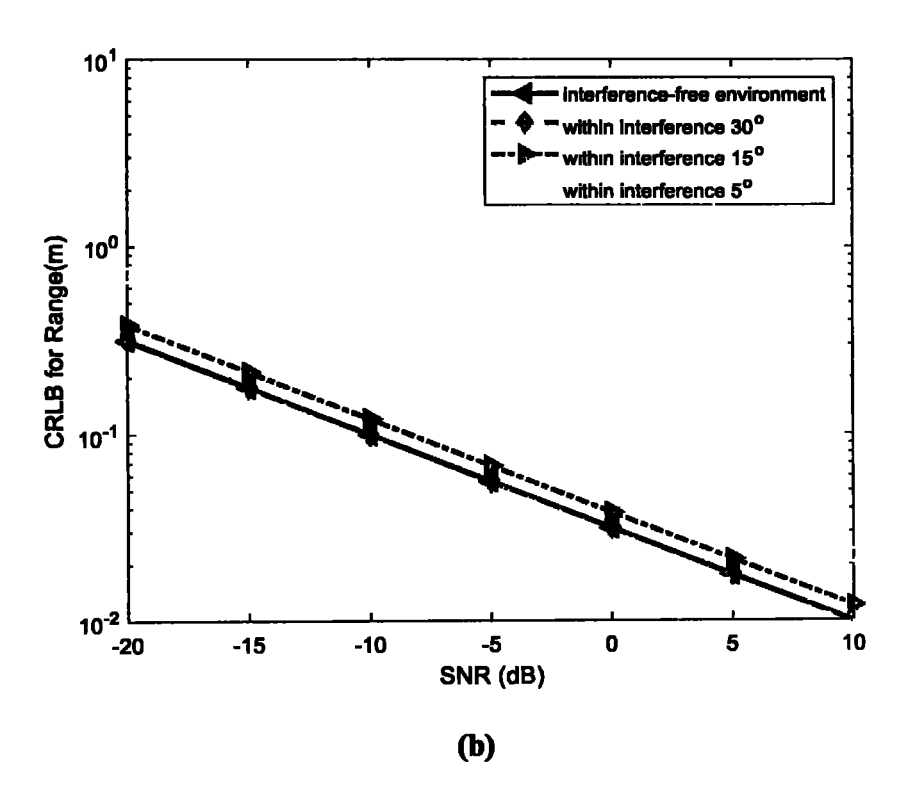


Figure 3.13: CRLB versus SNR (a) Angle parameter and (b) Range parameter.

We can observe the following: (1) the CRLB in the interference-free environment is smaller than of those in the interference environments, (2) the CRLBs are large when the interference is approaching the angle of the target, and (3) in the interference-free environment, the CRLB of the range is smaller than the $\delta r = 10$ meters.

Example 3.4 (Tracking of the maneuvering target (MT)):

This example illustrates the performance of tracking MT using various estimators including the proposed tracking scheme. The initial simulation parameters are provided in Table 3.3.

Table 3.3: Simulation parameters used for target tracking scenario in example 3.4.

Parameters	Setting Values	
The initial state of the target x_0	$[0,0,0,1,0,0]^T$	
The state covariance	diag([0.1, 0.1, 0.1, 0.1, 0.5, 0.5] ^T)	
The measurement matrix H	[100000; 010000]	
The prior probabilities model	$[0.9, 0.1]^T$	
The mode switching probabilities matrix Π	[0.98 0.02] [0.02 0.98]	

The measurement \mathbf{z}_n is made on the target position with Gaussian noise \mathbf{w}_n ,

where
$$E[\mathbf{w}_i \mathbf{w}_j^T] = \begin{bmatrix} 0.1 & 0 \\ 0 & 0.1 \end{bmatrix} \delta_{ij},$$
 (3.99)

where δ_{ij} is the Kronecker delta function. which equals to one if i = j and to zero otherwise.

The simulation is performed with 100 Monte Carlo runs, each has a randomly generated trajectory originating from the same starting point, and a corresponding observation series are generated independently. The motion of the target switches between CV with low process noise (such as PSD =0.1) and CA with high process noise (such as PSD =1). Four maneuvers operation are performed with revisit intervals for the sensor τ_n = 0.1s. In particular, the target motion is set to the CV model during 1-50 s and 71-120 s, while during 51-70 s and 121-150 s, the motion is set to the CA model. The actual trajectory, measurements, and estimates given by the proposed method in one run are shown in Fig. 3.14 (a) and (b), respectively.

For more insights, the RMSEs on the angle and range estimations over time given by KF and the proposed scheme are shown in Fig. 3.15 (a) and (b).

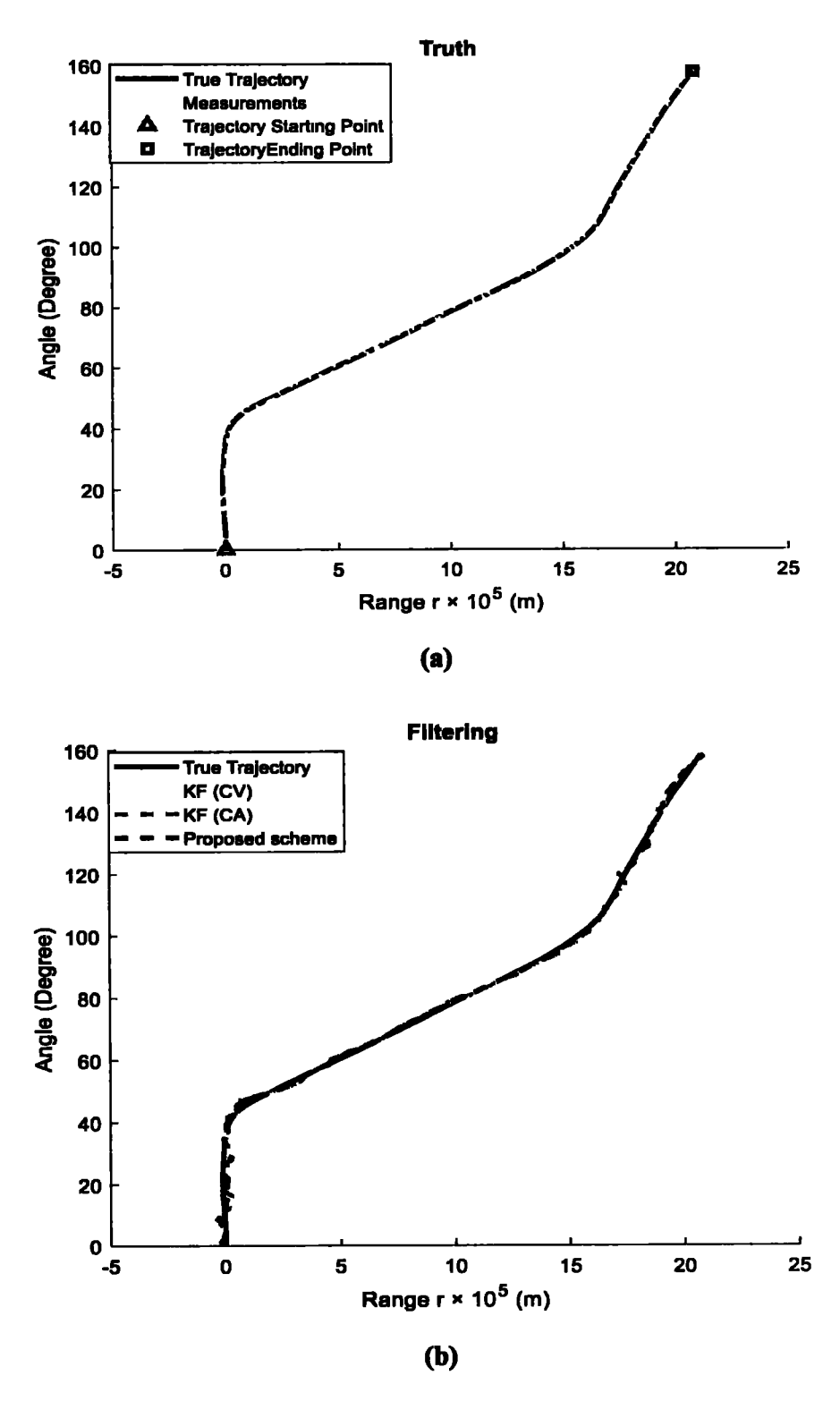
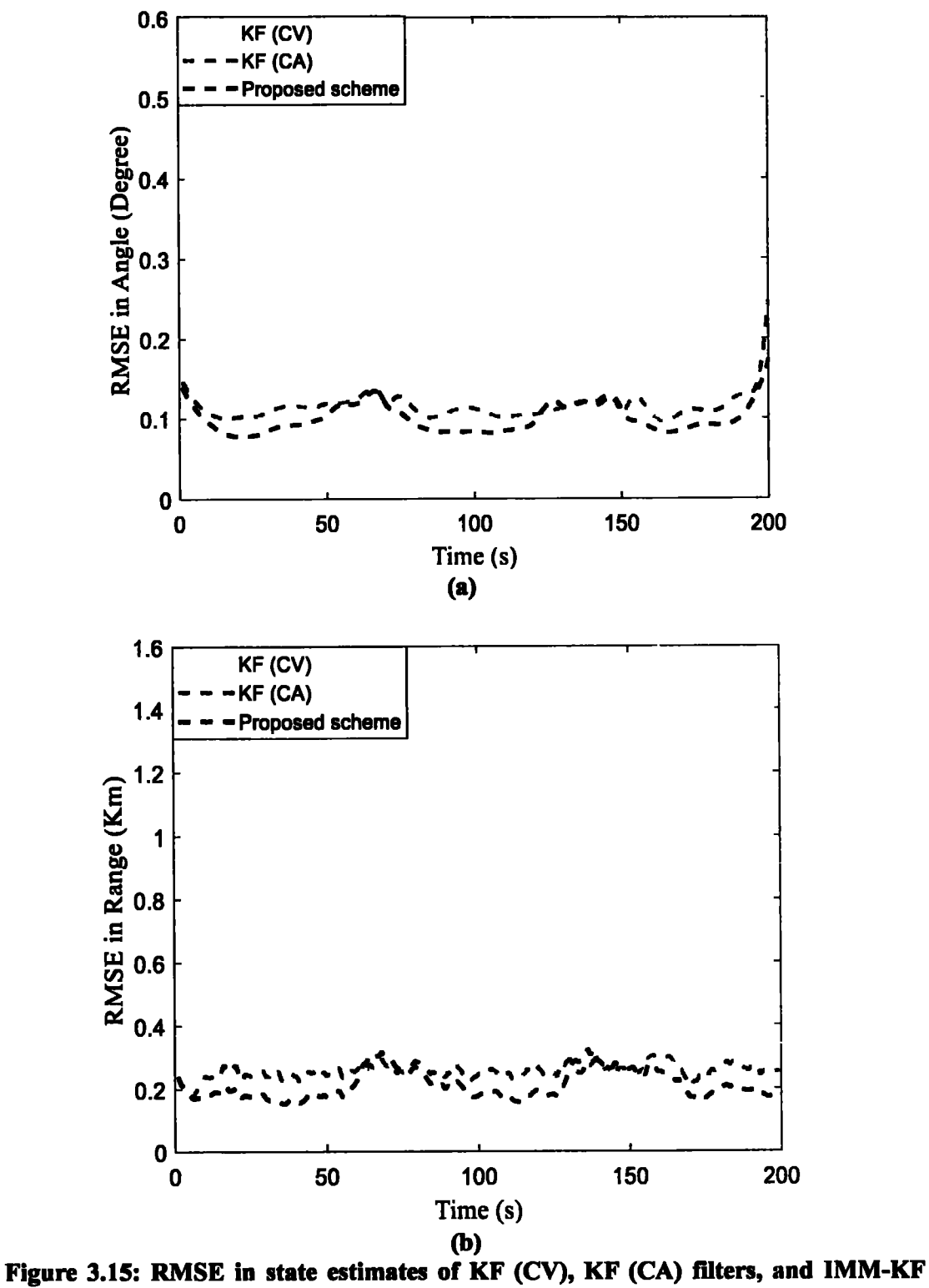


Figure 3.14: (a) Real trajectory and measurements and (b) estimates of the different estimators.



estimator for tracking a maneuvering target. (a) Angle errors. (b) Range errors.

The RMSEs of the angle and range parameters can be calculated, respectively, as:

RMSE
$$(\theta) = \sqrt{\frac{1}{M_c} \sum_{m=1}^{M_c} (\widehat{\theta_{t,m}} - \theta_{t,m})^2}$$
 (3.100)

RMSE
$$(r) = \sqrt{\frac{1}{M_c} \sum_{m=1}^{M_c} (\widehat{r_{t,m}} - r_{t,m})^2}$$
 (3.101)

where $M_c = 100$ is Monte Carlo runs, $\theta_{t,m}$ and $r_{t,m}$ stand for the true position of the target, and $\widehat{\theta_{t,m}}$ and $\widehat{r_{t,m}}$ represent the estimates of the angle and range for the target in the m^{th} Monte Carlo trial, respectively.

The average RMSE of the angle and range parameters and computing time per run performed in MATLAB software are provided in Tables 3.4 and 3.5, respectively.

Table 3.4: Average RMSE performance for angle parameters of different estimators.

Estimators	Average RMSE of Angle (Degree)	Computing Time (s) 0.0043		
KF (using CV)	0.2097			
KF (using CA)	0.1151	0.0047		
IMM-KF	0.0996	0.0727		

Table 3.5: Average RMSE performance for range parameters of different estimators.

Estimators	Average RMSE of Range (Km)	Computing Time (s)		
KF (using CV)	0.4439	0.0011		
KF (using CA)	0.2536	0.0013		
IMM-KF	0.2115	0.0209		

The proposed scheme outperforms the KF using the CV and CA models in terms of estimation accuracy but it is slower than the KF filter in terms of computing speed.

Fig. 3.16 shows the calculated probabilities of the two modes used in this example. It shows that target acceleration makes the CA model more likely, while the CV mode is considered more likely if the target is not accelerating [155].

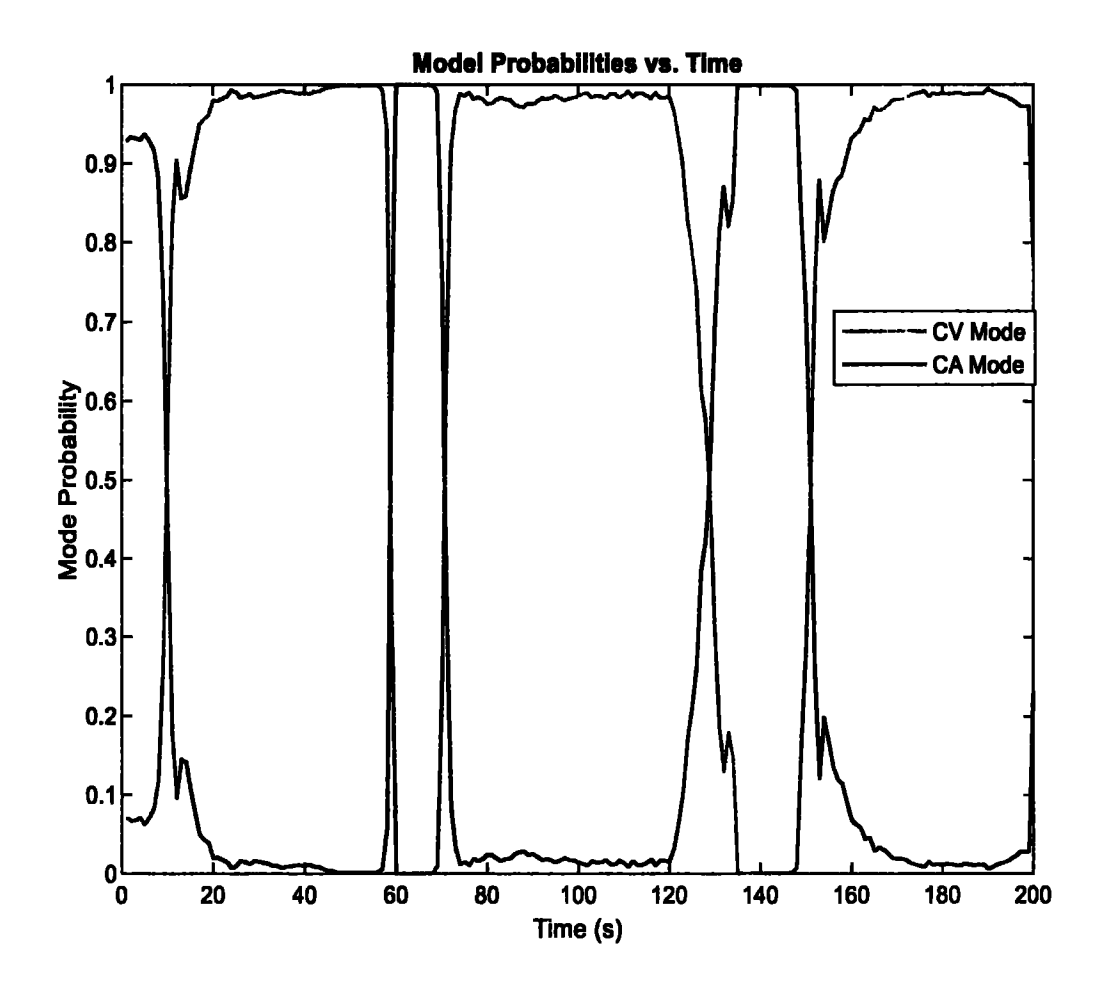


Figure 3.16: Mode probabilities of two-mode IMM algorithm for tracking a maneuvering target.

Fig. 3.17 illustrates the probability detection performance and it indicates that the proposed scheme outperforms the MIMO and FDA designs.

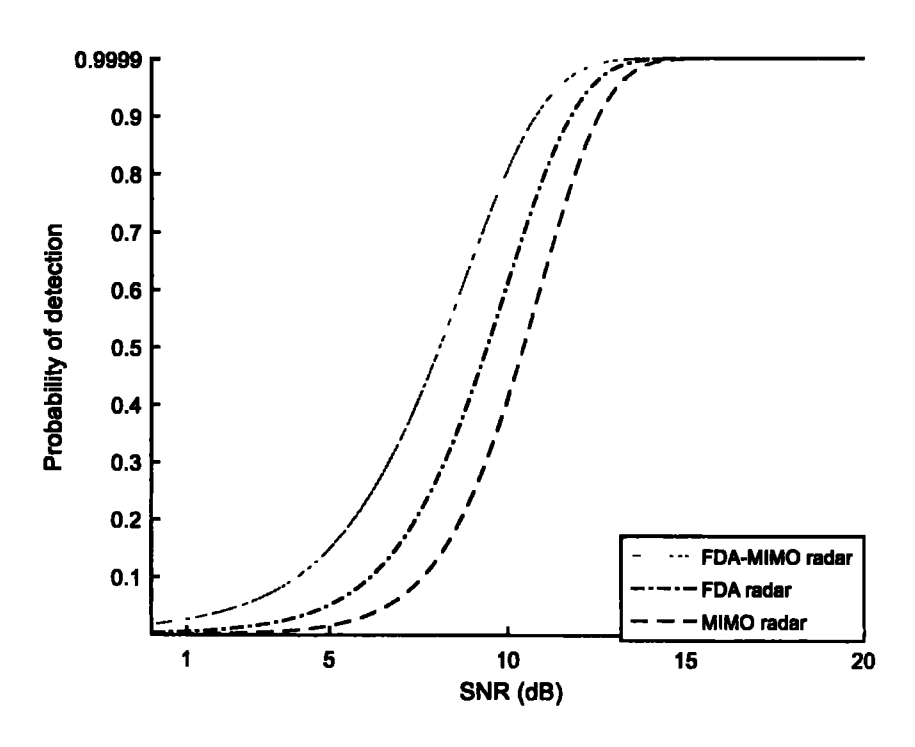


Figure 3.17: The detection performance of the proposed scheme design compared with MIMO and FDA radar systems.

Example 3.5 (Transmit BP synthesis and signal representation at the radar receiver):

The proposed RadCom platform aims to track the distant moving targets and simultaneously embed/deliver information symbols towards the intended communication receiver located at (θ_c, r_c) in the radar operation regions. Let's assume that, at the beginning of the tracking task, the target is moving away from the location of the communication station, and the operating region of the main beam is within the 2-D spatial sector $\theta_t = [-10^{\circ} \ 10^{\circ}]$ and $3 \times 10^{5} \ \text{m} \le r_t \le 3.5 \times 10^{5} \ \text{m}$, and for a communication receiver is $30^{\circ} \le \theta_c \le 40^{\circ}$ and $2 \times 10^{5} \ \text{m} \le r_c \le 2.5 \times 10^{5} \ \text{m}$.

During the current scan, the M-ary APSK strategy is selected by the transmitter for information transmission. In this case, during each radar pulse, the APSK strategy allows

the transmission of different gains towards the communication receiver direction by solving (3.12) and (3.13). Let us assume that, the K=3 (there are 12 radiating elements in each subarray) is selected, and there are two information symbols (assume each contains four bits i.e., $\beta=4$) that can be embedded during each radar pulse. Therefore, the 16-APSK with (5, 11) constellation in Fig. 3.3(a) is applied, where $A_i(i=1,2,...,11)$ are associated with $\overline{\mathbf{W_1}},...,\overline{\mathbf{W_{11}}}$ and $B_j(j=1,2,...,5)$ are associated with $\overline{\mathbf{W_{12}}},...,\overline{\mathbf{W_{16}}}$.

In such a case, the primary BF weight vector $\mathbf{w_1}$ is calculated by (3.12) while $\mathbf{w_2}$ and $\mathbf{w_3}$ are selected from $\mathbf{W} = \{\overline{\mathbf{w_1}}, ..., \overline{\mathbf{w_{16}}}\}$ according to the information available for transmission. Suppose that the information bits to be transmitted are 1010 0110, i.e. A_9B_2 , the equation in (3.30) can be rewritten as:

$$\mathbf{x}_{r}(t;\tau)|_{\mathbf{A}_{9}\mathbf{B}_{2}} = \sqrt{\frac{E}{3}} \alpha_{t}(\tau) \left[\mathbf{q}^{T}(\theta,r)|_{\mathbf{A}_{9}\mathbf{B}_{2}} \mathbf{\psi}(t) \right] \mathbf{b}(\theta) + \mathbf{n}_{d}(t;\tau) + \mathbf{n}_{r}(t;\tau)$$
(3.102)

where $q(\theta, r)|_{A_9B_2}$ can be expressed as:

$$\mathbf{q}(\theta,r)|_{A_{9}B_{2}} = \begin{bmatrix} \mathbf{w_{1}}^{H} \mathbf{a_{1}}(\theta,r) e^{-j \delta_{1,T}(\theta,r)} \\ \overline{\mathbf{w_{9}}}^{H} \mathbf{a_{2}}(\theta,r) e^{-j \delta_{2,T}(\theta,r)} \\ \overline{\mathbf{w_{13}}}^{H} \mathbf{a_{3}}(\theta,r) e^{-j \delta_{3,T}(\theta,r)} \end{bmatrix}$$
(3.103)

According to (3.12) and (3.13), we get:

$$\begin{cases} \mathbf{w_1}^H \mathbf{a_1}(\theta_t, r_t) = 1 \\ \mathbf{w_1}^H \mathbf{a_1}(\theta_c, r_c) = \varepsilon_{max} \\ \overline{\mathbf{w_9}}^H \mathbf{a_2}(\theta_c, r_c) = A_2 e^{-j\varphi_2} \\ \overline{\mathbf{w_{13}}}^H \mathbf{a_3}(\theta_c, r_c) = A_3 e^{-j\varphi_3} \end{cases}$$
(3.104)

It is clear from (3.104) that there are two different levels of magnitude ratios (ε_1 = 1 and ε_2 = 0.146) between each waveform pair. This leads to two gains in the transmit BPs towards the communication direction as shown in Fig. 3.18(a), while the detection performance of the radar target is not influenced by the information transmission process.

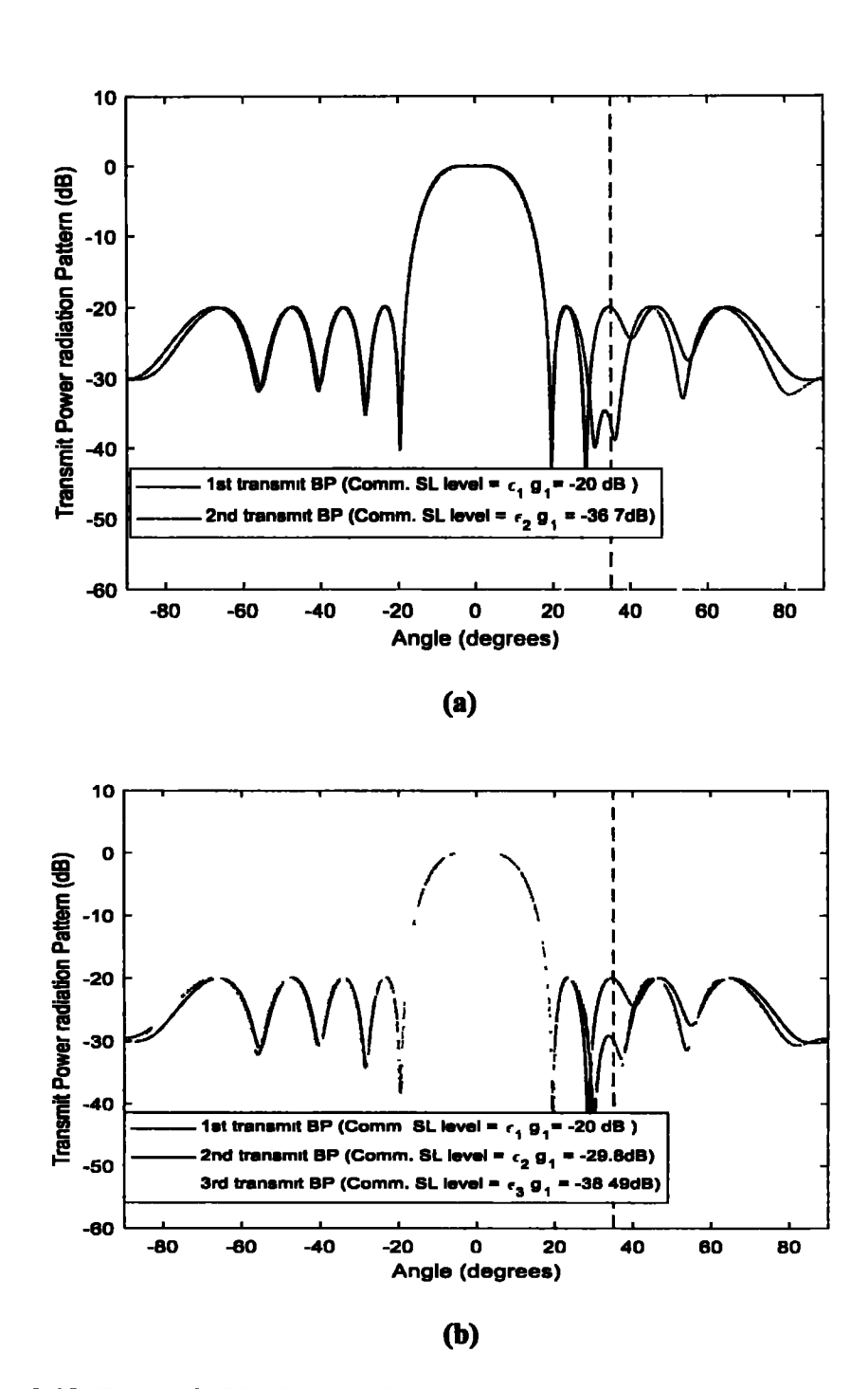


Figure 3.18: Transmit BPs for RadCom signaling strategies vs. angle when K=3 and apply: (a)16- APSK strategy and (b) 32-APSK strategy.

The transmit BP of the joint transmit RadCom platform when K=3 is plotted in Fig. 3.18(a). For the sake of clarification, a 32-APSK with (5, 11, 16) constellation is also plotted in Fig. 3.18(b) with three magnitude ratios (ε_1 =1, ε_2 =0.323, and ε_3 = 0.119). The direction of the communication receiver is represented by the red dashed line.

During the tracking operation, when the target is moving towards the communication receiver and both would be located within the main beam directions, then the M-ary PSK strategy is selected by the transmitter for information transmission. Let us assume that, the K=3 is selected, and there are two information symbols (assume each contains one bit) that can be embedded during each radar pulse. The binary PSK (BPSK) is applied where A_i (i=1,2) are associated with $\widetilde{W_1}$, $\widetilde{W_2}$.

The primary BF weight vector $\mathbf{w_1}$ is calculated by (3.12) while $\mathbf{w_2}$ and $\mathbf{w_3}$ are selected from $\mathbf{W} = \{\widetilde{\mathbf{w_1}}, \ \widetilde{\mathbf{w_2}}\}\$. To embed one bit of information, a phase constellation of the two symbols to be transmitted is assumed to be:

$$Q_{k} = \begin{cases} 1 & angle\left(\frac{\widetilde{w}_{1}^{H} \mathbf{a}_{k}(\theta_{c}, r_{c})}{g_{1}}\right) \in \left[-\frac{\pi}{2}, \frac{\pi}{2}\right] \\ 0 & angle\left(\frac{\widetilde{w}_{2}^{H} \mathbf{a}_{k}(\theta_{c}, r_{c})}{g_{1}}\right) \in \left[\frac{\pi}{2}, \frac{3\pi}{2}\right] \end{cases}$$
(3.105)

Suppose that the information bits to be transmitted are "10" bits, then (3.30) can be rewritten as:

$$\mathbf{x}_{r}(t;\tau)|_{10} = \sqrt{\frac{E}{3}} \alpha_{t}(\tau) [\mathbf{q}^{T}(\theta,r)|_{10} \mathbf{\psi}(t)] \mathbf{b}(\theta) + \mathbf{n}_{d}(t;\tau) + \mathbf{n}_{r}(t;\tau)$$
(3.106)

where $q(\theta, r)|_{10}$ can be expressed as:

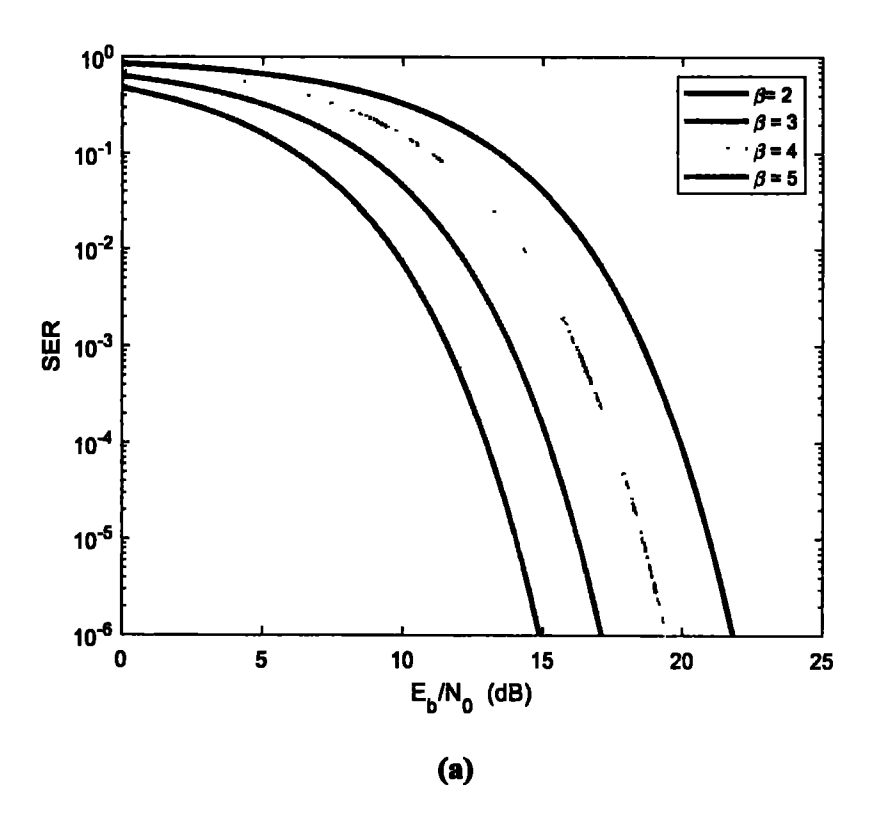
$$\mathbf{q}(\theta,r)|_{10} = \begin{bmatrix} \mathbf{w_1}^H & \mathbf{a_1}(\theta,r) e^{-j \delta_{1,T}(\theta,r)} \\ \widetilde{\mathbf{w_1}}^H & \mathbf{a_2}(\theta,r) e^{-j \delta_{2,T}(\theta,r)} \\ \widetilde{\mathbf{w_2}}^H & \mathbf{a_3}(\theta,r) e^{-j \delta_{3,T}(\theta,r)} \end{bmatrix}$$
(3.107)

According to (3.12) and (3.16), we get:

$$\begin{cases}
\mathbf{w_1}^H \mathbf{a_1}(\theta_t, r_t) = \widetilde{\mathbf{w_1}}^H \mathbf{a_2}(\theta_t, r_t) = \widetilde{\mathbf{w_2}}^H \mathbf{a_3}(\theta_t, r_t) = 1 \\
\mathbf{w_1}^H \mathbf{a_1}(\theta_c, r_c) = \widetilde{\mathbf{w_1}}^H \mathbf{a_2}(\theta_c, r_c) = \widetilde{\mathbf{w_2}}^H \mathbf{a_3}(\theta_c, r_c) = \varepsilon_{max}
\end{cases} (3.108)$$

Hence, we can conclude that the detection performance of the radar target is not influenced by the information transmission process towards the communication direction located at (θ_c, r_c) .

The SER of the proposed RadCom system when K = 3 is plotted in Fig. 3.19 for different information streams using APSK and PSK signaling strategies, respectively.



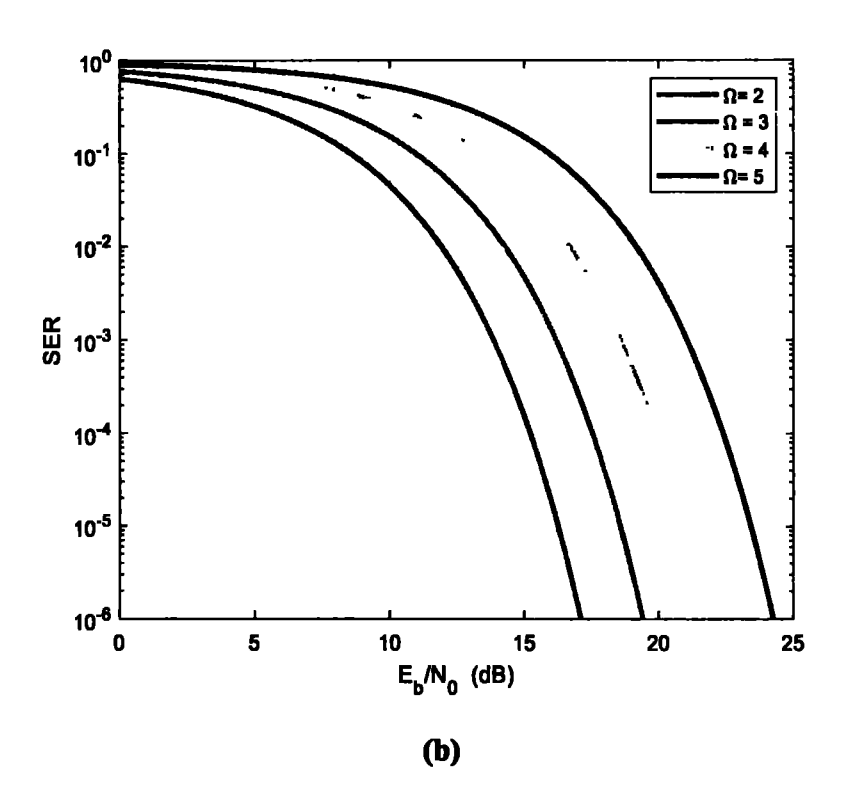


Figure 3.19: SER versus E_b/N_0 when K=3 and: (a) the intended communication receiver is located in the SL directions (b) the intended communication receiver is located within the main beam.

In Fig. 3.19(a), when $\beta = 5$, means that the ten bits of information are transmitted per radar pulse, and the data throughput of 300 Kbits/s can be achieved if the radar PRF is equal to 30 KHz. While in Fig. 3.19(b), when $\Omega = 4$, means that the 8 bits of information stream are transmitted per radar pulse, and the data throughput of 240 K bits/s can be achieved if the radar PRF is assumed to be 30 KHz.

Thus, the maximum achievable data throughput of the proposed system is:

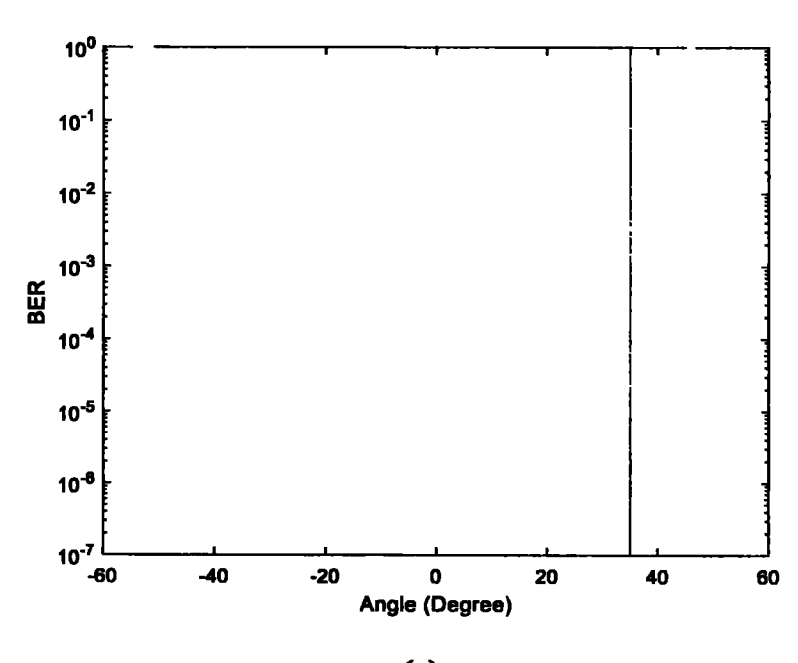
$$R = (K - 1) * (\beta + \Omega) * PRF \text{ bits/s}$$
(3.109)

Note that, we can increase the data throughput of the system by increasing the number of subarrays K while lowering the order of the signaling strategy to limit the SER.

In the SL-based signaling strategies, e.g., [125, 127, 134, 136, 160, 161], the communication receiver should be located in the SL directions so that it can decode the transmitted information symbols otherwise the performance will be significantly degraded. Our proposed design for the RadCom system maintains the communication link towards the intended communication direction during tracking operation.

Example 3.6 (BER performance in angle and range dimensions):

In this example, we evaluate the BER performance of the proposed RadCom system in angle and range dimensions. Let us assume that the communication receiver is located at (35°, 240 Km) and the SNR = 10 dB. Fig. 3.20(a) shows the angular BER for the proposed RadCom system.



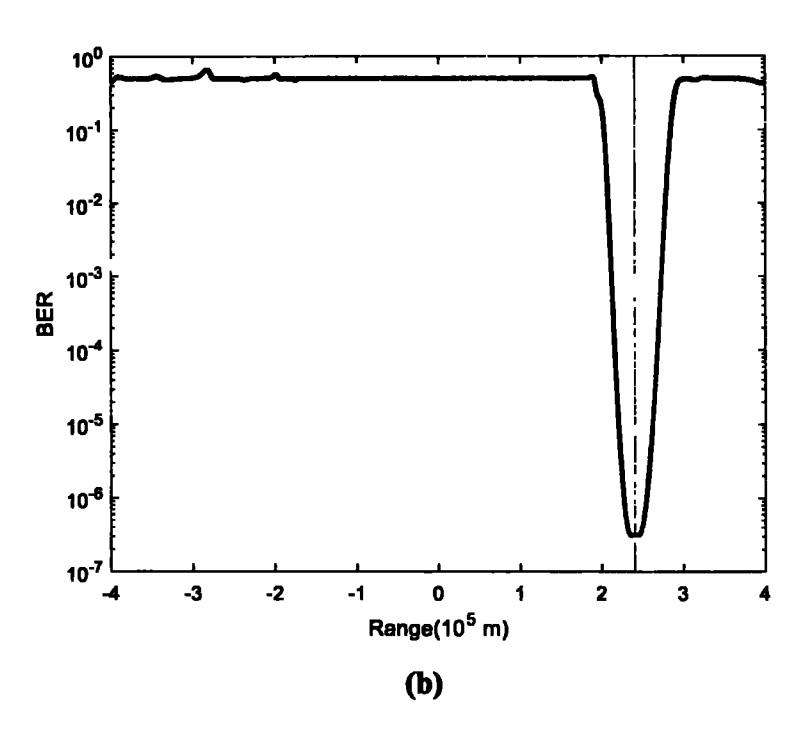


Figure 3.20: BER performance in the direction of the intended communication receiver in (a) angle dimension and (b) range dimension.

It is clear that the only direction that can decode the transmitted information is the direction where the communication station is located i.e., at 35°. The narrow BP towards the communication direction indicates that BP produced by the proposed method is focusing the energy towards the intended direction only. Hence, an inherent secure transmission against information interception is established. Fig. 3.20(b) shows the BER performance versus the range dimension. The only range that can decode the transmitted information is the range where the communication receiver is located i.e. at 240 Km.

In the current radar-communication framework, e.g., [125, 127, 134, 141, 160], the RadCom system is an angle-dependent BP and fixed for all ranges, whereas our proposed

RadCom system is an angle-range-dependent BP and provides a more secure transmission to a specific location.

In summary, the proposed design allows the angle-range dependent RadCom system to maintain the information transmission towards the communication receiver regardless of its location within radar regions. Hence, the overall communication throughput of the system is enhanced. Table 3.6 summarizes the contributions of the proposed design in comparison to the recent existing designs, where L and R denote the allowable SL levels and phases, respectively.

Table 3.6: Comparison between the proposed scheme design with recent existing designs.

Attribute	[134]	[135]	[136]	[141]	[142]	[160]	Proposed scheme design
Closed-loop design	No	No	No	No	No	No	Yes
Angle-range dependent optimization	No	No	Yes	No	No	No	Yes
Information embedding within side lobe (SL)/main lobe	SL	Either	SL	SL	broadcast	SL	Both
Altering the SL levels in pulse basis	Yes	No	Yes	Yes	No	Yes	Yes
Target position tracking	No	No	No	No	No	No	Yes
Achievable data rate	log ₂ L	$(K-1)\log_2 R$	K log ₂ L	K log ₂ LR	K log₂R	K log ₂ L	$(K-1)*(\beta+\Omega)$

3.5. Summary

In this chapter, we have embedded a closed-loop into the system's design to enable the RadCom system to utilize the resources more efficiently. We introduced two signaling strategies that will be selected by the transmitter according to the relative motion of the target. The system performs detection and tracking of the moving target and simultaneously maintains the information transmission towards the communication receiver during each scan. The simulation results verify that the communication performance is enhanced in terms of low SER, secure information transmission, and increased throughput. While for radar applications the performance is improved in terms of target detection and parameter estimation.

CHAPTER-4

MULTI-USER TRANSMISSION FOR RadCom SYSTEMS BASED ON APSK SIGNALING STRATEGY AND WAVEFORM DIVERSITY

In this chapter, an efficient MIMO RadCom system is proposed to improve the system's resource utilization. An alternative approach design is used for beamspace matrix **W** and waveform designs. We utilized either the amplitudes and/or phases of the transmitted radar waveforms, instead of utilizing the magnitude ratios and phase shifts between waveforms as used in Chapter 3 of this thesis, for information embedding towards the communication direction. Accordingly, the proposed APSK signaling strategy allows multi-user access via permitting distinct information bits to be transmitted simultaneously towards the intended communication users located in different directions at the SL region. The information embedding designs have been considered for both modes of communication (coherent and non-coherent). For the tracking applications, we considered two modes for the maneuvering target (MT), namely, constant velocity (CV) and coordinated turn motion (CTM) models in our proposed design. The CTM model characterizes the motion of MT under high acceleration maneuvers with control surfaces where the speed remains nearly constant during maneuvers.

Hence, during each radar illumination, the system carries out target tracking tasks while maintaining the communication symbols transmission towards the intended communication receiver. The simulation results verify the effective performance of the proposed design in terms of target tracking and angular BER. Furthermore, the proposed

APSK signaling strategy provides a significant improvement in terms of enhancing the overall throughput of the system and low BER performance in comparison with the existing SL-based communication signaling strategies.

4.1. Introduction

The RadCom co-design approach has received much attention in recent years [14, 17, 21-23, 125]. Since the system's operating resources are shared for both operations, it is assumed that the primary function of the RadCom system is to fulfill a radar emission and simultaneously allow a secondary information transmission function during the same radar pulse. For example, a multi-waveform SL-based communication used a convex optimization to produce multiple transmit BP having multiple SL power levels, where each level represents a distinct information symbol towards the communication direction in the SL region [125]. Different modulation schemes designs have been developed in the existing literature to embed information into the radar pulse emissions for the RadCom systems [23, 65, 126, 127, 135]. However, there are two constraints for the amplitude modulation SL-based approach: (1) the communication stations should be located in the SL of radar regions, which does not always occur in practical scenarios; (2) the communication throughput of the system is relatively very low. Moreover, the majority of these modulation schemes were proposed for broadcasting mode transmission, where the communication receivers are receiving the same information bits stream.

By employing MIMO configuration into RadCom system designs, multiple orthogonal waveforms are transmitted simultaneously, and thereby waveform diversity could be

exploited [20, 22, 29, 128]. To realize the dual function operation, the transmitted orthogonal waveforms are linearly combined in the far-field region to fulfill a radar emission in one direction and communication operation in another spatial direction [137, 138]. Communication symbols embedding into the emission of MIMO radars have been developed in [122, 142], where the achievable throughput is limited by the number of employed orthogonal waveforms and the PRF of the system.

In this chapter, we proposed a closed-loop design for the MIMO RadCom system where the information embedding strategy is cognitively selected for each illumination according to the location of the communication user in the operational environment. Hence, during each radar illumination, the system carries out target tracking tasks while maintaining the communication symbols transmission towards the intended communication receiver. Moreover, the proposed APSK signaling strategy allows multi-user access via permitting distinct information bits to be transmitted simultaneously towards the communication users located at the SL region in different directions. The performance of the proposed system is analyzed along with simulation results.

4.2. Proposed System Design

The cognitive cycle establishes a closed loop that embodies the transmitter, receiver, and operational environment. The system is reconfigured (updating the transmission parameters) according to the feedback information injected from the receiver to the transmitter. Fig. 4.1 depicts the functional blocks of the proposed system design. The receiver side includes the radar's receiver, memory, and position predictor blocks, while the transmitter includes five sub-blocks that contain signaling strategy selector, memory,

transmit BF weight vectors design, selector of the optimum weight vectors for transmission and lastly the joint transmit platform (JTP).

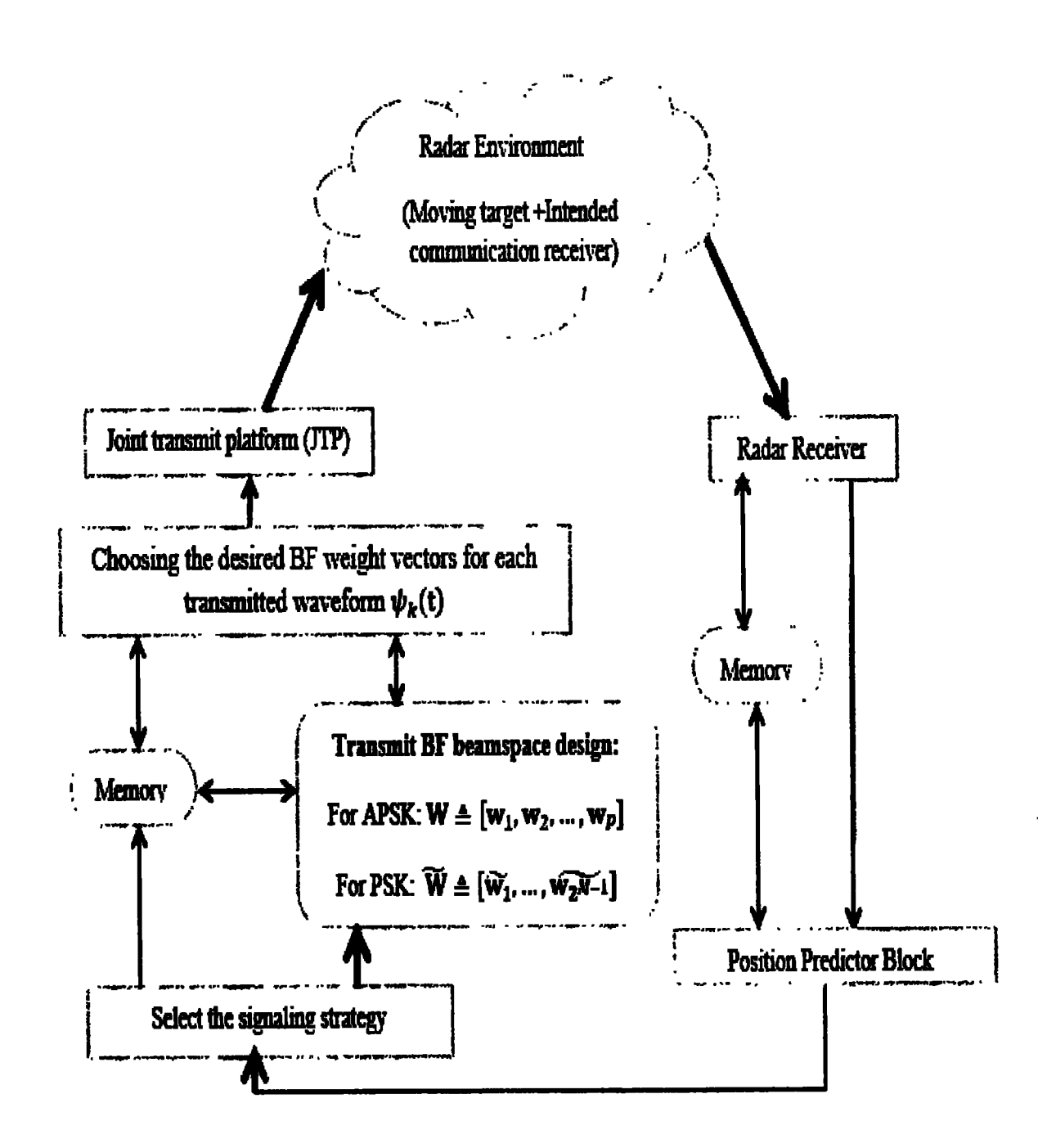


Figure 4.1: The proposed closed-loop design diagram for the RadCom system.

Once the proposed system is linked to the operational environment, the JTP illuminates the radar environment which contains potential moving target and intended communication receiver located at θ_t and θ_t respectively. The radar receiver estimates the target parameters such as DOA and velocity exploiting the reflected signals from the environment. It is worthy to mention that, from the initial scans a library is built which contains the previous and updated estimates of target parameters and then stored in the memory. The estimated target position $\widehat{P_n}$ at time n is forwarded to the prediction algorithm (extended Kalman filter- interacting multiple models (EKF-IMM) estimator) block to estimate the next target position $\widehat{P_{n+1}}$ at time n+1. Next, the receiver feeds back the predicted position of the target to the transmitter, where it compares $\widehat{P_{n+1}}$ with the known location of the communication receiver.

In this case, when the target and communication receiver are both located in the radar main beam directions, the information symbols transmitted towards the communication direction are embedded exclusively in the phases of transmitted waveforms by applying a PSK-based communication strategy. Therefore, the optimum performance for the target detection is maintained. On the other hand, when the communication station is located outside the main beam directions of the transmit BP, a proposed APSK strategy is applied to embed the information symbols by utilizing the amplitude and phase of the transmitted waveforms in the direction of the communication receiver.

Accordingly, the system carries out tracking the moving target as the primary function while maintaining the communication symbols transmission towards the intended communication direction as a secondary function during each illumination. As a result, the overall communication throughput of the proposed system is enhanced.

Note that, the system is operated iteratively and since the transmitter and the receiver are assumed to be co-located, i.e., monostatic system, the feedback is assumed to be always stable.

In the following, we elaborate on each part of the design paradigm independently.

4.2.1. Signal model

Consider a RadCom system with a common transmit antenna array consists of M radiating elements displaced as a uniform linear array (ULA) configuration with an inter-element spacing of d_T . Let $\{\psi_k(t)\}$, k=1,...,K, be the possible unity-energy transmit radar waveforms and they are orthogonal to each other, such that:

$$\int_{T} \left| \psi_{k}(t) \right|^{2} dt = 1 \tag{4.1}$$

$$\int_{T} \psi_{k}(t) \, \psi_{k'}^{*}(t) \, dt = 0, \qquad \text{for } k \neq k'$$
 (4.2)

where T and t denote the time duration of the radar pulse and the fast time, respectively, and (.)* denotes the complex conjugate operator. It is assumed that the co-located radar receiver consists of N receive antennas array with a ULA shape and an inter-element spacing of d_R . It is further assumed that a target in the far-field is seen via transmit and receive arrays from the same angle.

At the input of the JTP, the baseband representation of the transmitted signals can be expressed as:

$$s(t,\tau) = \sqrt{\frac{E}{K}} \sum_{k=1}^{K} \mathbf{w}_k^* \psi_k(t). \tag{4.3}$$

where τ denoting the pulse number, E is the total transmitted energy, and \mathbf{w}_k is the k^{th} transmit BF weight vector associated with the k^{th} waveform. Note that, the total energy E

is distributed equally among K waveforms so that during one radar pulse the transmitted energy equals to E.

The signals in (4.3) can be rewritten as:

$$\mathbf{s}(\mathbf{t},\tau) = \sqrt{\frac{E}{K}} \, \mathbf{W}^* \, \mathbf{\psi}(t) \tag{4.4}$$

where $\mathbf{W} \triangleq [\mathbf{w}_1, \mathbf{w}_2, ..., \mathbf{w}_k]$ is the $M \times K$ transmit weight BF matrix and $\mathbf{\psi}(t) \triangleq [\psi_1(t), ..., \psi_k(t)]$ is the $K \times 1$ orthogonal waveforms vector. Here, the \mathbf{W} and $\mathbf{\psi}(t)$ are assumed to be optimized to fulfill the requirements of the primary radar function while the information transmission being a secondary function can be achieved by modulating the transmit BPs. To utilize the waveform diversity at the radar receiver, the transmit signals should be orthogonal at all Doppler shifts and time-delays within the velocity and range specifications of the MIMO RadCom system. Achieving orthogonal signals with common spectrum contents is impractical and, therefore, in [147] several methods have been studied for designing waveforms with low cross-correlations.

The N \times 1 vector of the received array observations from far-field at an angle θ_t , assuming that the target of interest is located at θ_t , can be expressed as:

$$\mathbf{r}(t;\tau) = \alpha_t(\tau) [\mathbf{a}^T(\theta_t) \mathbf{s}(t,\tau)] \mathbf{b}(\theta_t) + \mathbf{n}(t;\tau)$$

$$= \sqrt{\frac{E}{K}} \alpha_t(\tau) [(\mathbf{W}^H \mathbf{a}(\theta_t))^T \mathbf{\psi}(t)] \mathbf{b}(\theta_t) + \mathbf{n}(t;\tau)$$
(4.5)

where $\alpha_t(\tau)$ is the reflection coefficient of the t^{th} the target which assumed to obey the Swerling-II model [106], (.)^T stands for the transpose operator, and $\mathbf{n}(t;\tau)$ is the $N\times 1$ zero-mean white Gaussian noise vector over the τ^{th} radar pulse.

Generally, $\mathbf{a}(\theta)$ and $\mathbf{b}(\theta)$ denote, respectively, the radar steering vectors of the transmit and the receive arrays towards angle θ and can be defined, respectively, as:

$$\mathbf{a}(\theta) = \left[1, e^{jk_0 d_T \sin \theta}, \dots, e^{jk_0 (M-1) d_T \sin \theta}\right]^T \tag{4.6}$$

$$\mathbf{b}(\theta) = \left[1, e^{jk_0 d_R \sin \theta}, \dots, e^{jk_0 (N-1) d_R \sin \theta}\right]^T \tag{4.7}$$

where $k_0 = 2\pi/\lambda$ is the wavenumber.

4.2.2. Transmit beamspace design and information embedding schemes

In this section, we present the design of transmitting BF weight vectors and proposed communication signaling schemes into radar radiation. Let $\Theta = [\theta_{min}, \theta_{max}]$ be the set of angles that form a spatial sector in which the radar main beam operates, i.e. where the transmitted power must be concentrated while keeping the power of the transmit emission pattern in the SL region below a certain predetermined threshold.

In the following, we introduce the signaling strategies applied for the information embedding process and their corresponding optimized transmit BF weight vectors designs that would be selected by the transmitter according to the location of the communication receiver in the transmit BP radiations during each illumination.

4.2.2.1. APSK-based information embedding scheme

During the tracking operation, when the radar target is moving within the radar operation region and the location of the communication receiver is outside the main lobe directions, i.e., within the radar SL region. In this case, as the communication receiver θ_l remains outside the main beam, a RadCom system can serve the communication receiver with information bits by selecting a proposed APSK communication scheme. Here, during each

radar pulse, the information embedded by controlling the amplitude levels as well as phase shifts of multiple radar waveforms radiated towards the communication receiver located in the SL region.

Thus, by solving the following convex optimization problem, the BF weight vectors for the proposed APSK signaling strategy can be calculated as:

$$\min_{\mathbf{w}_n} \max_{\theta_t} \left| e^{j\mu(\theta_t)} - \mathbf{w}_p^H \mathbf{a}(\theta_t) \right|, \qquad \theta_t \in \mathbf{\Theta}$$

Subject to
$$|\mathbf{w}_{n}^{H}\mathbf{a}(\theta_{s})| \leq \varepsilon_{max}$$
, $\theta_{s} \in \overline{\Theta}$ (4.8)

$$\mathbf{w}_{p}^{H}\mathbf{a}(\theta_{l}) = A_{p}(\theta_{l}) e^{j\varphi_{p}(\theta_{l})}, \qquad p = 1, 2, \dots, P. \quad \theta_{l} \in \overline{\Theta}$$
(4.9)

where $\mu(\theta)$ is the phase profile selected by the user, $\overline{\Theta}$ is representing the SL region, and ε_{max} is a positive number that indicates the highest allowable SL level. Here, \mathbf{w}_p is the p^{th} BF vector which achieves the desired SL level $A_p(\theta_l)$ as well as phase profile $e^{j\phi_p(\theta_l)}$ in the direction of θ_l . Note that, each SL level term $A_p(\theta_l)$ can assign any of the L permissible SL levels and also this applied for the phase term $e^{j\phi_p(\theta_l)}$ which can take any of the R permissible phases.

Thus, each \mathbf{w}_p , p=1,...,P, is representing a distinct APSK symbol in the direction of the communication receiver during each radar pulse. Accordingly, by solving (4.9) for P times all possible transmit BF weight vectors are produced, and the \mathbf{w}_p , p=1,...,P, that corresponds to the desired APSK symbol is selected for transmission towards the communication receiver.

Therefore, the transmitted signal (4.4) can be rewritten as:

$$\mathbf{s}(\mathbf{t},\tau) = \sqrt{\frac{E}{K}} \mathbf{W}^* \mathbf{B} (\tau) \mathbf{\psi}(t)$$
 (4.10)

Here, $\mathbf{W} \triangleq [\mathbf{w}_1, \mathbf{w}_2, ..., \mathbf{w}_P]$ is the $M \times P$ transmit weight BF matrix that includes P transmit BF weight vectors and $\mathbf{B}(\tau) \triangleq [\mathbf{b}_1(\tau), \mathbf{b}_2(\tau), ..., \mathbf{b}_K(\tau)]$ is $P \times K$ selection matrix that selects the desired transmit BF weight vectors from \mathbf{W} for each transmitted waveform $\psi_k(t), k = 1, ..., K$. The k^{th} selection vector $\mathbf{b}_k(\tau) \triangleq [b_{1,k}(\tau), b_{2,k}(\tau), ..., b_{P,k}(\tau)]^T$, k = 1, ..., K, is the $P \times 1$ vector such that only one element in $\mathbf{b}_k(\tau)$ is equal to 1 and the remaining elements are zeros.

Notice that, the transmit beamspace matrix **W** acts as the dictionary for the optimized transmit BF weight vectors.

For coherent transmission mode, where the phase synchronization is required to achieve accurate detection, the embedded APSK communication symbol is transmitted towards the communication direction θ_t is given by:

$$g_{p(APSK)}(\theta_i) \triangleq \mathbf{w}_p^H \mathbf{a}(\theta_i) = A_p(\theta_i) e^{j\varphi_p(\theta_i)}, \qquad 1 \leq p \leq K$$
 (4.11)

Any synchronization mismatch results in performance degradation. To avoid this limitation, a non-coherent communication mode is applied in which $\psi_1(t)$ is selected as reference waveform along with \mathbf{w}_1 as reference transmit BF weight vector by setting $\mathbf{b}_1(\tau) = [1, \mathbf{0}_{P-1}]^T$. In this case, the transmitted embedded message in the communication direction θ_l is given by:

$$g_{p(APSK)}(\theta_l) \triangleq \frac{\mathbf{w}_p^H \mathbf{a}(\theta_l)}{\mathbf{w}_1^H \mathbf{a}(\theta_l)}, \qquad 2 \le p \le P \le K \qquad (4.12)$$

Note that from (4.11) and (4.12), the transmitted APSK symbol has a magnitude component $|g_{p(APSK)}(\theta_i)|$ and phase component $angle(g_{p(APSK)}(\theta_i))$ in the communication direction of θ_i .

4.2.2.2. PSK-based information embedding scheme

Here, during the tracking task scenario, when the target is moving within the operational radar environment and the communication receiver and the target are both located within the radar main lobe region Θ as shown in Fig. 3.2(b) in chapter 3. Thus, to maintain the target detection performance, PSK-based communication is selected by the transmitter for information embedding that would be transmitted towards the communication receiver.

According to [162], there exists $(2^{M-1}-1)$ BF weight vectors that can be produced from the principle BF weight vector such that all vectors would exhibit the same transmit BP radiation but each vector has a distinct phase profile. Therefore, if the $\widetilde{\mathbf{w}}_1$ is selected as the principle transmit BF weight vector from $\widetilde{\mathbf{W}} = [\widetilde{\mathbf{w}}_1, ..., \widetilde{\mathbf{w}}_{2^{M-1}}]$, which can be determined by solving the optimization problem in (4.9) and (4.10) as follows:

$$\min_{\mathbf{W}_1} \max_{\theta} \left| e^{j\mu(\theta)} - \widetilde{\mathbf{W}_1}^H \mathbf{a}(\theta) \right|$$

Subject to
$$\widetilde{\mathbf{W}_1}^H \mathbf{a}(\theta_t) = 1$$
, $\theta_t \in \mathbf{\Theta}$ (4.13)

$$\widehat{\mathbf{w}_{1}}^{H}\mathbf{a}(\theta_{i}) = A e^{j\phi_{1}} \qquad \qquad \theta_{i} \in \mathbf{\Theta}$$
 (4.14)

Here, A is a constant value and can be set to one, and ϕ_1 represents the phase information associated with the principal BF weight vector. i.e, \mathbf{W}_1 .

The remaining transmit BF weight vectors in \mathbf{W} can be determined using the technique developed in [133], where the information bits are embedded by controlling only the phases of the transmitted waveforms.

In this case, the signal transmitted from the JTP is given as:

$$\mathbf{s}(\mathsf{t},\tau) = \sqrt{\frac{E}{K}} \ \widetilde{\mathbf{W}}^* \mathbf{B} (\tau) \, \psi(t) \tag{4.15}$$

Here, $\widetilde{\mathbf{W}}$ is the $M \times 2^{M-1}$ transmit beamspace matrix while the dimension of the selection matrix $\mathbf{B}(\tau)$ is $2^{M-1} \times K$. The k^{th} selection vector $\mathbf{b}_k(\tau)$ is with the dimension of $2^{M-1} \times 1$.

For coherent transmission mode, the phase-embedded communication symbol is transmitted towards the communication direction θ_i is given by:

$$g_{k(PSK)}(\theta_i) \triangleq angle\left(\widetilde{\mathbf{W}_k}^H \mathbf{a}(\theta_i)\right) = A e^{j\phi_k}, \quad 1 \leq k \leq 2^{M-1} \leq K \quad (4.16)$$

For non-coherent communication, $\psi_1(t)$ is selected as the reference waveform along with \widetilde{w}_1 as the reference transmit BF weight vector via setting $\mathbf{b}_1(\tau) = [1, \ \mathbf{0}_{2^{M-1}-1}]^T$. In this case, the transmitted phase-embedded message towards the communication direction θ_l can be expressed as:

$$g_{k(PSK)}(\theta_l) \triangleq angle\left(\frac{\widetilde{w_k}^H a(\theta_l)}{\widetilde{w_l}^H a(\theta_l)}\right), \qquad 2 \leq k \leq 2^{M-1} \leq K$$
 (4.17)

Notice that the transmit beamspace matrix $\widetilde{\mathbf{W}}$ acts as the dictionary of the optimized BF weight vectors.

Hence, our proposed design for the MIMO RadCom system is different from the current literature of the radar-communication framework. It maintains the communication link towards the intended communication receiver during each illumination. As a result, the overall performance and the throughput of the system are enhanced.

Algorithm 4.1. illustrates the selection mechanism of the information embedding strategy during each radar scan.

ALGORITHM 4.1: Algorithm for information embedding scheme selection during each radar scan.

At the RadCom receiver (one cognitive cycle): $P_{n-1} = [\theta_{t,n-1}, v_{t,n-1}]$ (previous estimated target's parameters).

- 1: Estimate the parameters for the moving target at a time t_n , i.e. currently estimated parameters \widehat{P}_n .
- 2: Update the information library with new estimated values.
- 3: Forward the new estimated values to the predictor position algorithm (EKF-IMM algorithm) to estimate the next position of the moving target $\widehat{P_{n+1}}$.
- 4: Feedback $\widehat{P_{n+1}}$ to the transmitter.
- 5: At the transmitter: Compare $\widehat{P_{n+1}}$ with the known location of the communication receiver θ_l .
- 6: if $(\theta_i \in \Theta)$
- 7: Select PSK modulation scheme for information embedding towards θ_i , then (4.14) and (4.16) are used.
- 8: else
- 9: $\theta_i \in \overline{\Theta}$
- 10: Select APSK modulation scheme for information embedding, then (4.9) and (4.11) are applied.
- 11: end if
- 12: Go to step 1

In Algorithm 4.1, the radar receiver estimates the target parameters such as the direction of arrival (DOA), range, and velocity utilizing the reflected signals from the environment. The estimated target position \widehat{P}_n at time n is forwarded to the predictor position block to estimate the next target position \widehat{P}_{n+1} at time n+1. Next, the receiver feeds back the predicted position of the target to the transmitter, which compares \widehat{P}_{n+1} with the prior knowledge of the communication receiver location θ_l . Then, whenever the location of the communication receiver is within the main beam directions, the transmitter selects the PSK-based communication strategy for information transmission. On the other hand, whenever the location of the communication receiver is outside the main beam directions, the transmitter selects the proposed APSK strategy for information transmission. Thus, during each radar scan, the proposed cognitive selection of the information embedding strategies maintains the communication symbols transmission to the intended communication receiver.

Note that, such a transmit beamspace design requires careful design to make sure that the radar operation is not disturbed. This demands that the autocorrelation for different waveform designs remains constant regardless of the alteration in transmitting information symbols. In the context of the communications operation, the cross-correlation between different pairs of transmitting information symbols and associated waveforms should be as small as possible.

The transmission framework of the proposed system configuration is illustrated in Fig. 4.2.

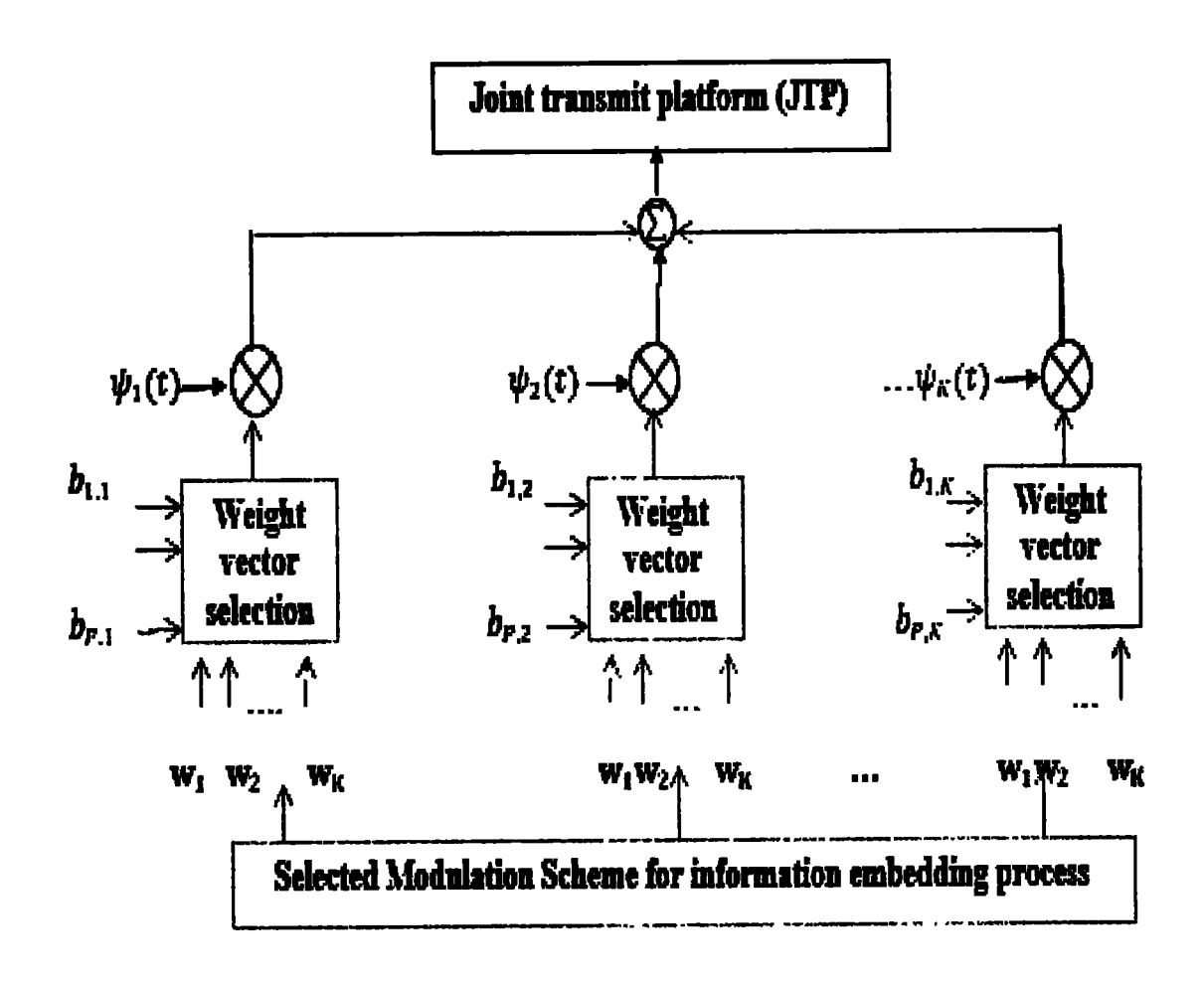


Figure 4.2: Signal Transmission diagram for the proposed MIMO RadCom system.

4.2.3. Communication symbol detection at the communication receiver

For communication symbol detection, the communication receiver located at θ_i , within the system illumination regions, is assumed to have a perfect knowledge of the $\psi_k(t)$, k=1,2,...,K. Therefore, the received signal at the output of the communication receiver can be written as:

$$x_i(t; \tau) = \alpha_{ch}(\tau) \left[\mathbf{a}^T(\theta_i) \ \mathbf{s}(t; \tau) \right] + z_i(t; \tau) \tag{4.18}$$

where $\alpha_{ch}(\tau)$ represents a complex channel response during the τ^{th} radar pulse and $z_i(t;\tau)$ is the white Gaussian noise with zero mean and variance σ^2_i .

Equation (4.18) can be rewritten as:

$$x_{i}(t; \tau) = \sqrt{\frac{E}{K}} \alpha_{ch}(\tau) \left[\sum_{k=1}^{K} g_{k} \psi_{k}(t) \right] + z_{i}(t; \tau), \quad 1 \le k \le K \quad (4.19)$$

where $g_k \triangleq \mathbf{w}_k^H \mathbf{a}(\theta_i)$ is the received gain associated with the k^{th} BF weight vector towards the communication receiver located at θ_i .

Then, by matched-filtering the $x_l(t; \tau)$ to $\psi_k(t)$, $1 \le k \le K$, during each radar pulse yields:

$$y_{i,k}(\tau) = \frac{1}{T} \int_0^T x_i(t; \tau) \psi_k(t) dt$$

$$= \sqrt{\frac{E}{K}} \alpha_{ch}(\tau) \left(\mathbf{w}_k^H \mathbf{a}(\theta_i) \right) + \widetilde{z_k}(\tau)$$

$$= \sqrt{\frac{E}{K}} \alpha_{ch}(\tau) g_k + \widetilde{z_k}(\tau), \qquad 1 \le k \le K \quad (4.20)$$

Here $\widetilde{z}_k(\tau)$ represents the output noise obtained after matched filtering and modeled as zero-mean white Gaussian noise with variance σ^2_k .

For coherent and non-coherent communication modes, let's define the k^{th} received communication symbol at the communication receiver located at θ_l , respectively, as:

$$s_{kc}(\theta_i) \triangleq y_{i,k}(\tau), \qquad 1 \le k \le K$$
 (4.21)

$$s_{kn}\left(\theta_{i}\right) \triangleq \frac{y_{i,k}(\tau)}{y_{i,1}(\tau)}, \qquad 1 \leq k \leq K \qquad (4.22)$$

The received communication symbol would have a magnitude component and a phase component. Thus, during the tracking operation, if the intended communication receiver is located at the SL region, then it can decode the transmitted APSK communication symbols by determining the SL levels and phases during each radar pulse as:

$$\widehat{A_p} = |s_k(\theta_i)| \tag{4.23}$$

and

$$\widehat{\varphi_p} = angle(s_k(\theta_i)) \tag{4.24}$$

On the other hand, if the communication receiver is located within the main beam directions during the tracking operation, then A_p in (4.23) is set as 1, and the k^{th} embedded phase symbol ϕ_k can be estimated using (4.24) and mapped to the embedded phase-bits.

4.2.4. Echo processing at the radar receiver

The N \times 1 vector of the received array observations from the far-field point located at θ_t , assuming that the target of interest is located at θ_t , is modeled in (4.5). Then, by matched-filtering the received signal $\mathbf{r}(t;\tau)$ to the $\psi_k(t)$, k=1,...,K, yields the $KN\times 1$ vector of virtual received data, that is:

$$y(\tau) = Vec\left(\int_{T} \mathbf{r}(t;\tau) \, \mathbf{\psi}^{H}(t) \, dt\right),$$

$$= \sqrt{\frac{B}{K}} \, \alpha_{t}(\tau) \left[\left(\mathbf{W}^{H} \mathbf{a}(\theta_{t}) \right) \otimes \mathbf{b}(\theta_{t}) \right] + \widetilde{\mathbf{n}}(\tau) \tag{4.25}$$

where Vec(.) is the operator that stacks the columns of a matrix into one column vector, \otimes denotes the Kronecker product, and $\widetilde{\mathbf{n}}(\tau)$ is the $KN \times 1$ noise term after matched-filtering and modeled as additive Gaussian with zero mean and variance $\sigma^2 \mathbf{I}_{KN}$, where \mathbf{I}_{KN} is the identity matrix of dimension $KN \times KN$, and can be defined as:

$$\widetilde{\mathbf{n}}(\tau) = \operatorname{Vec}\left(\int_{T} \mathbf{n}(t;\tau) \, \mathbf{\psi}^{H}(t) \, dt\right) \tag{4.26}$$

Thus, the $KN \times 1$ virtual received data vector after matched filtering can be rewritten as:

$$\mathbf{y}_{r} = \left[\mathbf{y}_{r,1}^{T}(\tau), \dots, \mathbf{y}_{r,K}^{T}(\tau) \right]^{T}$$

$$= \sqrt{\frac{E}{K}} \alpha_{t} \left[\mathbf{h}(\theta_{t}) \otimes \mathbf{b}(\theta_{t}) \right] + \widetilde{\mathbf{n}}$$
(4.27)

where $\mathbf{h}(\theta_t) \triangleq \mathbf{W}^H \mathbf{a}(\theta_t)$. For Doppler application, if the target has a radial velocity v_r , then the received signals are shifted in frequency by Doppler shift, $f_d = \frac{2v_r}{\lambda}$, where λ is the wavelength. Let

$$\mathbf{a}_r(\theta_t) = \mathbf{h}(\theta_t) \otimes \mathbf{b}(\theta_t) \tag{4.28}$$

Then, we further extend the (4.27) to include the moving target scenario as:

$$\mathbf{y}_{r(mov)} = \sqrt{\frac{E}{K}} \alpha_t \left[\mathbf{a}_d(f_d) \otimes \mathbf{a}_r(\theta_t) \right] + \widetilde{\mathbf{n}}$$
 (4.29)

where $a_d(f_d)$ is the Doppler vector which can be expressed as:

$$\mathbf{a}_{d}(f_{d}) = \left[1, e^{j2\pi f_{d}T}, \dots, e^{j2\pi(L-1)f_{d}T}\right]^{T}$$
(4.30)

where L is the sampling number. Then (4.27) can be rewritten as:

$$\mathbf{y}_{r(mov)} = \sqrt{\frac{E}{\kappa}} \alpha_t \mathbf{u}_{mov} (\theta_t, f_d) + \widetilde{\mathbf{n}}$$
 (4.31)

where $\mathbf{u}_{mov}(\theta_t, f_d)$ represents a joint angle-Doppler steering vector and is given by:

$$\mathbf{u}_{mov}(\theta_t, f_d) = \mathbf{a}_d(f_d) \otimes \mathbf{a}_r(\theta_t) \tag{4.32}$$

The Doppler frequency can be expressed, for the constant velocity and accelerated moving target, respectively, as:

$$f_d = \frac{2v_0}{\lambda} \tag{4.33}$$

and

$$f_d = \frac{2(v_o + a_s t_s)}{\lambda}$$
 (4.34)

where v_o , a_s , and t_s denote the constant velocity, acceleration, and slow time dimension, respectively.

It may be visible from the (4.31) that, the joint estimation of angle-Doppler parameters for the moving targets can be achieved by utilizing the MIMO RadCom array arrangement and when it is combined with the MIMO coherent-time integration, the Doppler resolution can be significantly improved.

4.2.5. Tracking algorithm

In tracking scenarios, a maneuvering target (MT) is considered as a nonlinear dynamical system characterized by several possible operation regimes, which can be described as a sudden change in the dynamic motion equation of the system. An efficient and robust approach for tracking the MT scenario is modeling the situation as the state estimation problem with Markovian switching coefficients [153].

In this chapter, we consider two modes for the MT, namely, constant velocity (CV) and coordinated turn motion (CTM) models in our proposed design. The CTM model characterizes the motion of MT under high acceleration maneuvers with control surfaces where the speed remains nearly constant during maneuvers. The EKF-IMM estimator is a typical approach for such an estimation problem [154, 163, 164].

The dynamical constraint for CV and CTM motion models can be expressed in Cartesian coordinate's space as:

$$\mathbf{F}_{n} = \begin{bmatrix} \mathbf{A}_{n} & \mathbf{0}_{m \times m} & \mathbf{0}_{m \times m} \\ \mathbf{0}_{m \times m} & \mathbf{A}_{n} & \mathbf{0}_{m \times m} \\ \mathbf{0}_{m \times m} & \mathbf{0}_{m \times m} & \mathbf{A}_{n} \end{bmatrix}$$
(4.35)

where $\mathbf{0}_{m \times m}$ denotes m by m matrix of zeros and \mathbf{A}_n is expressed for CA and CTM motions respectively, as:

$$\mathbf{A}_{CV} = \begin{bmatrix} 1 & \tau_n \\ 0 & 1 \end{bmatrix} \tag{4.36}$$

$$\mathbf{A}_{CTM} = \begin{bmatrix} 1 & \frac{\sin(\Omega_n \tau_n)}{\Omega_n} & \frac{1-\cos(\Omega_n \tau_n)}{\Omega_n^2} \\ 0 & \cos(\Omega_n \tau_n) & \frac{\sin(\Omega_n \tau_n)}{\Omega_n} \\ 0 & -\Omega_n \sin(\Omega_n \tau_n) & \cos(\Omega_n \tau_n) \end{bmatrix}$$
(4.37)

where $\tau_n = t_n - t_{n-1}$ denotes the sampling time, t_n represents the period of measurement n and Ω_n represents the turn rate at the time t_n , which can be expressed as:

$$\Omega_n = \frac{\sqrt{\dot{x_n}^2 + \dot{y_n}^2 + \ddot{z_n}^2}}{\sqrt{\dot{x_n}^2 + \dot{y_n}^2 + \dot{z_n}^2}}$$
(4.38)

where $(\dot{x_n}, \dot{y_n}, \dot{z_n})$ and $(\ddot{x_n}, \ddot{y_n}, \ddot{z_n})$ denote the velocity and the acceleration components of the target at discrete time t_n , respectively.

The covariance matrix of the input process noise for CV and CTM motion models are characterized by $G_nQ_nG_n^T$ that is given by:

$$\mathbf{G}_{n}\mathbf{Q}_{n}\mathbf{G}_{n}^{T} = \begin{bmatrix} q_{n}^{x} \mathbf{B}_{n} \mathbf{B}_{n}^{T} & \mathbf{0}_{m \times m} & \mathbf{0}_{m \times m} \\ \mathbf{0}_{m \times m} & q_{n}^{y} \mathbf{B}_{n} \mathbf{B}_{n}^{T} & \mathbf{0}_{m \times m} \\ \mathbf{0}_{m \times m} & \mathbf{0}_{m \times m} & q_{n}^{z} \mathbf{B}_{n} \mathbf{B}_{n}^{T} \end{bmatrix}$$
(4.39)

where $\mathbf{B}_n \mathbf{B}_n^T$ is expressed for CV and CTM motions, respectively, as:

$$(\mathbf{B}_n \mathbf{B}_n^T)_{CV} = \begin{bmatrix} \frac{\tau_n^4}{4} & \frac{\tau_n^3}{2} \\ \frac{\tau_n^3}{2} & \tau_n^2 \end{bmatrix}$$
(4.40)

$$\mathbf{B}_{n}\mathbf{B}_{n}^{T} = \begin{bmatrix} \frac{\tau_{n}^{4}}{4} & \frac{\tau_{n}^{3}}{2} & \frac{\tau_{n}^{2}}{2} \\ \frac{\tau_{n}^{3}}{2} & \tau_{n}^{2} & \tau_{n} \\ \frac{\tau_{n}^{2}}{2} & \tau_{n} & 1 \end{bmatrix}$$
(4.41)

4.3. Performance Evaluation

In this part of the chapter, we present simulation examples to demonstrate the performance of the proposed system design. In all examples, we assume a ULA consisting of M = N = 10 antenna elements spaced $^{\lambda}/_{2}$ apart. Noise is assumed to be zero-mean, Gaussian, and white both spatially and temporally. The targets in each example are assumed to lie within a given spatial sector. Moreover, the surveillance region where the RadCom system operates is $-90^{\circ} \le \theta \le 90^{\circ}$. Besides radar functions within the main beam, we assumed that the information bits are delivered to the communication receiver located at θ_{l} . It is also assumed that the power level in the SL region is at least 20 dB lower than the main beam thus the maximum allowable value of $\varepsilon_{max} = 0.1$ is selected.

Example 4.1 (Performance of the proposed beamspace design in terms of a target resolution and the RMSE):

In this example, the performance of the proposed optimum transmit beamspace **W** design approach is compared to that of the traditional MIMO radar with uniform power density transmission, and the approach presented in [165], maps the transmit steering vector to the appropriate corresponding of a ULA based on convex optimization formulation. The main beam of the BPs is assumed to be within the spatial sector $\Theta = [-15^{\circ} \ 15^{\circ}]$, and the number of pulses applied is 50. The probability of the target resolution and the RMSE are calculated using 500 Monte-Carlo trials.

Fig. 4.3 illustrates the transmit BPs of the conventional MIMO radar with uniform transmit power distribution, the approach presented in [165], and the proposed design for

the optimum transmit **W**. For designing the optimal **W** we used four beams while for the approach of [165] only two beams are used as proposed therein (see example 3 in [165]). It can be seen from the figure that the proposed design concentrates more power in the desired sector with relatively low SL levels compared with the method used in [165].

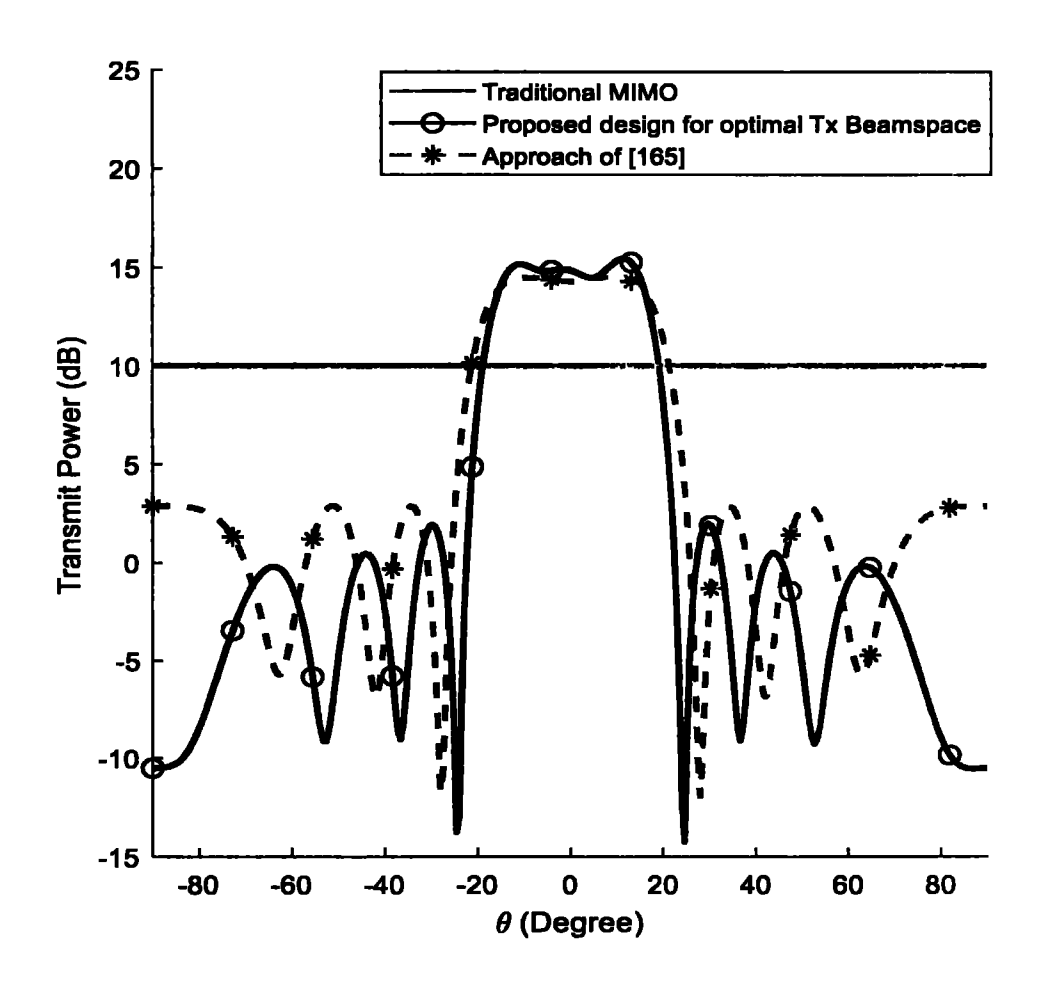


Figure 4.3: Transmit BPs of the Traditional MIMO, Approach of [165], and the proposed optimal beamspace design.

To investigate the RMSE performance of the approaches under test, assume that there are two targets located at $\theta_{t1} = -9^{\circ}$ and $\theta_{t2} = -8^{\circ}$. Here, RMSE is used as a performance criterion, which can be calculated as follows:

RMSE
$$(\theta) = \sqrt{\frac{1}{TM_c} \sum_{t=1}^{T} \sum_{m=1}^{M_c} (\widehat{\theta_{t,m}} - \theta_t)^2}$$
 (4.42)

where $\widehat{\theta_{t,m}}$ denotes the estimates of the angle for the t^{th} target in the m^{th} Monte Carlo run, and T and M_c denote the total number of targets and Monte Carlo runs, respectively. Fig. 4.4 shows the RMSEs versus SNR for the approaches under test. As we can be seen from the figure, the RMSE of the proposed optimal beamspace design and the method used in [165] have lower RMSEs as compared to the RMSE of the traditional MIMO radar.

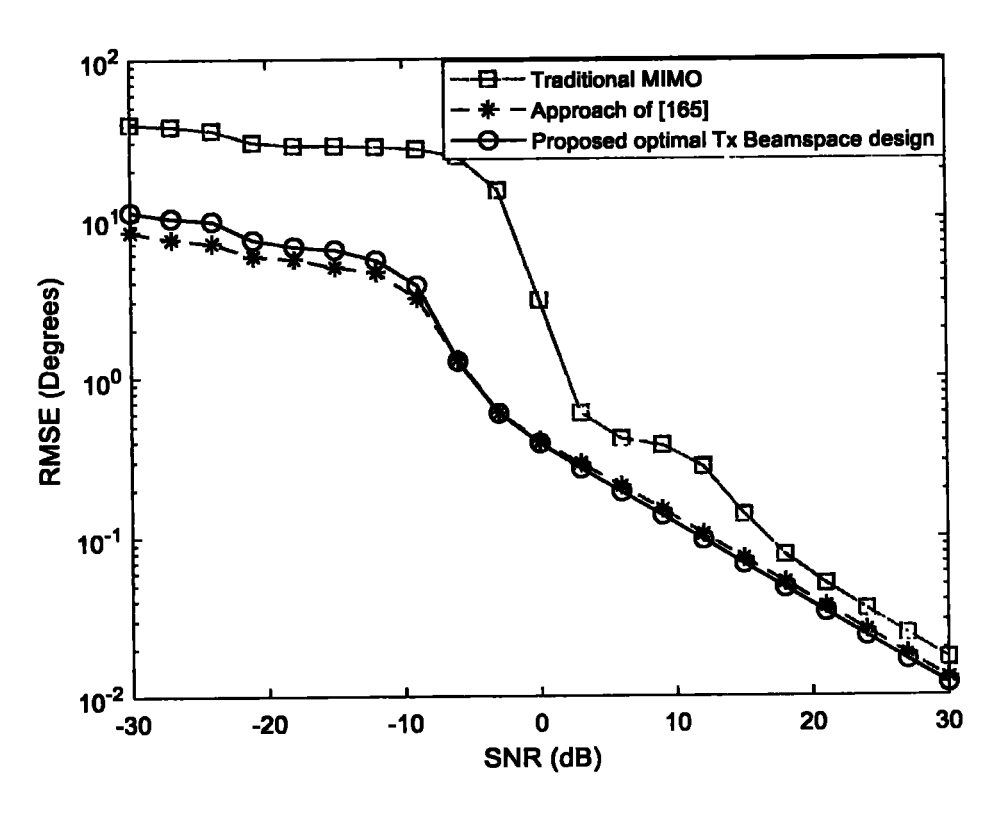


Figure 4.4: RMSE performance comparison between the approaches under test, Traditional MIMO, Approach of [165], and the proposed optimal beamspace design.

It is also observed from the figure that, the performance of the method [165] is very close to the performance of the proposed optimal beamspace design. Moreover, the proposed method outperformed the other methods as SNR is more than -10 dB.

To examine the resolution capability of each approach, it can be observed from Fig. 4.5 that the proposed design outperforms the other approaches under the test.

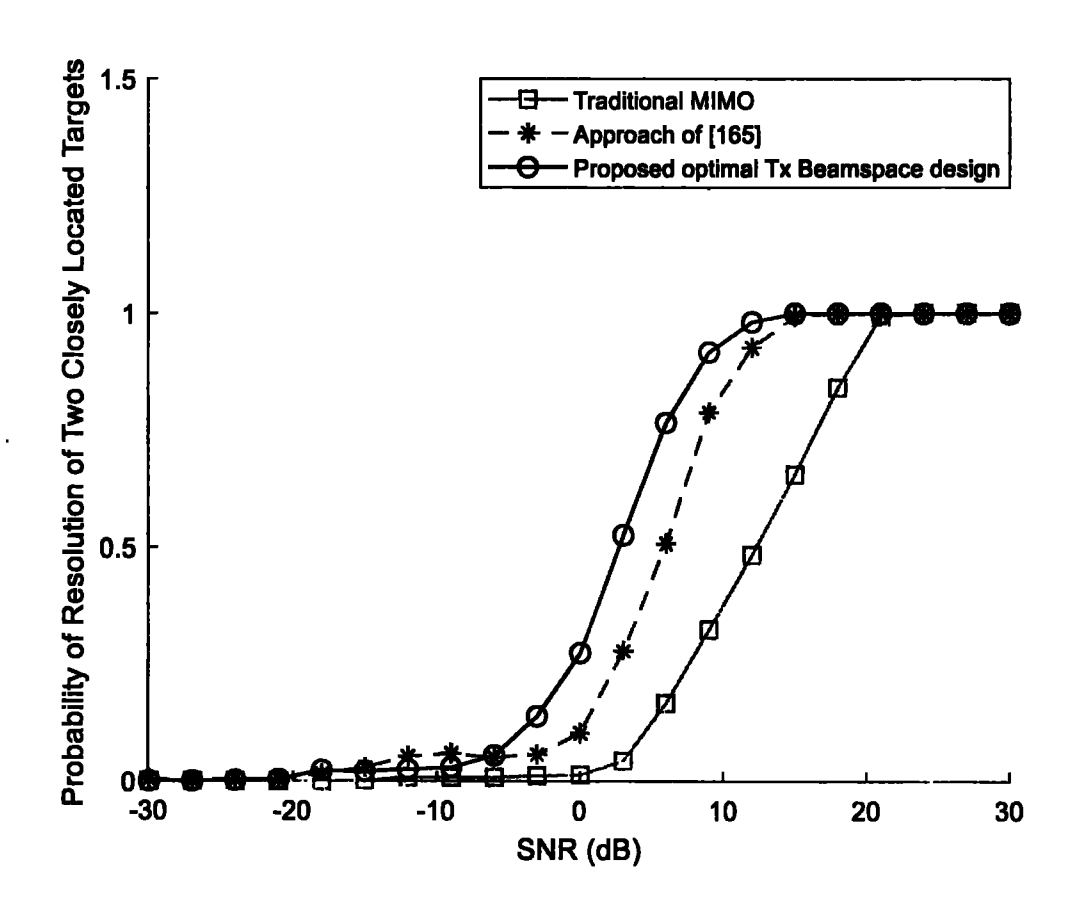


Figure 4.5: Resolution performance comparison between the approaches under test, Traditional MIMO, Approach of [165], and the proposed optimal beamspace design.

Example 4.2 (Tracking of the maneuvering target (MT)):

This example illustrates the performance of tracking MT using various estimators including the proposed tracking scheme. The motion of the target modeled as two Markov models with $\tau_n = 0.1 \text{s}$ and insignificant noises are used. The first model of the target motion is a linear CV with noise modeled as zero-mean with power spectral density (PSD) equal to 0.01. The second model of the motion is a combination of CV with a non-linear CTM model with noise modeled as zero-mean turn rate with covariance equal to 0.15. In the non-linear estimation problems with the multi-model design, the EKF-IMM approach is required for filtering and smoothing. The initial simulation parameters are provided in Table 4.1.

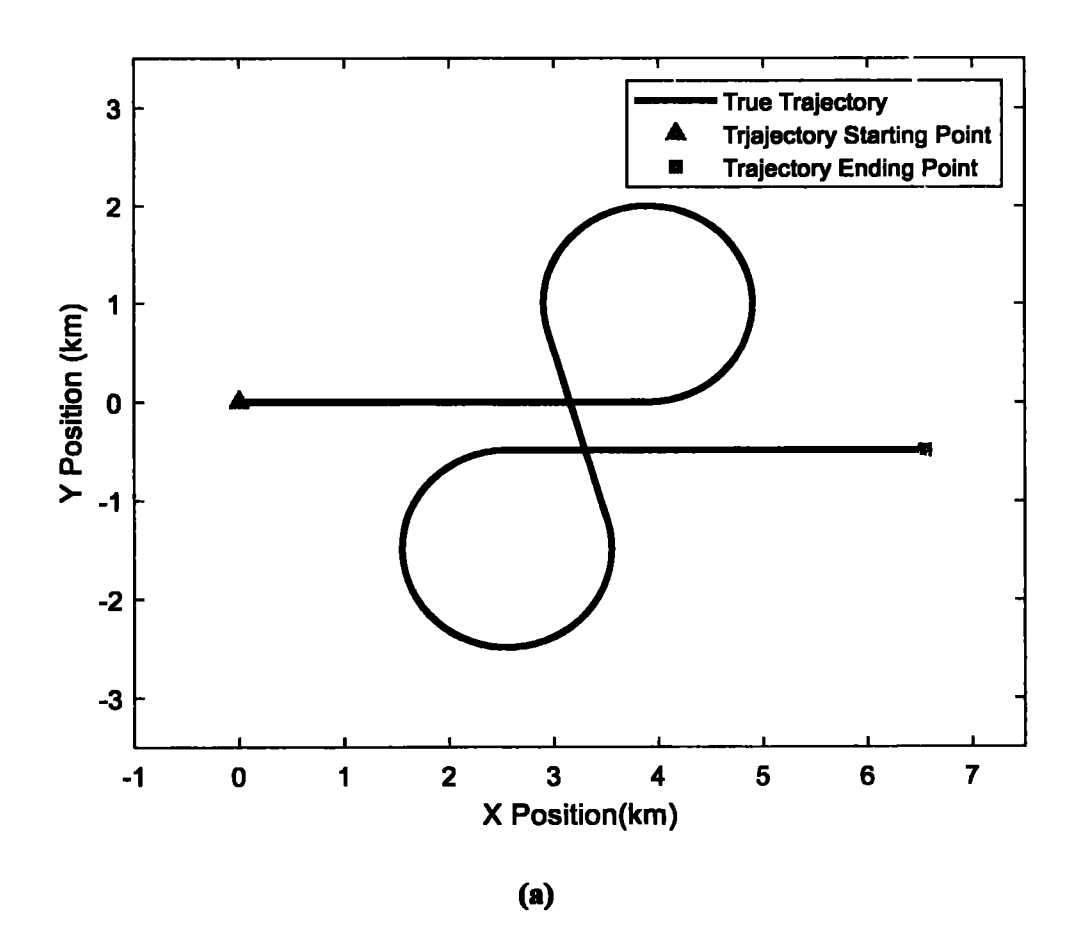
The measurement \mathbf{z}_n is made on the target position with real Gaussian noise \mathbf{w}_n modeled as $\mathbf{w}_n \sim \mathcal{N}(0, \Sigma_{\mathbf{w}})$ where $\Sigma_{\mathbf{w}} = 0.01$ is used.

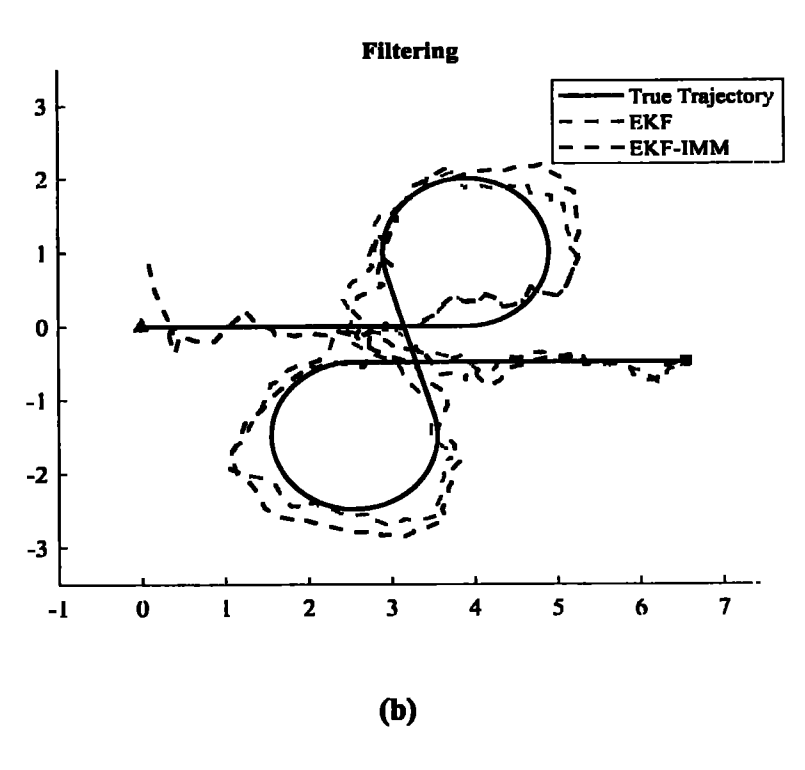
Table 4.1: Simulation parameters used for target tracking scenario in example 4.2.

Parameters	Setting Values	
The initial state of the target x ₀	$[0,0,1,0,0]^T$	
The state covariance	$diag([10.1, 10.1, 1.1, 1.1, 1]^T)$	
The measurement matrix H	[1 0 0 0 0; 0 1 0 0 0]	
The prior probabilities model	$[0.9, 0.1]^T$	
The model transition probability matrix Π	[0.9 0.1] [0.1 0.9]	

The simulation is performed with 100 Monte Carlo runs, each containing 200 sampling steps and using the same generated trajectory originating from the same starting point, but the corresponding observation series are generated randomly. The actual

trajectory and estimates generated by EK and EK-IMM filters and smoothers in one run are shown in Fig. 4.6 (a), (b), and (c) respectively. As shown from Fig. 4.6 (a) that, the target starts to move from starting point (the origin) with a velocity of 1 Km/s along the x-axis then at point x= 4 it starts to maneuver along the y-axis. At point (x= 2, y= -1) the target moves in a straight line along the x-axis till the ending point. We can observe from Figs. 4.6 (b) and (c) that, the EK and EK-IMM smoothers appropriately capture the trend of the trajectory better than their corresponding filters.





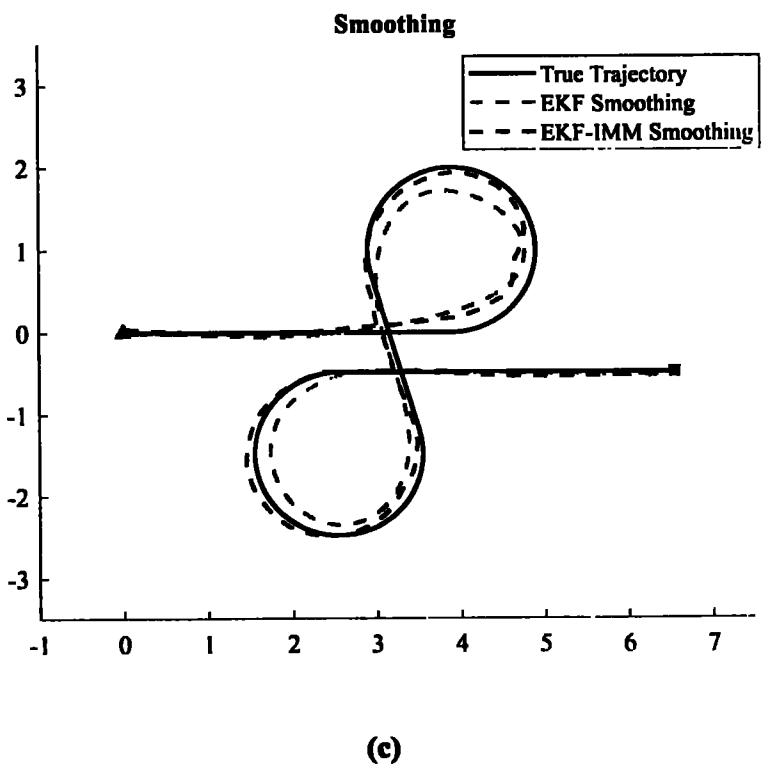


Figure 4.6: (a) Real trajectory, (b) estimates of the EKF and the proposed EKF-IMM filters, and (c) estimates of the EKF and the proposed EKF-IMM smoothers.

For more insights, the average performance of the RMSE angle estimation over 100 Monte Carlo runs for the proposed and other estimation approaches are shown in Fig. 4.7. The RMSEs of the angle parameter can be calculated as:

RMSE
$$(\theta_t) = \sqrt{\frac{1}{M_c} \sum_{m=1}^{M_c} (\widehat{\theta_{t,m}} - \theta_{t,m})^2}$$
 (4.43)

where M_c is the total number of the Monte Carlo runs, $\theta_{t,m}$ and $\widehat{\theta_{t,m}}$ represent the true and the estimated angle of the target in the m^{th} run, respectively.

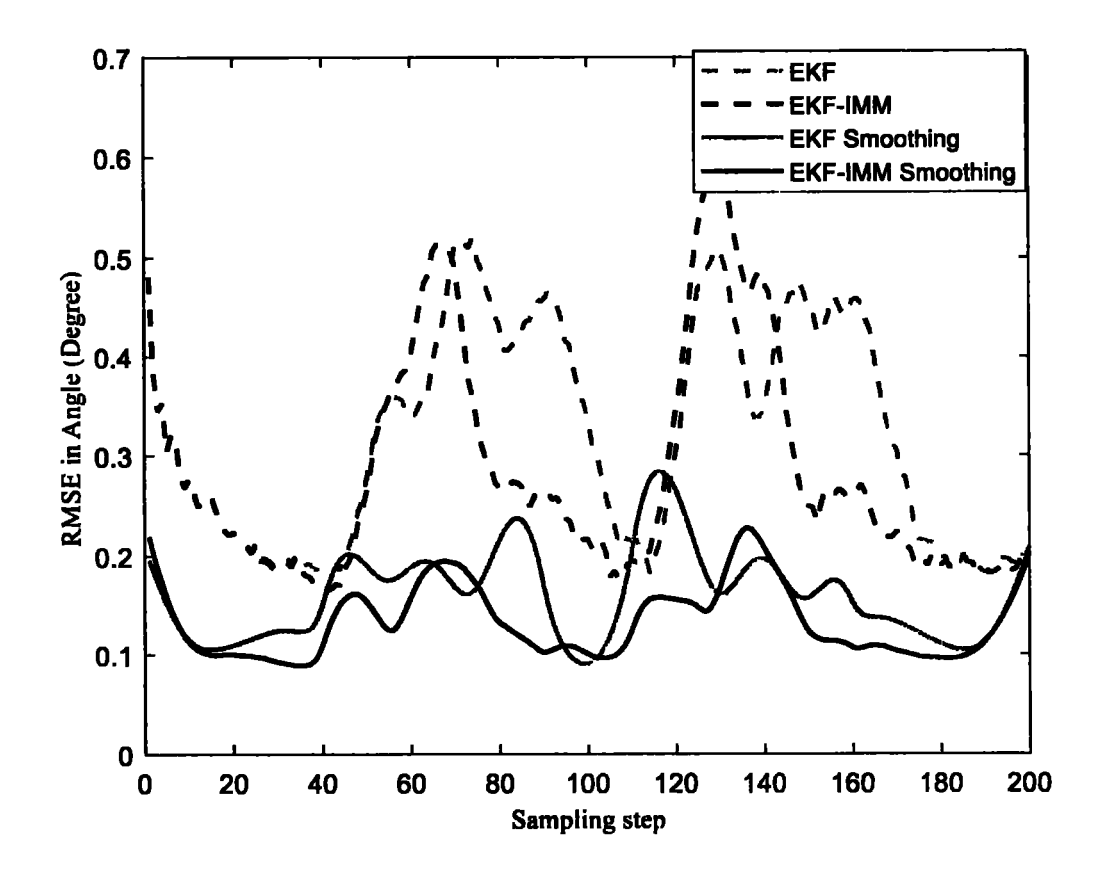


Figure 4.7: RMSE in angle estimates of different non-linear filters and smoothers over sampling steps in the scenario of tracking a maneuvering target.

The RMSE of the angle parameter and average computing time per Monte Carlo run is provided in Table 4.2.

Table 4.2: Average RMSE performance for angle parameters of different non-linear estimators.

Estimators	Average RMSE of Angle	Computing Time (s)
	(Degree)	
EKF (using CV)	0.3234	0.0122
EK smoother (using CA)	0.1607	0.0152
EKF-IMM	0.2860	0.0311
EKF-IMM smoother	0.1333	0.0970

The proposed scheme outperforms the EKF and EK smoother using the CV model in terms of estimation accuracy but at the cost of computing speed, in which the proposed method is slower in time computation which is performed in MATLAB software.

Fig. 4.8 shows the calculated probabilities for the modes used in this example.

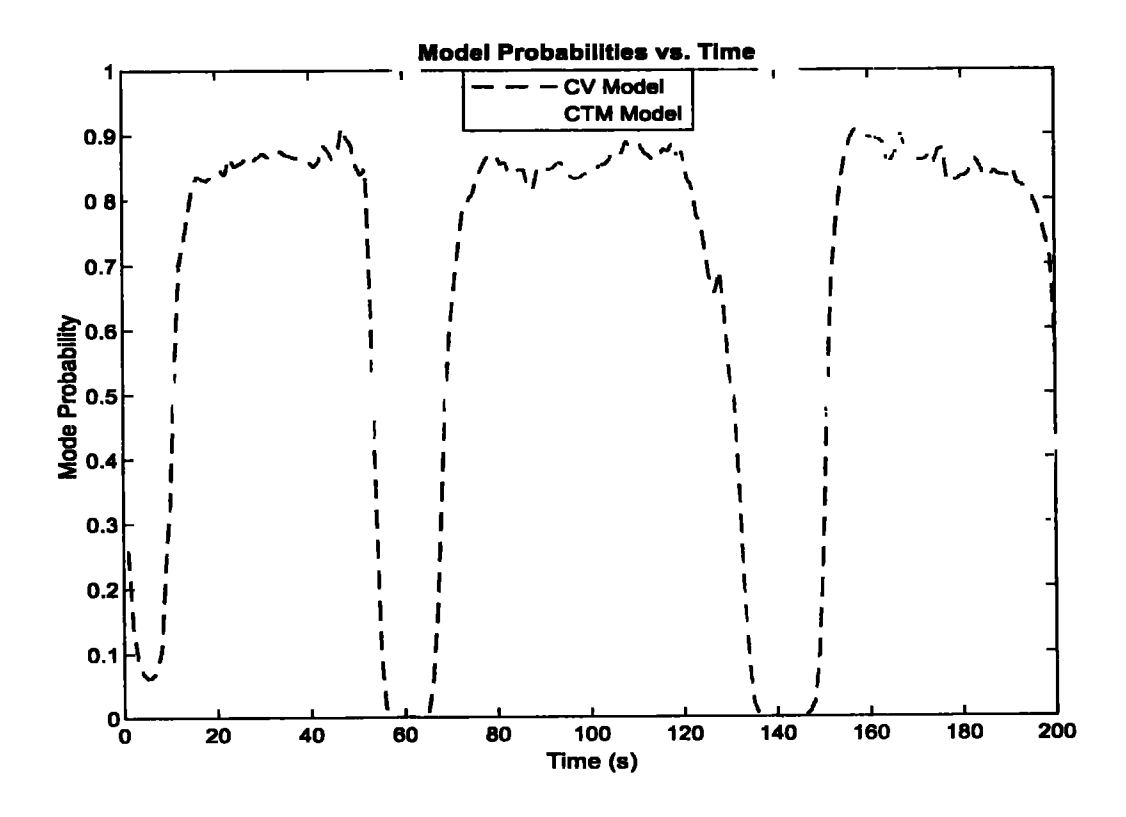


Figure 4.8: Model probabilities for two-mode (CV and CTM models) of maneuvering target during tracking operation.

Example 4.3 (Transmit BPs synthesis towards the communication receiver located within the RadCom transmission directions):

The proposed MIMO RadCom system aims to track the distant moving targets and simultaneously embed/deliver information symbols towards the intended communication receiver located at θ_i within the RadCom operation regions. Let's assume that, at the beginning of the tracking scenario, the operating region of the main beam is within the spatial region $\Theta = [-10^{\circ} \ 10^{\circ}]$ and a single communication receiver is located outside the main lobe Θ directions, assume that it is located at $\theta_i = 45^{\circ}$. Thus, during the current scans, as long as the communication receiver is located outside the main lobe directions, the APSK strategy is selected by the transmitter for information symbols transmission towards the communication directions.

In this case, during each radar pulse, the communication symbols are embedded by utilizing the magnitudes as well as the phases of the transmitted waveforms. Thus, by solving (4.9) and (4.11), the APSK strategy enables the system to transmit L different SL levels with R unique phases towards the communication user. Therefore, each transmitted waveform carries ($\log_2 LR$) bits of information to the communication user. Let's assume that there are two bits of information are embedded in each transmitted communication symbol, the possible number of different SL levels or phases transmitted towards the communication direction is four possibilities. Thus, in the APSK strategy, each BP radiation corresponds to the BF weight vector, $\mathbf{W} = [\mathbf{w}_1, \mathbf{w}_2, ..., \mathbf{w}_P]$, that projects one SL level associated with one phase response towards the communication receiver during each radar pulse. For the non-coherent transmission case, \mathbf{W} contains four pairs of BF vectors associated with suitable four of APSK constellation points. The transmit BPs radiations of

the proposed MIMO RadCom system when the communication receiver is located within the SL region and two bits are embedded towards the communication direction is plotted in Fig. 4.9.

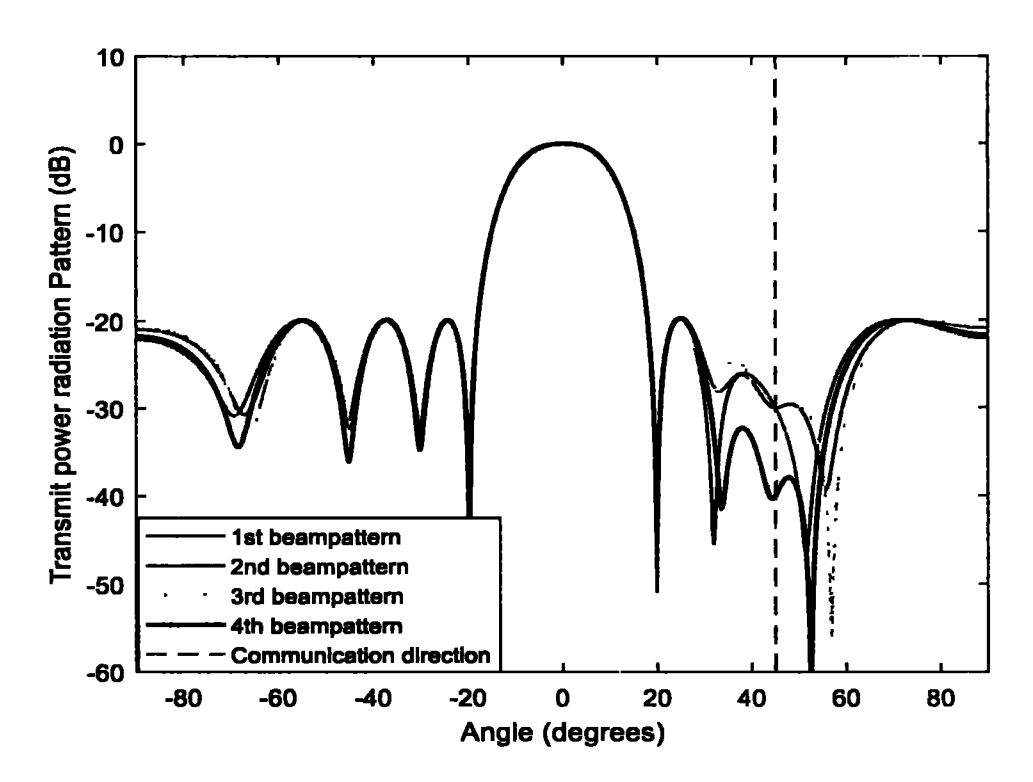


Figure 4.9: Transmit BPs radiations for RadCom APSK-based signaling strategy vs. angle when two bits are embedded towards the communication direction located in the SL at $\theta_t = 45^{\circ}$.

Fig. 4.9 shows that each BP radiation corresponds to one SL level associated with one phase response during each radar pulse, and it represents a single communication symbol containing two bits of transmitted information towards the communication receiver.

On the other hand, During the tracking operation, when the target is moving towards the communication receiver and both would be located within the main beam directions.

To maintain the information transmission towards the intended communication receiver

and also detection performance for the RadCom system, the PSK strategy is selected by the transmitter. In this case, the information symbols are embedded only by controlling the phases of transmitted signals during each radar pulse. For two bits of information that can be embedded during each radar pulse, four constellation points of phases are formed each representing one communication symbol. Thus, the principle transmit BF vector \mathbf{W}_1 can be determined by solving (4.8) and the remaining BF weight vectors are selected from $\mathbf{W} = \{\mathbf{W}_2, \dots, \mathbf{W}_{2^{M-1}-1}\}$ associated with each constellation point applying the method presented in [133].

For a coherent PSK based method, four BF vectors are selected from $\widetilde{\mathbf{W}}$ and using (4.14) while for the non-coherent case, $\widetilde{\mathbf{W}}$ is used to build four pairs of BF weight vectors associated with four suitable points of phase rotations using (4.16). The transmit BP radiation of the proposed joint transmit platform when communication direction $\theta_l \in \Theta$ during one radar pulse is plotted in Fig. 4.10. It shows that the BP radiation corresponds to one SL level associated with one phase response during each radar pulse, and it represents a single communication symbol that contains two bits of transmitted information towards the communication receiver.

Hence, we can conclude that the detection performance of the radar target is not influenced by the information transmission process towards the communication direction located at θ_i and the proposed design for the RadCom system maintains the communication link towards the intended communication direction during tracking operation.

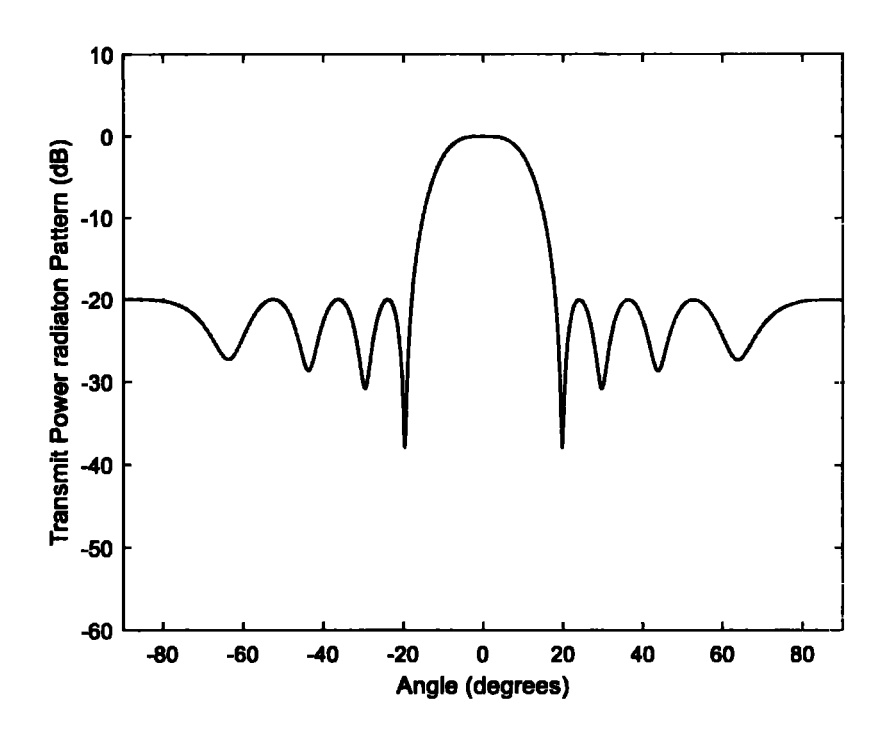


Figure 4.10: Single transmit BP radiation for RadCom PSK-based signaling strategy vs. angle represents a single embedded communication symbol towards the communication direction located at $\theta_l \in \Theta = [-10^{\circ} \ 10]$.

Example 4.4 (Transmission of distinct communication streams towards different communication stations located within the SL region):

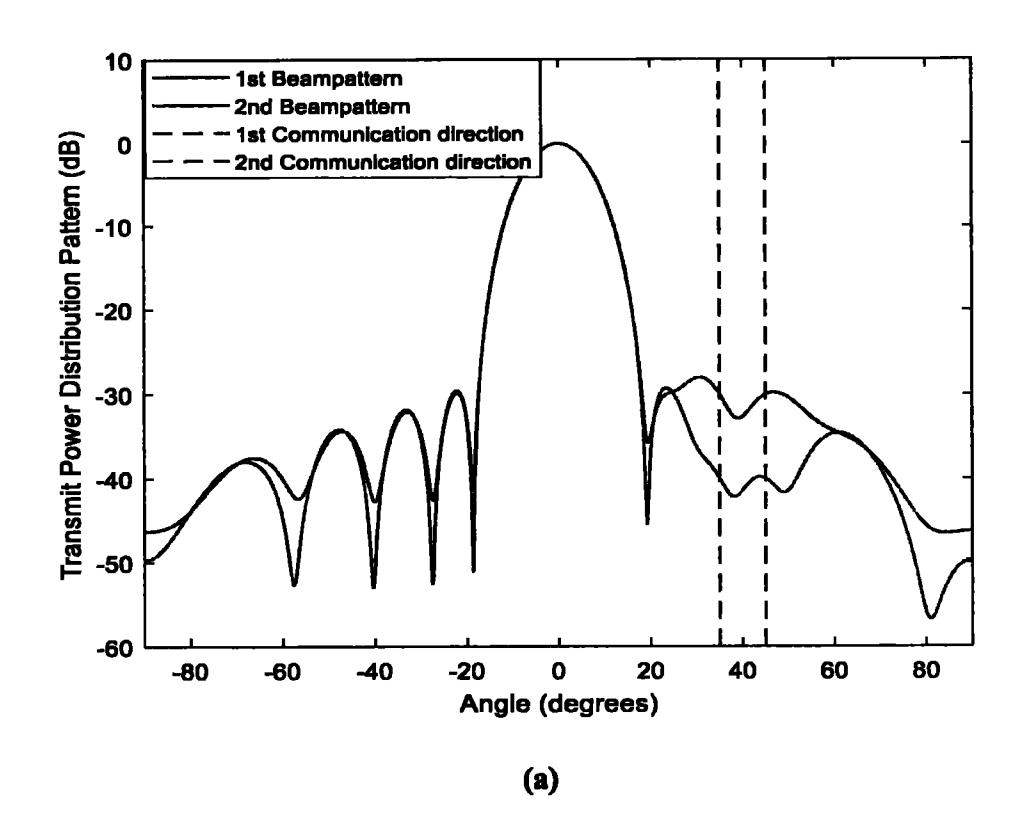
In this example, we examined the capability of the proposed MIMO RadCom system to transmit distinct communication symbols towards different communication receivers located within the SL region. Also, we compared the proposed APSK-based communication strategy with the existing SL-based communication strategies in terms of the overall throughput of the system and BER performance. Here, the same simulation parameters in example 4.3 are used with the assumption that there are two communication receivers located in the radar SL directions at angles 35° and 45°. Assume that the

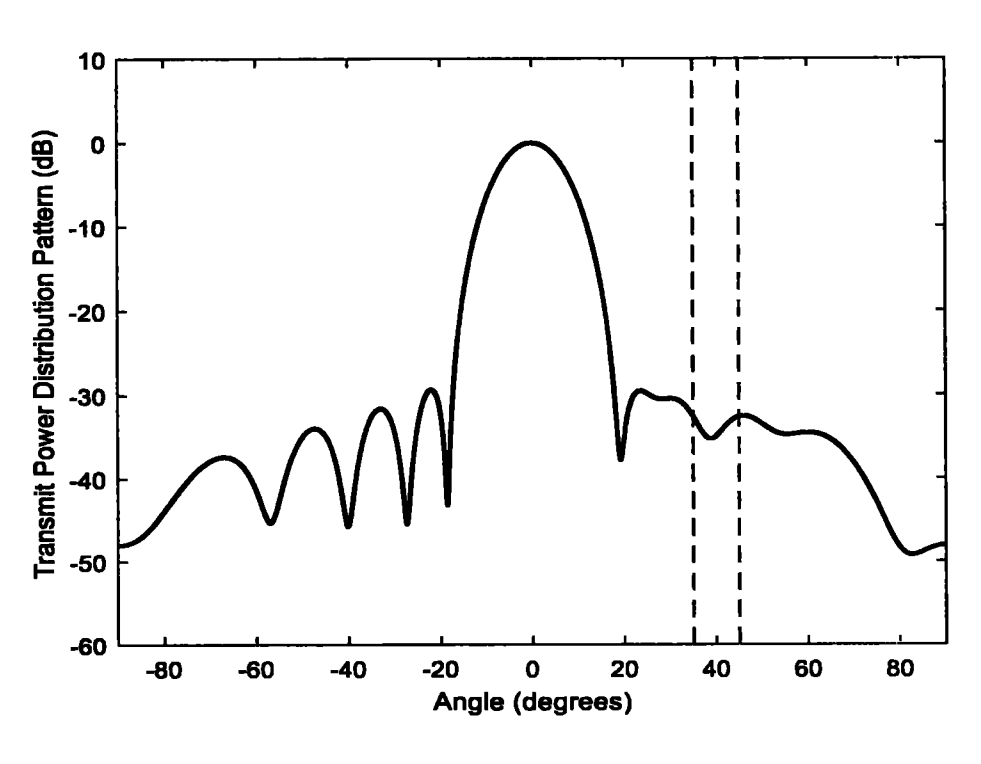
secondary objective of the proposed RadCom system is to project two SL levels and at the same time transmit the waveforms with two distinct phases towards different communication users located at angles 35° and 45°, respectively, to embed two distinct bits of information to each user.

PSK and ASK SL-based communication strategies will have the capability to utilize only the phase or magnitude variations of the transmitted waveform, respectively. In contrast, the proposed APSK-based communication strategy can exploit the difference in both the amplitude and the phase parameters of the transmitted waveform.

Fig. 4.11(a) shows the transmit BP radiations corresponding to two BF weight vectors for the ASK-based communication schemes [125, 134, 136, 161]. These BF vectors are designed to broadcast the SL level of either -40 dB or -30 dB, which are selected from $0 < L_k \le \varepsilon_{max}$, (k = 1, 2), towards the communication receivers. During each radar pulse, the SL level remains identical at both communication units for the existing ASK-based communication schemes [125, 134, 136, 161]. For the PSK-based communication schemes [126, 133, 135, 142], two BF weight vectors are designed to have the same amplitude response but exhibit unique phase responses, uniformly distributed from 0° to 360°, at the communication receivers. Fig. 4.11(b) shows that the BP radiations of these BF weight vectors have an SL level of -32.64 dB at both communication users. During each radar pulse, each of the BF vectors broadcast a unique response of phase in the direction of all communication stations. Similar to the ASK-based communication schemes, the transmitted communication symbol is broadcast to all communication unit's directions.

Different from the ASK-based communication schemes, the proposed APSK-based communication scheme allows to project different SL levels at the two communication receivers. Furthermore, unlike the PSK-based communication schemes, the proposed APSK-based communication scheme, at the same time, can transmit distinct phases to different communication receivers. Thus, the APSK-based communication scheme can independently assign two different amplitudes levels and two unique phases at the two different communication directions to transmit distinct symbols to each communication user. Using (4.9) to generate 16 BF weight vectors for L = R = C = 2, where C denotes the number of communication receivers. Fig. 4.11(c) demonstrates the four possible BPs power radiation for the proposed APSK-based communication scheme generated by using (4.9). Since there are two possibilities for phase responses transmitted towards each communication receiver, each BP power radiation for the proposed APSK-based communication scheme corresponds to four distinct BF weight vectors that project the identical magnitude but exhibit different response of phases towards each communication receiver. The direction of the communication receivers is represented by the red dashed lines.





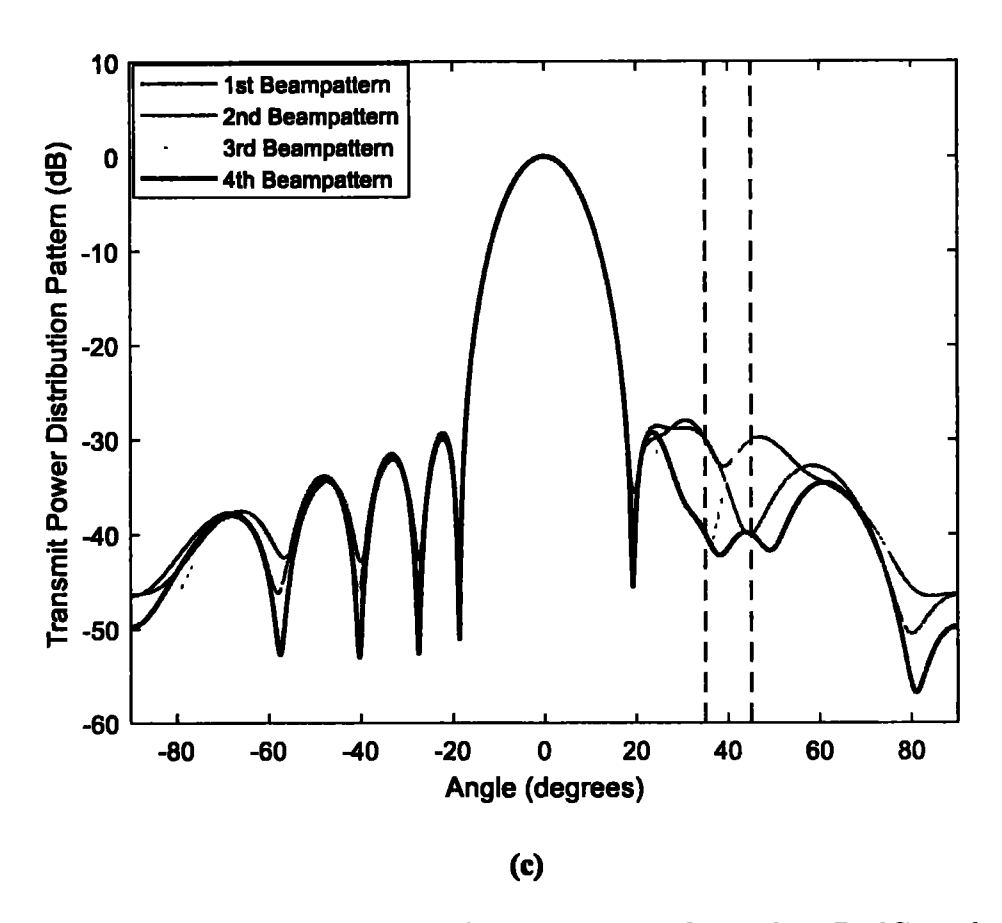


Figure 4.11: Transmit BPs power radiations vs. angle for various RadCom signaling strategies: (a) ASK-based communication scheme when (L=C=2), (b) PSK-based communication scheme when (R=C=2), and (c) proposed APSK-based communication scheme when (L=R=C=2).

Example 4.5 (Data rates analysis and BER performance):

In this example, we analyze the throughput that can be achieved by each existing SL-based communication scheme and also evaluates the BER performance for each of them.

Using the same simulation parameters used in example 4.4 with the assumption that there are two orthogonal waveforms used for transmission.

During each radar pulse, the ASK-based communication scheme exploits two SL levels and will be capable to transmit $(K \log_2 L) = 2$ bits. In the case of the PSK-based method

utilizes two phases and will be able to deliver $(K \log_2 R) = 2$ bits. On the other hand, for coherent APSK-based signaling strategy can transmit $(K \log_2 LR) = 4$ bits. In the case of non-coherent communication schemes, we will have 32 BF weight vectors to be generated to achieve the same throughput. To reduce the error, grey coded is employed for all symbols in all modulation schemes before transmission.

Thus, the overall achievable throughput of the proposed MIMO RadCom scheme design is given as:

$$K * (\log_2 LR + \log_2 Q) * PRF \text{ bits/s}$$
 (4.44)

where Q represents the number of bits transmitted by the system when the communication receiver is located within the main lobe directions of the BP radiations of the RadCom system transmission.

In the case of non-coherent communication mode, the overall achievable throughput of the proposed scheme design will be:

$$(K-1) * (\log_2 LR + \log_2 Q) * PRF$$
 bits/s (4.45)

For multi-user applications, the overall achievable throughput of the proposed APSK-based communication scheme will be:

$$C * K * \log_2 LR * PRF \text{ bits/s}$$
 (4.46)

Fig. 4.12 illustrates the comparison of BER performance for the proposed APSK signaling strategy with the existing SL control-based strategies. It is evident from Fig. 4.12 that the proposed signaling strategy outperforms the existing SL control-based strategies in terms of BER performance. This is due to the proposed strategy is designed to increase the sum data rate with the same resources which result in a further increase of the effective distance between the transmitted symbol in the space constellation along with the ability to transmit

distinct communication symbols to different receivers results in BER reduction for the proposed APSK-based signaling strategy.

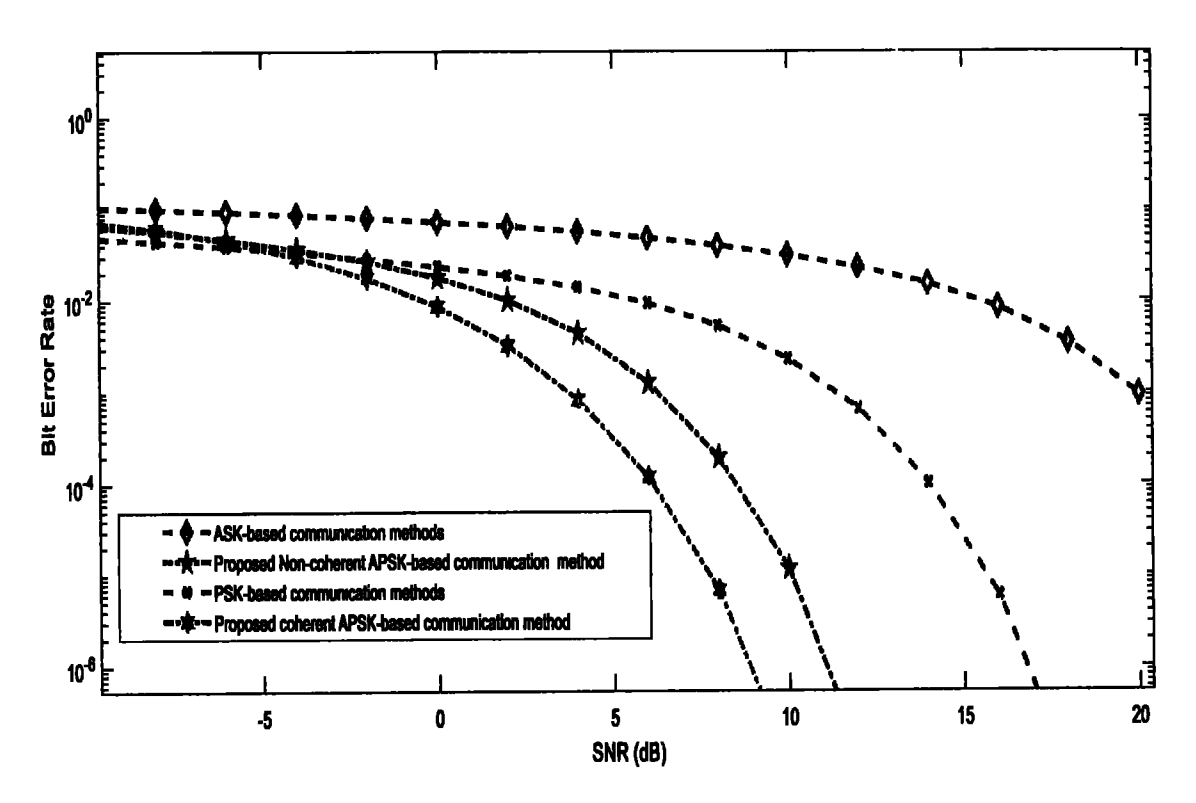


Figure 4.12: BER versus SNR for various SL-based signaling strategies; ASK, PSK, and the proposed APSK.

Also, the figure shows that the coherent APSK-based communication mode achieves better BER performance in comparison to the counterpart of the non-coherent mode. This is because for non-coherent communication the number of transmitted symbols in the constellation space is increased and since the transmitted power is divided between the waveforms causing the error rate becomes higher.

Example 4.6 (Angular BER performance):

In this example, we evaluate the performance of the proposed MIMO RadCom system in terms of angular BER. The same parameters are used except that the intended communication receiver is located at $\theta_i = 30^\circ$ at the initial time of the tracking scenario. Thus, the information embedding/delivering towards the communication direction by applying the APSK-based communication signaling as the communication receiver remains outside the main beam spatial sector $\mathbf{\Theta} = [-10^\circ \ 10]$. Fig. 4.13(a) shows the BER versus the angle $\theta_i = 30^\circ$, where the communication station is located.

During tracking operation, when the target and communication receiver are both located within the main beam directions Θ , assuming that the communication station is located at $\theta_i = 6^{\circ}$, then the PSK is selected for information embedding/delivering towards the communication receiver. Therefore, the target detection performance and communication link are maintained. Fig. 4.13(b) shows the BER versus the spatial angle $\theta_i = 6^{\circ}$.

It is clear from Fig. 4.13 that the only direction that can decode/decipher the transmitted information is the intended communication direction where the communication station is located. The narrow BP towards the communication direction indicates that BP produced by the proposed design schemes is focusing the energy towards the intended communication direction only. Hence, an inherent secure transmission against information interception is established.

In summary, unlike the existing RadCom scheme designs, the proposed design maintains the communication link towards the communication direction regardless of its location within the RadCom operation regions.

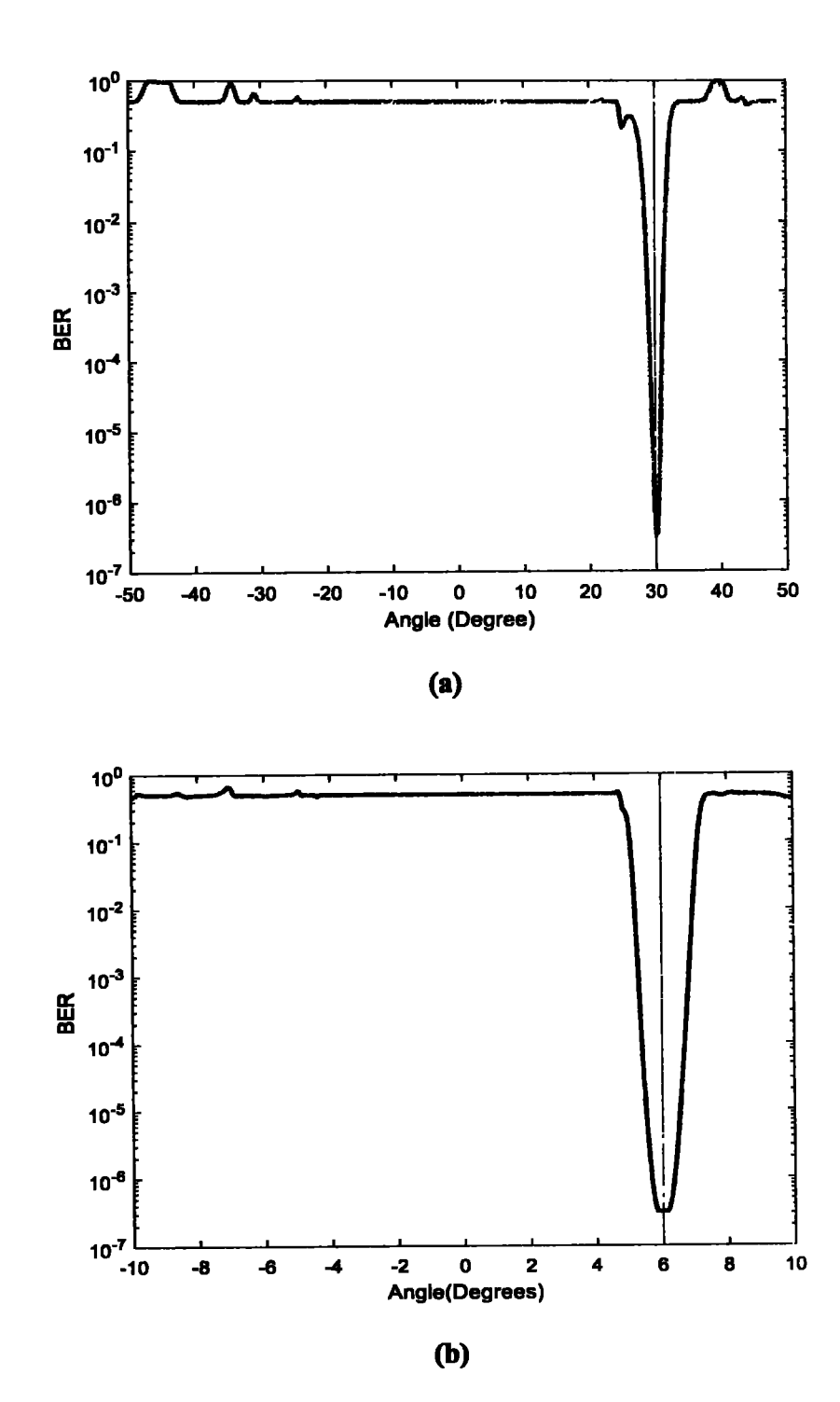


Figure 4.13: Angular BER: when (a) the intended communication receiver is located at $\theta_t = 30^\circ$ in the SL directions and (b) the intended communication receiver is located within the main beam spatial sector $\in \Theta = [-10^\circ \ 10]$, i.e., at $\theta_i = 6^\circ$.

4.4. Summary

In this chapter, we proposed a closed-loop into the RadCom system design that allows the system to perform detection and tracking the moving target while simultaneously maintaining the information delivery to the intended communication receivers present in the operation region during each scan. The joint transmit platform (JTP) of the system is composed of M antenna elements where the transmitted waveforms are orthogonal to each other, Also, we introduced two signaling strategies, APSK and PSK, used for information embedding into the system emissions towards the communication direction located either in SL or main lobe directions, respectively, during the tracking operation. The information embedding designs have been formulated for both modes of communication (coherent and non-coherent). The simulation results verify that the communication performance is improved in terms of low BER, secure information transmission, and throughput is enhanced. While for radar applications the performance is improved in terms of resolution and parameter estimation. Moreover, the proposed APSK-based communication scheme is capable to transmit distinct streams of information towards different communication receivers located within the SL region. In contrast to ASK and PSK SL-based communication schemes, the proposed APSK scheme is capable to project different SL levels and at the same time transmitting the waveforms with different phases to different communication stations located within the SL region.

CHAPTER-5

SUMMARY AND FUTURE RESEARCH

At the end of this work, the most important contributions are summarized. A brief discussion of future research trends and open problems will wrap up this thesis.

5.1. Summary

To remedy the problem of congestion within the spectrum space and utilize most of this limited resource, technologies have been developed that allow a single system to simultaneously perform radar and communications operations. RadCom systems are an evolving field of research, in which both functions radar and communications, share the same platform hardware and spectrum resources, establishing a specific category of RF technology. RadCom systems can support applications that require communication data, which can be target parameter information or radar-independent information, to be efficiently transmitted using the same frequency bandwidth and radar aperture. This is attained by embedding communication symbols into radar emissions.

In this thesis, we reviewed the principles of RadCom systems and described the progress made in the development of various design approaches for the RadCom system and different forms of communication symbols embedding schemes into radar emissions. While the major current design schemes for the RadCom system are open-loop designs, this thesis develops a closed-loop design into the RadCom system architecture. The feedback information provided from the receiver side is utilized by the transmitter to select

the appropriately optimized transmit BF weight vectors from the beamspace library suitable for both target detection and information transmission towards the communication receiver located either in the SL or main lobe directions of the RadCom BPs radiations. In Chapter 3, we developed an angle-range dependent RadCom system that utilizes an FDA-MIMO configuration. We have used an unambiguous joint estimation algorithm for the angle and range parameters of the radar target. For embedding the communication symbols into RadCom emissions, we utilize either the magnitude ratio and/or the phase shifts between the (K-1) transmitted waveform pairs. We have designed two signaling strategies, the proposed APSK and PSK schemes for embedding the transmitted communication symbols towards the communication receiver located either in SL or main lobe directions, respectively. In the tracking scenario, we considered two motion modes for the moving target, CV and CA models in our proposed design. The simulation results verified the effectiveness of the proposed designs. The performance of the radar functionality is improved in terms of target detection, parameters estimation, CRLB for range and angle estimations, and the SINR. While for the communication functionality, the performance is improved in terms of SER, secure information transmission, and overall throughput of the system.

Chapter 4 extends the beamspace design of the APSK information embedding strategy to allow different communication symbols to be transmitted to different users located in the SL region. As a result, the overall throughput of the RadCom system is enhanced as distinct information bits are transmitted to different users. In this chapter, we developed a MIMO RadCom system that utilizes the property of waveform diversity. For embedding the

communication symbols into RadCom emissions, we utilized the amplitudes and phases of the transmitted waveforms in the direction of the communication receivers. We have designed two signaling strategies, the proposed APSK and PSK schemes for embedding the transmitted communication symbols towards the communication receiver located either in SL or main lobe directions, respectively. Also, in the tracking scenario, we considered different motion modes, CTM and CV models, for the moving target in our proposed design. The simulation results verified the effectiveness of the proposed designs. The performance of the radar functionality is improved in terms of resolution, estimation, and tracking performance. While for the communication functionality, the performance is improved in terms of BER, secure information transmission, and the overall throughput of the system is enhanced.

5.2. Future trends and challenges

While many efforts have been contributed towards RadCom systems, the field remains to be further investigated within a wide-ranging of scenarios and constraints. To this end, the future trends to be researched are listed as follows

- Further research is required to explore the ability of the proposed RadCom system to
 deliver information to the moving communication receivers during the tracking operation.
 The cognitive control and machine learning (ML) algorithms in the system design are
 essential to enable the system to distinguish between communication and target locations.
- Ideally, the receiver of the RadCom system should be a dual function receiver, i.e, used for processing the target returns and demodulating the communication symbols. Thus, the key

challenge for the receiver of the RadCom system is to separate the target returns/echoes from the received communication signals in presence of interference and noise. This signal classification processing is vital for both channel estimation and signal demodulation. As an example, in [166] the authors proposed to employ the compressed sensing method for symbol demodulation and joint parameter estimation. For signal classification purposes, given the independent statistical properties of the two types of signals, advanced ML-based methods such as the independent component analysis (ICA) algorithms can be used to well-address the design of the dual-function receiver.

- Interference produced by clutter scattering would affect the detection performance of the communication symbols, thus, further studies are required for clutter cancelation in the RadCom system [22].
- In this thesis, we considered a monostatic configuration for the RadCom system and we assumed that the receiver side knows the transmitted communication symbols. Thus, matched filtering (MF) processing can be applied in the monostatic receiver case. Bistatic configuration for the RadCom system would introduce additional challenges. In a bistatic configuration case, the receiver lacks knowledge of the transmitted communication symbols, thus, it neither can perform the matched filtering properly nor separate or remove the communication signal from the original transmitted waveform.
- RadCom systems research has recently raised privacy and security concerns. Since the spectrum is shared, the system may accidentally reveal vital information to the opponent eavesdroppers or commercial users. Thus, in the spectrum sharing scenarios, physical layer security has to be taken into consideration. One possible approach is transmitting an artificial noise (AN) by the system to the opponent target to contaminate and disturb the

eavesdropping activity while the desired transmit BPs are formulated. In the meantime, the performance of the communication function also must be guaranteed. Accordingly, numerous performance trade-offs including target detection and parameters estimation performance, and the communication and secrecy rates are still to be investigated. Some preliminary efforts on this issue can be found in [167-169].

- As a potential application of the RadCom systems, vehicular networks have drawn a lot of attention from both academia and industry. RadCom design schemes might be extended to vehicle-to-everything (V2X) applications with specific consideration of channel models for vehicle-to-infrastructure (V2I) and vehicle-to-vehicle (V2V) scenarios. Such schemes require novel signaling/beamforming design approaches [48, 170].
- An intelligent reflecting surface (IRS) [171, 172] is a promising beamforming technique used for improving the performance of wireless communication systems. IRS technology employed a large number of passive low-cost-complexity reflecting elements. Each element can reflect the incident signals on it with adaptable phase shifts and hence a passive BF can be established with the green energy-efficient property. RadCom systems can benefit from the deployment of IRS technology in the environment via a joint optimization of their design parameters with the IRS phase shift. Advanced approximation algorithms are required to solve such complex optimization problems to meet the time requirements for both functions.

APPENDIX A

Representation of the Received Data after Compensation Process at the Radar Receiver:

As shown in (3.42), the $f_{s,R}$ depends only on an angle, and thus, the compensating vector $\mathbf{g}(r_a)$, which is defined in (3.43), can be expressed in the joint transmit-receive spatial frequency domain as:

$$\mathbf{h} = \mathbf{1}_N \otimes \mathbf{g}(r_a) \tag{A.1}$$

where $\mathbf{1}_N$ is $N \times 1$ vector, all elements of the vector are equal to 1.

The received data after the compensation process is applied can be expressed as:

$$\mathbf{y}_{r,comp} = \left(\sqrt{\frac{E}{K}} \, \alpha_t \, [\, \mathbf{q}(\theta_t, \, r_t) \, \otimes \mathbf{b}(\theta_t) \,] + \widetilde{\mathbf{n}_d} \, + \, \widetilde{\mathbf{n}_r} \, \right) \odot \mathbf{h}$$

$$= \sqrt{\frac{E}{K}} \, \alpha_t [\, (\mathbf{q}(\theta_t, r_t) \odot \, \mathbf{h}) \otimes \mathbf{b}(\theta_t) \,] + \widetilde{\mathbf{n}_d} \, \odot \, \mathbf{h} \, + \, \widetilde{\mathbf{n}_r} \, \odot \, \mathbf{h} \quad (A.2)$$

Since the received interference signals and received noise are circularly Gaussian distribution with zero mean, the compensation process does not affect the joint transmit-receive spectrum distribution of the noise and interferences signals.

Therefore, $y_{r,comp}$ can be written as:

$$y_{r,comp} = \sqrt{\frac{E}{K}} \alpha_t \mathbf{W}^H [(\mathbf{a}(\theta_t) \odot \mathbf{a}(r_t) \odot \mathbf{g}(r_a)) \otimes \mathbf{b}(\theta_t)] + \widetilde{\mathbf{n}_i} + \widetilde{\mathbf{n}_r}$$

$$= \sqrt{\frac{E}{K}} \alpha_t \mathbf{W}^H [(\mathbf{a}(\theta_t) \odot \mathbf{a}(r_t - r_a)) \otimes \mathbf{b}(\theta_t)] + \widetilde{\mathbf{n}_d} + \widetilde{\mathbf{n}_r}$$

$$= \sqrt{\frac{E}{K}} \alpha_t \mathbf{W}^H [(\mathbf{a}(\theta_t) \odot \mathbf{a}(r_f + (i-1)r_{uamg} + \Delta r - r_f)) \otimes \mathbf{b}(\theta_t)] + \widetilde{\mathbf{n}_d} + \widetilde{\mathbf{n}_r} (A.3)$$

Note that, for the sake of simplicity, the term $e^{-j \delta_{k,T}(\theta_t,r_t)}$, k=1,...,K, is absorbed into the α_t .

APPENDIX B

Distance Calculation between the Symbols of the 16-APSK Constellation:

Assume that each symbol (signal point) to be transmitted towards the communication receiver located in the SL region is mapped into 4 bits, i.e. $\beta = 4$ bits, (see Fig. 3.3(a)), and these symbols are equally probable. For the 16-APSK modulation scheme, (5, 11) structure is used, the distances between the symbols in the inner and outer circles can be calculated as:

$$d_{A_1A_l}^2 = 4R_A^2 \left[\sin^2 \left(\frac{(i-1)\pi}{11} \right) \right]$$
 (B.1)

$$d_{B_1A_i}^2 = R_B^2 \left[1 + \left(\frac{R_B}{R_A} \right)^2 - 2 \left(\frac{R_B}{R_A} \right) \cos \left(\Theta + \frac{2(i-1)\pi}{11} \right) \right]$$
 (B.2)

$$d_{B_1B_j}^2 = 4R_B^2 \left[\sin^2 \left(\frac{(j-1)\pi}{5} \right) \right]$$
 (B.3)

$$d_{A_1B_j}^2 = R_B^2 \left[1 + \left(\frac{R_B}{R_A} \right)^2 - 2 \left(\frac{R_B}{R_A} \right) \cos \left(\Theta + \frac{2(j-1)\pi}{5} \right) \right]$$
 (B.4)

where R_B and R_A denote the radius of the inner and outer rings, respectively, and Θ represents the angle formed between the first communication symbol of the inner and outer rings.

APPENDIX C

Probability Density Function (PDF) Derivation for the 16-PSK Constellation:

Assume that A_1 (see Fig. 3.3(b)) is transmitted, the received vector at the communication receiver can be written as:

$$\mathbf{r} = (r_1, r_2) = (R_A + n_1, n_2)$$
 (C.1)

Where r_1 and r_2 are independent Gaussian random variables with mean R_A and zero, respectively, and variance $\frac{N_0}{2}$. Hence, the joint PDF of (r_1, r_2) is given by:

$$f_R = \frac{1}{\pi N_0} e^{-\frac{(r_1 - R_A)^2 + r_2^2}{N_0}}$$
 (C.2)

We introduce polar coordinates transformations of (r_1, r_2) as:

$$V = \sqrt{r_1^2 + r_2^2} \tag{C.3}$$

$$\Theta = \arctan\left(\frac{r_2}{r_1}\right) \tag{C.4}$$

The joint PDF of V and Θ can be derived as:

$$f_{V,\Theta}(v,\phi) = \frac{v}{\pi N_o} e^{-\frac{v^2 + R_A - 2\sqrt{R_A} v \cos \phi}{N_o}}$$
 (C.5)

We derive the marginal PDF of Θ , Integrating over v, as [173]:

$$f_{\Theta}(\phi) = \int_{0}^{\infty} f_{V,\Theta}(v,\phi) dv$$

$$= \frac{1}{2\pi} e^{-\xi \sin^2 \phi} \int_{0}^{\infty} v e^{-\frac{(v - \sqrt{2\xi} \cos \phi)^2}{2}} dv \qquad (C.6)$$

where $\xi = \frac{R_A^2}{N_a}$ is the SNR per symbol.

REFERENCES

- [1] P. Brown, "75.4 Billion devices connected to the internet of things by 2025," ed: Electronics, 2016.
- [2] F. Liu, C. Masouros, A. P. Petropulu, H. Griffiths, and L. Hanzo, "Joint radar and communication design: Applications, state-of-the-art, and the road ahead," *IEEE Transactions on Communications*, vol. 68, pp. 3834-3862, 2020.
- [3] A. Morris, "German spectrum auction raises more than 5B," ed, 2015.
- [4] R. Frieden, "The evolving 5G case study in United States unilateral spectrum planning and policy," *Telecommunications Policy*, vol. 44, p. 102011, 2020.
- [5] M. Calabrese, "Use it or Share It: A New Default Policy for Spectrum Management," Available at SSRN 3762098.
- [6] H. Griffiths, L. Cohen, S. Watts, E. Mokole, C. Baker, M. Wicks, et al., "Radar spectrum engineering and management: Technical and regulatory issues," *Proceedings of the IEEE*, vol. 103, pp. 85-102, 2014.
- [7] H. Wang, J. T. Johnson, and C. J. Baker, "Spectrum sharing between communications and ATC radar systems," *IET Radar, Sonar & Navigation*, vol. 11, pp. 994-1001, 2017.
- [8] J. H. Reed, A. W. Clegg, A. V. Padaki, T. Yang, R. Nealy, C. Dietrich, et al., "On the co-existence of TD-LTE and radar over 3.5 GHz band: An experimental study," *IEEE Wireless Communications Letters*, vol. 5, pp. 368-371, 2016.
- [9] F. Hessar and S. Roy, "Spectrum sharing between a surveillance radar and secondary Wi-Fi networks," *IEEE Transactions on Aerospace and Electronic Systems*, vol. 52, pp. 1434-1448, 2016.
- [10] H. Griffiths, S. Blunt, L. Cohen, and L. Savy, "Challenge problems in spectrum engineering and waveform diversity," in 2013 IEEE Radar Conference (RadarCon13), 2013, pp. 1-5.
- [11] H. Hayvaci and B. Tavli, "Spectrum sharing in radar and wireless communication systems:

 A review," in 2014 International Conference on Electromagnetics in Advanced Applications (ICEAA), 2014, pp. 810-813.
- [12] B. Paul, A. R. Chiriyath, and D. W. Bliss, "Survey of RF communications and sensing convergence research," *IEEE Access*, vol. 5, pp. 252-270, 2016.

- [13] J. Mitola, J. Guerci, J. Reed, Y.-D. Yao, Y. Chen, T. C. Clancy, et al., "Accelerating 5G QoE via public-private spectrum sharing," *IEEE Communications Magazine*, vol. 52, pp. 77-85, 2014.
- [14] J. Qian, Z. He, N. Huang, and B. Li, "Transmit designs for spectral coexistence of MIMO radar and MIMO communication systems," *IEEE Transactions on Circuits and Systems II:* Express Briefs, vol. 65, pp. 2072-2076, 2018.
- [15] K.-W. Huang, M. Bică, U. Mitra, and V. Koivunen, "Radar waveform design in spectrum sharing environment: Coexistence and cognition," in 2015 IEEE Radar Conference (RadarCon), 2015, pp. 1698-1703.
- [16] J. G. Metcalf, C. Sahin, S. D. Blunt, and M. Rangaswamy, "Analysis of symbol-design strategies for intrapulse radar-embedded communications," *IEEE Transactions on Aerospace and Electronic Systems*, vol. 51, pp. 2914-2931, 2015.
- [17] E. Grossi, M. Lops and L. Venturino, "Energy Efficiency Optimization in Radar-Communication Spectrum Sharing," in *IEEE Transactions on Signal Processing*, vol. 69, pp. 3541-3554, 2021.
- [18] X. Wang, J. Xu, A. Hassanien and E. Aboutanios, "Joint Communications with FH-MIMO Radar Systems: An Extended Signaling Strategy," *ICASSP 2021 2021 IEEE International Conference on Acoustics, Speech and Signal Processing (ICASSP)*, 2021, pp. 8253-8257.
- [19] S. H. Dokhanchi, M. R. B. Shankar, M. Alaee-Kerahroodi and B. Ottersten, "Adaptive Waveform Design for Automotive Joint Radar-Communication Systems," in *IEEE Transactions on Vehicular Technology*, vol. 70, no. 5, pp. 4273-4290, May 2021.
- [20] J. A. Mahal, A. Khawar, A. Abdelhadi, and T. C. Clancy, "Spectral coexistence of MIMO radar and MIMO cellular system," *IEEE Transactions on Aerospace and Electronic Systems*, vol. 53, pp. 655-668, 2017.
- [21] N. C. Luong, X. Lu, D. T. Hoang, D. Niyato and D. I. Kim, "Radio Resource Management in Joint Radar and Communication: A Comprehensive Survey," in *IEEE Communications Surveys & Tutorials*, vol. 23, no. 2, pp. 780-814, 2021.
- [22] X. Zhang, X. Wang and E. Aboutanios, "Effect Analysis of Spatial Modulation on Clutter Mitigation for Joint RadCom Systems and Solutions," 2020 IEEE Radar Conference (RadarConf20), pp. 1-6, 2020.
- [23] A. Hassanien, M. G. Amin, Y. D. Zhang, and F. Ahmad, "Signaling strategies for dual-function radar communications: An overview," *IEEE Aerospace and Electronic Systems Magazine*, vol. 31, pp. 36-45, 2016.

- [24] Y. Li, X. Wu and R. Tao, "Waveform Design for the Joint MIMO Radar and Communications with Low Integrated Sidelobe Levels and Accurate Information Embedding," ICASSP 2021 2021 IEEE International Conference on Acoustics, Speech and Signal Processing (ICASSP), pp. 8263-8267, 2021.
- [25] H. Wymeersch, G. Seco-Granados, G. Destino, D. Dardari, and F. Tufvesson, "5G mmWave positioning for vehicular networks," *IEEE Wireless Communications*, vol. 24, pp. 80-86, 2017.
- [26] C. Yang and H.-R. Shao, "WiFi-based indoor positioning," *IEEE Communications Magazine*, vol. 53, pp. 150-157, 2015.
- [27] L. Wang, J. McGeehan, C. Williams, and A. Doufexi, "Application of cooperative sensing in radar-communications coexistence," *IET communications*, vol. 2, pp. 856-868, 2008.
- [28] R. Saruthirathanaworakun, J. M. Peha, and L. M. Correia, "Opportunistic sharing between rotating radar and cellular," *IEEE Journal on Selected Areas in Communications*, vol. 30, pp. 1900-1910, 2012.
- [29] J. Li and P. Stoica, "MIMO radar with colocated antennas," *IEEE Signal Processing Magazine*, vol. 24, pp. 106-114, 2007.
- [30] J. Li and P. Stoica, MIMO radar signal processing: John Wiley & Sons, 2008.
- [31] M. Biguesh and A. B. Gershman, "Training-based MIMO channel estimation: a study of estimator tradeoffs and optimal training signals," *IEEE transactions on signal processing*, vol. 54, pp. 884-893, 2006.
- [32] B. Li and A. P. Petropulu, "Joint transmit designs for coexistence of MIMO wireless communications and sparse sensing radars in clutter," *IEEE Transactions on Aerospace and Electronic Systems*, vol. 53, pp. 2846-2864, 2017.
- [33] F. Liu, A. Garcia-Rodriguez, C. Masouros, and G. Geraci, "Interfering channel estimation in radar-cellular coexistence: How much information do we need?," *IEEE Transactions on Wireless Communications*, vol. 18, pp. 4238-4253, 2019.
- [34] A. Khawar, A. Abdel-Hadi, and T. C. Clancy, "Target detection performance of spectrum sharing MIMO radars," *IEEE Sensors Journal*, vol. 15, pp. 4928-4940, 2015.
- [35] A. Khawar, A. Abdel-Hadi, and T. C. Clancy, "MIMO radar waveform design for coexistence with cellular systems," in 2014 IEEE International Symposium on Dynamic Spectrum Access Networks (DYSPAN), 2014, pp. 20-26.

- [36] Y. Noam and A. J. Goldsmith, "Blind null-space learning for MIMO underlay cognitive radio with primary user interference adaptation," *IEEE Transactions on Wireless Communications*, vol. 12, pp. 1722-1734, 2013.
- [37] A. Babaei, W. H. Tranter, and T. Bose, "A nullspace-based precoder with subspace expansion for radar/communications coexistence," in 2013 IEEE Global Communications Conference (GLOBECOM), 2013, pp. 3487-3492.
- [38] B. Li and A. Petropulu, "Spectrum sharing between matrix completion based MIMO radars and a MIMO communication system," in 2015 IEEE International Conference on Acoustics, Speech and Signal Processing (ICASSP), 2015, pp. 2444-2448.
- [39] B. Li, A. P. Petropulu, and W. Trappe, "Optimum co-design for spectrum sharing between matrix completion based MIMO radars and a MIMO communication system," *IEEE Transactions on Signal Processing*, vol. 64, pp. 4562-4575, 2016.
- [40] F. Liu, C. Masouros, A. Li, and T. Ratnarajah, "Robust MIMO beamforming for cellular and radar coexistence," *IEEE Wireless Communications Letters*, vol. 6, pp. 374-377, 2017.
- [41] Y. Cui, V. Koivunen, and X. Jing, "Interference alignment based spectrum sharing for MIMO radar and communication systems," in 2018 IEEE 19th International Workshop on Signal Processing Advances in Wireless Communications (SPAWC), 2018, pp. 1-5.
- [42] Z. Cheng, B. Liao, S. Shi, Z. He, and J. Li, "Co-Design for Overlaid MIMO Radar and Downlink MISO Communication Systems via Cramér—Rao Bound Minimization," *IEEE Transactions on Signal Processing*, vol. 67, pp. 6227-6240, 2019.
- [43] F. Liu, C. Masouros, A. Li, T. Ratnarajah, and J. Zhou, "MIMO radar and cellular coexistence: A power-efficient approach enabled by interference exploitation," *IEEE Transactions on Signal Processing*, vol. 66, pp. 3681-3695, 2018.
- [44] C. Masouros and G. Zheng, "Exploiting known interference as green signal power for downlink beamforming optimization," *IEEE Transactions on Signal processing*, vol. 63, pp. 3628-3640, 2015.
- [45] G. C. Tavik, C. L. Hilterbrick, J. B. Evins, J. J. Alter, J. G. Crnkovich, J. W. de Graaf, et al., "The advanced multifunction RF concept," *IEEE Transactions on Microwave Theory and Techniques*, vol. 53, pp. 1009-1020, 2005.
- [46] L. Reichardt, C. Sturm, F. Grünhaupt, and T. Zwick, "Demonstrating the use of the IEEE 802.11 p car-to-car communication standard for automotive radar," in 2012 6th European Conference on Antennas and Propagation (EUCAP), 2012, pp. 1576-1580.

- [47] P. Kumari, N. Gonzalez-Prelcic, and R. W. Heath, "Investigating the IEEE 802.11 ad standard for millimeter wave automotive radar," in 2015 IEEE 82nd Vehicular Technology Conference (VTC2015-Fall), 2015, pp. 1-5.
- [48] P. Kumari, J. Choi, N. González-Prelcic, and R. W. Heath, "IEEE 802.11 ad-based radar: An approach to joint vehicular communication-radar system," *IEEE Transactions on Vehicular Technology*, vol. 67, pp. 3012-3027, 2017.
- [49] G. R. Muns, K. V. Mishra, C. B. Guerra, Y. C. Eldar, and K. R. Chowdhury, "Beam alignment and tracking for autonomous vehicular communication using IEEE 802.11 adbased radar," in *IEEE INFOCOM 2019-IEEE Conference on Computer Communications Workshops (INFOCOM WKSHPS)*, 2019, pp. 535-540.
- [50] P. Kumari, R. W. Heath, and S. A. Vorobyov, "Virtual pulse design for IEEE 802.11 AD-based joint communication-radar," in 2018 IEEE International Conference on Acoustics, Speech and Signal Processing (ICASSP), 2018, pp. 3315-3319.
- [51] E. Grossi, M. Lops, L. Venturino, and A. Zappone, "Opportunistic automotive radar using the IEEE 802.11 ad standard," in 2017 IEEE Radar Conference (RadarConf), 2017, pp. 1196-1200.
- [52] P. Kumari, M. E. Eltayeb, and R. W. Heath, "Sparsity-aware adaptive beamforming design for IEEE 802.11 ad-based joint communication-radar," in 2018 IEEE Radar Conference (RadarConf18), 2018, pp. 0923-0928.
- [53] P. Kumari, D. H. Nguyen, and R. W. Heath, "Performance trade-off in an adaptive IEEE 802.11 ad waveform design for a joint automotive radar and communication system," in 2017 IEEE International Conference on Acoustics, Speech and Signal Processing (ICASSP), 2017, pp. 4281-4285.
- [54] P. Kumari, S. A. Vorobyov, and R. W. Heath, "Adaptive Virtual Waveform Design for Millimeter-Wave Joint Communication-Radar," *IEEE Transactions on Signal Processing*, vol. 68, pp. 715-730, 2019.
- [55] A. Ahmed, S. Zhang, and Y. D. Zhang, "Optimized Sensor Selection for Joint Radar-communication Systems," in *ICASSP 2020-2020 IEEE International Conference on Acoustics, Speech and Signal Processing (ICASSP)*, 2020, pp. 4682-4686.
- [56] S. Sodagari, A. Khawar, T. C. Clancy, and R. McGwier, "A projection based approach for radar and telecommunication systems coexistence," in 2012 IEEE Global Communications Conference (GLOBECOM), 2012, pp. 5010-5014.
- [57] F. Liu, C. Masouros, A. Li, H. Sun, and L. Hanzo, "MU-MIMO communications with MIMO radar: From co-existence to joint transmission," *IEEE Transactions on Wireless Communications*, vol. 17, pp. 2755-2770, 2018.

- [58] D. Ma, T. Huang, Y. Liu, and X. Wang, "A novel joint radar and communication system based on randomized partition of antenna array," in 2018 IEEE International Conference on Acoustics, Speech and Signal Processing (ICASSP), 2018, pp. 3335-3339.
- [59] J. G. Proakis and M. Salehi, *Digital Communication*, 5th ed. New York, NY, USA: McGraw-Hill, 2007.
- [60] A. Mohammadi and F. M. Ghannouchi, "Digital Modulation Techniques in MIMO Systems," in *RF Transceiver Design for MIMO Wireless Communications*, ed: Springer, 2012, pp. 27-54.
- [61] J. Wang, S. Jia, and J. Song, "Generalised spatial modulation system with multiple active transmit antennas and low complexity detection scheme," *IEEE Transactions on Wireless Communications*, vol. 11, pp. 1605-1615, 2012.
- [62] X. Wang, A. Hassanien, and M. G. Amin, "Sparse transmit array design for dual-function radar communications by antenna selection," *Digital Signal Processing*, vol. 83, pp. 223-234, 2018.
- [63] X. Wang, A. Hassanien, and M. G. Amin, "Dual-function MIMO radar communications system design via sparse array optimization," *IEEE Transactions on Aerospace and Electronic Systems*, vol. 55, pp. 1213-1226, 2018.
- [64] M. Jiang, G. Liao, Z. Yang, Y. Liu, and Y. Chen, "Integrated radar and communication waveform design based on a shared array," Signal Processing, p. 107956, 2020.
- [65] C. Sturm and W. Wiesbeck, "Waveform design and signal processing aspects for fusion of wireless communications and radar sensing," *Proceedings of the IEEE*, vol. 99, pp. 1236-1259, 2011.
- [66] E. Uchiyama and R. Kohno, "Inter-vehicle spread spectrum communication and ranging system with interference canceller," in *Proceedings 199 IEEE/IEEJ/JSAI International Conference on Intelligent Transportation Systems (Cat. No. 99TH8383)*, 1999, pp. 778-782.
- [67] K. Mizutani and R. Kohno, "Inter-vehicle spread spectrum communication and ranging system with concatenated EOE sequence," *IEEE Transactions on intelligent transportation systems*, vol. 2, pp. 180-191, 2001.
- [68] F. E. Nathanson, J. P. Reilly, and M. N. Cohen, "Radar design principles-Signal processing and the Environment," *STIA*, vol. 91, p. 46747, 1991.
- [69] T. Kasami, "Weight distribution formula for some class of cyclic codes," Coordinated Science Laboratory Report no. R-285, 1966.

- [70] T. Hwang, C. Yang, G. Wu, S. Li, and G. Y. Li, "OFDM and its wireless applications: A survey," *IEEE transactions on Vehicular Technology*, vol. 58, pp. 1673-1694, 2008.
- [71] T. S. Rappaport, A. Annamalai, R. Buehrer, and W. H. Tranter, "Wireless communications: past events and a future perspective," *IEEE communications Magazine*, vol. 40, pp. 148-161, 2002.
- [72] N. Levanon, "Multifrequency radar signals," in Record of the IEEE 2000 International Radar Conference [Cat. No. 00CH37037], 2000, pp. 683-688.
- [73] G. Franken, H. Nikookar, and P. Van Genderen, "Doppler tolerance of OFDM-coded radar signals," in 2006 European radar conference, 2006, pp. 108-111.
- [74] C. Sturm, T. Zwick, and W. Wiesbeck, "An OFDM system concept for joint radar and communications operations," in VTC Spring 2009-IEEE 69th Vehicular Technology Conference, 2009, pp. 1-5.
- [75] Y. L. Sit, C. Sturm, L. Reichardt, T. Zwick, and W. Wiesbeck, "The OFDM joint radar-communication system: An overview," in *Proc. Int. Conf. Advances in Satellite and Space Communications (SPACOMM 2011)*, 2011, pp. 69-74.
- [76] Y. L. Sit, L. Reichardt, C. Sturm, and T. Zwick, "Extension of the OFDM joint radar-communication system for a multipath, multiuser scenario," in 2011 IEEE RadarCon (RADAR), 2011, pp. 718-723.
- [77] Y. L. Sit, C. Sturm, and T. Zwick, "Doppler estimation in an OFDM joint radar and communication system," in 2011 German Microwave Conference, 2011, pp. 1-4.
- [78] T. Liang, Z. Li, M. Wang, and X. Fang, "Design of radar-communication integrated signal based on OFDM," in *International Conference on Artificial Intelligence for Communications and Networks*, 2019, pp. 108-119.
- [79] S. Han, L. Ye, and W. Meng, Artificial Intelligence for Communications and Networks: First EAI International Conference, AICON 2019, Harbin, China, May 25-26, 2019, Proceedings, Part II vol. 287: Springer, 2019.
- [80] L. Welch, "Lower bounds on the maximum cross correlation of signals (corresp.)," *IEEE Transactions on Information theory*, vol. 20, pp. 397-399, 1974.
- [81] T. W. Tedesso and R. Romero, "Code shift keying based joint radar and communications for EMCON applications," *Digital Signal Processing*, vol. 80, pp. 48-56, 2018.
- [82] X. Tian and Z. Song, "On radar and communication integrated system using OFDM signal," in 2017 IEEE Radar Conference (RadarConf), 2017, pp. 0318-0323.

- [83] J. A. Davis and J. Jedwab, "Peak-to-mean power control in OFDM, Golay complementary sequences, and Reed-Muller codes," *IEEE Transactions on information theory*, vol. 45, pp. 2397-2417, 1999.
- [84] W. Li, Z. Xiang, and P. Ren, "Waveform Design for Dual-Function Radar-Communication System With Golay Block Coding," *IEEE Access*, vol. 7, pp. 184053-184062, 2019.
- [85] I. Podkurkov, J. Zhang, A. F. Nadeev, and M. Haardt, "Efficient multidimensional wideband parameter estimation for OFDM based joint radar and communication systems," *IEEE Access*, vol. 7, pp. 112792-112808, 2019.
- [86] J. Zhang, I. Podkurkov, M. Haardt, and A. Nadeev, "Efficient multidimensional parameter estimation for joint wideband radar and communication systems based on OFDM," in 2017 IEEE International Conference on Acoustics, Speech and Signal Processing (ICASSP), 2017, pp. 3096-3100.
- [87] A. V. Oppenheim, Discrete-time signal processing: Pearson Education India, 1999.
- [88] B. Schweizer, C. Knill, D. Schindler, and C. Waldschmidt, "Stepped-carrier OFDM-radar processing scheme to retrieve high-resolution range-velocity profile at low sampling rate," *IEEE Transactions on Microwave Theory and Techniques*, vol. 66, pp. 1610-1618, 2017.
- [89] G. Lellouch, A. K. Mishra, and M. Inggs, "Stepped OFDM radar technique to resolve range and Doppler simultaneously," *IEEE Transactions on Aerospace and Electronic Systems*, vol. 51, pp. 937-950, 2015.
- [90] M. C. P. Paredes and M. Garcia, "The problem of peak-to-average power ratio in OFDM systems," arXiv preprint arXiv:1503.08271, 2015.
- [91] Y. Yang, J. Mei, D. Hu, Y. Lei, and X. Luo, "Research on reducing PAPR of QAM-OFDM radar-communication integration sharing signal," *The Journal of Engineering*, vol. 2019, pp. 8042-8046, 2019.
- [92] K. Bae, J. G. Andrews, and E. J. Powers, "Adaptive active constellation extension algorithm for peak-to-average ratio reduction in OFDM," *IEEE Communications Letters*, vol. 14, pp. 39-41, 2009.
- [93] R. A. Shafik, M. S. Rahman, A. R. Islam, and N. S. Ashraf, "On the error vector magnitude as a performance metric and comparative analysis," in 2006 International Conference on Emerging Technologies, 2006, pp. 27-31.
- [94] T. Huang and T. Zhao, "Low PMEPR OFDM radar waveform design using the iterative least squares algorithm," *IEEE Signal Processing Letters*, vol. 22, pp. 1975-1979, 2015.

- [95] A. Turlapaty, Y. Jin, and Y. Xu, "Range and velocity estimation of radar targets by weighted OFDM modulation," in 2014 IEEE Radar Conference, 2014, pp. 1358-1362.
- [96] X. Lv, J. Wang, Z. Jiang, and W. Wu, "A Joint Radar-Communication System Based on OCDM-OFDM Scheme," in 2018 International Conference on Microwave and Millimeter Wave Technology (ICMMT), 2018, pp. 1-3.
- [97] X. Lv, J. Wang, Z. Jiang, and W. Jiao, "A novel PAPR reduction method for OCDM-based radar-communication signal," in 2018 IEEE MTT-S International Microwave Workshop Series on 5G Hardware and System Technologies (IMWS-5G), 2018, pp. 1-3.
- [98] X. Ouyang, C. Antony, F. Gunning, H. Zhang, and Y. L. Guan, "Discrete Fresnel transform and its circular convolution," arXiv preprint arXiv:1510.00574, 2015.
- [99] Y. Liu, G. Liao, J. Xu, Z. Yang, and Y. Zhang, "Adaptive OFDM integrated radar and communications waveform design based on information theory," *IEEE Communications Letters*, vol. 21, pp. 2174-2177, 2017.
- [100] Y. Liu, G. Liao, and Z. Yang, "Robust OFDM integrated radar and communications waveform design based on information theory," *Signal Processing*, vol. 162, pp. 317-329, 2019.
- [101] M. Braun, C. Sturm, A. Niethammer, and F. K. Jondral, "Parametrization of joint OFDM-based radar and communication systems for vehicular applications," in 2009 IEEE 20th International Symposium on Personal, Indoor and Mobile Radio Communications, 2009, pp. 3020-3024.
- [102] C. Knill, F. Roos, B. Schweizer, D. Schindler, and C. Waldschmidt, "Random multiplexing for an MIMO-OFDM radar with compressed sensing-based reconstruction," *IEEE Microwave and Wireless Components Letters*, vol. 29, pp. 300-302, 2019.
- [103] C. Sturm, Y. L. Sit, M. Braun, and T. Zwick, "Spectrally interleaved multi-carrier signals for radar network applications and multi-input multi-output radar," *IET Radar, Sonar & Navigation*, vol. 7, pp. 261-269, 2013.
- [104] G. Hakobyan and B. Yang, "A novel OFDM-MIMO radar with non-equidistant subcarrier interleaving and compressed sensing," in 2016 17th International Radar Symposium (IRS), 2016, pp. 1-5.
- [105] G. Hakobyan and B. Yang, "A novel intercarrier-interference free signal processing scheme for OFDM radar," *IEEE Transactions on Vehicular Technology*, vol. 67, pp. 5158-5167, 2017.
- [106] M. Skolnik, "Introduction to Radar systems," *IEEE Aerospace and Electronic Systems Magazine*, vol. 16, pp. 19-19, 2001.

- [107] C. Sahin, J. Jakabosky, P. M. McCormick, J. G. Metcalf, and S. D. Blunt, "A novel approach for embedding communication symbols into physical radar waveforms," in 2017 IEEE Radar Conference (RadarConf), 2017, pp. 1498-1503.
- [108] C.-H. Wang, C. D. Ozkaptan, E. Ekici, and O. Altintas, "Poster: Multi-carrier Modulation on FMCW Radar for Joint Automotive Radar and Communication," in 2018 IEEE Vehicular Networking Conference (VNC), 2018, pp. 1-2.
- [109] O. Altintas and C.-h. Wang, "Multi-carrier modulation on FMCW radar for integrated automotive radar and communication systems," ed: Google Patents, 2020.
- [110] Z. Dou, "Radar-communication integration based on MSK-LFM spread spectrum signal," International Journal of Communications, Network and System Sciences, vol. 10, p. 108, 2017.
- [111] X. Chen, Z. Liu, Y. Liu, and Z. Wang, "Energy leakage analysis of the radar and communication integrated waveform," *IET Signal Processing*, vol. 12, pp. 375-382, 2017.
- [112] L. Zhipeng, C. Xingbo, W. Xiaomo, S. Xu, and F. Yuan, "Communication analysis of integrated waveform based on LFM and MSK," in *IET International Radar Conference* 2015, 2015, pp. 1-5.
- [113] Y. Ni, Z. Wang, Q. Huang, and M. Zhang, "High Throughput Rate-Shift Integrated System for Joint Radar-Communications," *IEEE Access*, vol. 7, pp. 78228-78238, 2019.
- [114] Y. Zhang, Q. Li, L. Huang, C. Pan, and J. Song, "A modified waveform design for radar-communication integration based on LFM-CPM," in 2017 IEEE 85th Vehicular Technology Conference (VTC Spring), 2017, pp. 1-5.
- [115] X.-B. Li, R.-J. Yang, and W. Cheng, "Integrated radar and communication based on multicarrier frequency modulation chirp signal," *Dianzi Yu Xinxi Xuebao(Journal of Electronics and Information Technology)*, vol. 35, pp. 406-412, 2013.
- [116] Y. Zhang, Q. Li, L. Huang, and J. Song, "Waveform design for joint radar-communication system with multi-user based on MIMO radar," in 2017 IEEE Radar Conference (RadarConf), 2017, pp. 0415-0418.
- [117] Q. Li, K. Dai, Y. Zhang, and H. Zhang, "Integrated waveform for a joint radar-communication system with high-speed transmission," *IEEE Wireless Communications Letters*, vol. 8, pp. 1208-1211, 2019.
- [118] T. K. Moon, Error correction coding: mathematical methods and algorithms: John Wiley & Sons, 2020.

- [119] L. Bahl, J. Cocke, F. Jelinek, and J. Raviv, "Optimal decoding of linear codes for minimizing symbol error rate (corresp.)," *IEEE Transactions on information theory*, vol. 20, pp. 284-287, 1974.
- [120] D. Gaglione, C. Clemente, C. V. Ilioudis, A. R. Persico, I. K. Proudler, J. J. Soraghan, et al., "Waveform design for communicating radar systems using fractional Fourier transform," Digital Signal Processing, vol. 80, pp. 57-69, 2018.
- [121] M. B. Alabd, L. G. de Oliveira, B. Nuss, W. Wiesbeck, and T. Zwick, "Time-Frequency Shift Modulation for Chirp Sequence based Radar Communications," in 2020 IEEE MTT-S International Conference on Microwaves for Intelligent Mobility (ICMIM), 2020, pp. 1-4
- [122] A. Hassanien, B. Himed, and B. D. Rigling, "A dual-function MIMO radar-communications system using frequency-hopping waveforms," in 2017 IEEE Radar Conference (RadarConf), 2017, pp. 1721-1725.
- [123] J. P. Costas, "A study of a class of detection waveforms having nearly ideal range—Doppler ambiguity properties," *Proceedings of the IEEE*, vol. 72, pp. 996-1009, 1984.
- [124] X. Wang and J. Xu, "Co-design of joint radar and communications systems utilizing frequency hopping code diversity," in 2019 IEEE Radar Conference (RadarConf), 2019, pp. 1-6.
- [125] A. Hassanien, M. G. Amin, Y. D. Zhang, and F. Ahmad, "Dual-function radar-communications: Information embedding using sidelobe control and waveform diversity," *IEEE Transactions on Signal Processing*, vol. 64, pp. 2168-2181, 2015.
- [126] A. Hassanien, M. G. Amin, Y. D. Zhang, and F. Ahmad, "Phase-modulation based dual-function radar-communications," *IET Radar, Sonar & Navigation*, vol. 10, pp. 1411-1421, 2016.
- [127] A. Ahmed, Y. D. Zhang, and Y. Gu, "Dual-function radar-communications using QAM-based sidelobe modulation," *Digital Signal Processing*, vol. 82, pp. 166-174, 2018.
- [128] E. BouDaher, A. Hassanien, E. Aboutanios, and M. G. Amin, "Towards a dual-function MIMO radar-communication system," in 2016 IEEE Radar Conference (RadarConf), 2016, pp. 1-6.
- [129] A. Hassanien, E. Aboutanios, M. G. Amin, and G. A. Fabrizio, "A dual-function MIMO radar-communication system via waveform permutation," *Digital Signal Processing*, vol. 83, pp. 118-128, 2018.

- [130] P. Antonik, M. C. Wicks, H. D. Griffiths, and C. J. Baker, "Range-dependent beamforming using element level waveform diversity," in 2006 International Waveform Diversity & Design Conference, 2006, pp. 1-6.
- [131] S. W. Golomb and H. Taylor, "Constructions and properties of Costas arrays," *Proceedings* of the IEEE, vol. 72, pp. 1143-1163, 1984.
- [132] S. Y. Nusenu and W.-Q. Wang, "Dual-function FDA MIMO radar-communications system employing costas signal waveforms," in 2018 IEEE Radar Conference (RadarConf18), 2018, pp. 0033-0038.
- [133] A. Hassanien, M. G. Amin, Y. D. Zhang, and F. Ahmad, "Dual-function radar-communications using phase-rotational invariance," in 2015 23rd European Signal Processing Conference (EUSIPCO), 2015, pp. 1346-1350.
- [134] J. Euziere, R. Guinvarc'h, M. Lesturgie, B. Uguen, and R. Gillard, "Dual function radar communication time-modulated array," in 2014 International Radar Conference, 2014, pp. 1-4.
- [135] A. Hassanien, M. G. Amin, Y. D. Zhang, F. Ahmad, and B. Himed, "Non-coherent PSK-based dual-function radar-communication systems," in 2016 IEEE Radar Conference (RadarConf), 2016, pp. 1-6.
- [136] A. R. Al-Salehi, I. M. Qureshi, A. N. Malik, W. Khan, and A. Basit, "Dual-function radar-communications: information transmission during FDA radar listening mode," *International Journal of Microwave and Wireless Technologies*, vol. 12, pp. 1-12, 2020.
- [137] P. M. McCormick, S. D. Blunt, and J. G. Metcalf, "Simultaneous radar and communications emissions from a common aperture, part 1: Theory," in 2017 IEEE Radar Conference (RadarConf), 2017, pp. 1685-1690.
- [138] P. M. McCormick, B. Ravenscroft, S. D. Blunt, A. J. Duly, and J. G. Metcalf, "Simultaneous radar and communication emissions from a common aperture, part II: experimentation," in 2017 IEEE Radar Conference (RadarConf), 2017, pp. 1697-1702.
- [139] J. Li and P. Stoica, MIMO radar signal processing vol. 7: Wiley Online Library, 2009.
- [140] J. Li and P. Stoica, "MIMO radar—diversity means superiority," MIMO radar signal processing, vol. 1: Wiley Online Library, 2009.
- [141] A. Ahmed, Y. D. Zhang, and B. Himed, "Multi-user dual-function radar-communications exploiting sidelobe control and waveform diversity," in 2018 IEEE Radar Conference (RadarConf18), 2018, pp. 0698-0702.

- [142] A. Hassanien, M. G. Amin, Y. D. Zhang, and B. Himed, "A dual-function MIMO radar-communications system using PSK modulation," in 2016 24th European Signal Processing Conference (EUSIPCO), 2016, pp. 1613-1617.
- [143] M. N. El Korso, R. Boyer, A. Renaux, and S. Marcos, "Statistical resolution limit for source localization in a MIMO context," in 2011 IEEE International Conference on Acoustics, Speech and Signal Processing (ICASSP), 2011, pp. 2756-2759.
- [144] W.-Q. Wang, "Range-angle dependent transmit beampattern synthesis for linear frequency diverse arrays," *IEEE Transactions on Antennas and Propagation*, vol. 61, pp. 4073-4081, 2013.
- [145] P. Baizert, T. B. Hale, M. A. Temple, and M. C. Wicks, "Forward-looking radar GMTI benefits using a linear frequency diverse array," *Electronics Letters*, vol. 42, pp. 1311-1312, 2006.
- [146] P. Antonik, M. C. Wicks, H. D. Griffiths, and C. J. Baker, "Multi-mission multi-mode waveform diversity," in 2006 IEEE Conference on Radar, 2006, p. 3 pp.
- [147] S. D. Blunt and E. L. Mokole, "Overview of radar waveform diversity," *IEEE Aerospace and Electronic Systems Magazine*, vol. 31, pp. 2-42, 2016.
- [148] M. Baldi, F. Chiaraluce, A. De Angelis, R. Marchesani, and S. Schillaci, "A comparison between APSK and QAM in wireless tactical scenarios for land mobile systems," EURASIP Journal on Wireless Communications and Networking, vol. 2012, p. 317, 2012.
- [149] H. K. D. Sarma, S. Borah, and N. Dutta, Advances in Communication, Cloud, and Big Data: Proceedings of 2nd National Conference on CCB 2016 vol. 31: Springer, 2018.
- [150] D. D. Sworder and J. E. Boyd, *Estimation problems in hybrid systems*: Cambridge University Press, 1999.
- [151] A. Alouani, P. Xia, T. Rice, and W. Blair, "A two-stage Kalman estimator for state estimation in the presence of random bias and for tracking maneuvering targets," in [1991] Proceedings of the 30th IEEE Conference on Decision and Control, 1991, pp. 2059-2062.
- [152] T. Kirubarajan and Y. Bar-Shalom, "Kalman filter versus IMM estimator: when do we need the latter?," *IEEE Transactions on Aerospace and Electronic Systems*, vol. 39, pp. 1452-1457, 2003.
- [153] H. A. Blom and Y. Bar-Shalom, "The interacting multiple model algorithm for systems with Markovian switching coefficients," *IEEE Transactions on Automatic Control*, vol. 33, pp. 780-783, 1988.

- [154] Y. Bar-Shalom, X. R. Li, and T. Kirubarajan, Estimation with applications to tracking and navigation: theory algorithms and software: John Wiley & Sons, 2004.
- [155] X. R. Li and V. P. Jilkov, "Survey of maneuvering target tracking. Part I. Dynamic models," *IEEE Transactions on Aerospace and Electronic Systems*, vol. 39, pp. 1333-1364, 2003.
- [156] G. A. Watson and W. D. Blair, "IMM algorithm for tracking targets that maneuver through coordinated turns," in *Signal and Data Processing of Small Targets* 1992, 1992, pp. 236-247.
- [157] W.-Q. Wang and H. Shao, "Range-angle localization of targets by a double-pulse frequency diverse array radar," *IEEE Journal of Selected Topics in Signal Processing*, vol. 8, pp. 106-114, 2013.
- [158] S. M. Kay, "Statistical signal processing: Detection theory," *Prentice Hall*, vol. 146, p. 222, 1998.
- [159] J. Xu, G. Liao, S. Zhu, L. Huang, and H. C. So, "Joint range and angle estimation using MIMO radar with frequency diverse array," *IEEE Transactions on Signal Processing*, vol. 63, pp. 3396-3410, 2015.
- [160] A. de Oliveira Ferreira, R. Sampaio-Neto, and J. M. Fortes, "Robust sidelobe amplitude and phase modulation for dual-function radar-communications," *Transactions on Emerging Telecommunications Technologies*, vol. 29, p. e3314, 2018.
- [161] A. Basit, W.-Q. Wang, and S. Y. Nusenu, "Adaptive transmit array sidelobe control using FDA-MIMO for tracking in joint radar-communications," *Digital Signal Processing*, vol. 97, p. 102619, 2020.
- [162] A. Hassanien, S. A. Vorobyov, and A. Khabbazibasmenj, "Transmit radiation pattern invariance in MIMO radar with application to DOA estimation," *IEEE Signal Processing Letters*, vol. 22, pp. 1609-1613, 2015.
- [163] H. Liu and W. Wu, "Interacting multiple model (IMM) fifth-degree spherical simplex-radial cubature Kalman filter for maneuvering target tracking," *Sensors*, vol. 17, p. 1374, 2017.
- [164] M. W. Owen and A. R. Stubberud, "NEKF IMM tracking algorithm," in Signal and Data Processing of Small Targets 2003, 2004, pp. 223-233.
- [165] A. Hassanien and S. A. Vorobyov, "Transmit energy focusing for DOA estimation in MIMO radar with colocated antennas," *IEEE Transactions on Signal Processing*, vol. 59, pp. 2669-2682, 2011.

- [166] L. Zheng, M. Lops, and X. Wang, "Adaptive interference removal for uncoordinated radar/communication coexistence," *IEEE Journal of Selected Topics in Signal Processing*, vol. 12, pp. 45-60, 2017.
- [167] A. Deligiannis, A. Daniyan, S. Lambotharan, and J. A. Chambers, "Secrecy rate optimizations for MIMO communication radar," *IEEE Transactions on Aerospace and Electronic Systems*, vol. 54, pp. 2481-2492, 2018.
- [168] B. K. Chalise and M. G. Amin, "Performance tradeoff in a unified system of communications and passive radar: A secrecy capacity approach," *Digital Signal Processing*, vol. 82, pp. 282-293, 2018.
- [169] A. Dimas, M. A. Clark, B. Li, K. Psounis, and A. P. Petropulu, "On radar privacy in shared spectrum scenarios," in *ICASSP 2019-2019 IEEE International Conference on Acoustics, Speech and Signal Processing (ICASSP)*, 2019, pp. 7790-7794.
- [170] S. H. Dokhanchi, B. S. Mysore, K. V. Mishra, and B. Ottersten, "A mmWave automotive joint radar-communications system," *IEEE Transactions on Aerospace and Electronic Systems*, vol. 55, pp. 1241-1260, 2019.
- [171] Q. Wu and R. Zhang, "Intelligent reflecting surface enhanced wireless network via joint active and passive beamforming," *IEEE Transactions on Wireless Communications*, vol. 18, pp. 5394-5409, 2019.
- [172] S. Abeywickrama, R. Zhang, Q. Wu, and C. Yuen, "Intelligent reflecting surface: Practical phase shift model and beamforming optimization," *IEEE Transactions on Communications*, vol. 68, pp. 5849-5863, 2020.
- [173] J. G. Proakis and M. Salehi, Fundamentals of communication systems: Pearson Education India, 2007.

